Masterarbeit

Design and testing of a yaw mechanism for a small scale wind turbine

Juan Llobell Buigues

WE-MT-17-01

Author: Juan Llobell Buigues
Registration number: 03707584
Professor: Carlo L. Bottasso
Supervisor: Franz Mühle

Garching bei München, November 2021

I, Juan Llobell Buigues, confirm that the work presented in this thesis has been performed and interpreted solely by myself except where explicitly identified to the contrary. All verbatim extracts have been distinguished by quotation marks, and all sources of information have been specifically acknowledged. I confirm that this work has not been submitted elsewhere in any other form for the fulfillment of any other degree or qualification.

Garching bei München, November 2021
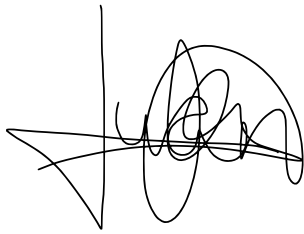
ABSTRACT

The main objective of this thesis is to have assembled one functional wind turbine sub-scaled G06 model. The G06 machine is a work in progress TUM wind turbine model, primarily designed by E.M Nanos. The final version, which includes active collective pitch, has never been assembled, and a solution for a suitable yaw mechanism has not yet been implemented. Thus two workflows are pivotal in this project: the assembly (including the documentation of the process) of one G06 machine and the design and implementation of a suitable yaw system.

E.M Nanos primarily designed the G06 model intending to perform wake and wind farm control studies in complex wind farm configurations and complex terrain. The challenge was to ensure a good aerodynamic performance and instrumentation while having a compact model, which allows setting several columns of at least five models in a 4 m by 14 m section in an atmospheric boundary layer wind tunnel. The smaller the model is, the more difficult it is to ensure a realistic aerodynamic performance similar to real wind turbine wake behaviour and also, the more difficult it gets to dispose of an instrumentation and control system suitable for wind farm control studies. [1]

A first design with manual pitch and lower instrumentation level was running in the Dallas Wind Tunnel. Afterwards, a prototype with active collective pitch control and strain gauges in the shaft was developed. The final design pieces were designed by Nanos and manufactured but never assembled. Work was resumed from this point, being the assembly of one turbine documented in this thesis. Besides, it was still necessary to solve how to implement a compact and powerful yaw system, which is pivotal to perform wind farm control studies (one of the main motivations of the model). The small size of the tower limits the design of such a system. Due to this restriction, alternative solutions to the ones implemented for the bigger scaled models of the TUM family (G1 and G2) are considered and evaluated in this thesis.

The work results is a G1 turbine with active pitch and an effective yaw mechanism system implemented, whose negligible effect on the wake has been proved in the wind tunnel. The yaw system was also tested to prove that it can perform the desired dynamic yawing movements. For the G1 machine, the most demanding dynamic yaw is a sinusoidal wave with 2° amplitude at 2 Hz. Not only will this be the design point, but other specifications such as a 0.2° accuracy position and slight backlash will be required. A Simulink model is built to design the components of the system, and finally tests are performed with the aim of finding the system operation limits.

List of Figures

Contents

Introduction

The introduction chapter aims to justify why a yaw mechanism in a small scale turbine as the G06 can be interesting. First, an overview of the role of the wind industry in the energy transition will be given, which justifies why the industry and its technology are growing at such a fast rate. This rapid growth must be supported with constant improvement in research and testing (both in the field and in wind tunnels). The future seems bright for small scale wind turbines, and the focus will be laid on their usefulness for wind tunnel testing. The introduction will finish analyzing the foundation of yaw aerodynamics and commenting state of the art of small wind turbines design (being yaw mechanisms design for small scale wind turbines almost nonexistent in the literature), which will lead to a more detailed explanation of the project's objective.

In Chapter 2 the G06 model is described, summarizing effectively all the information published by E.M.Nanos in his final work: "Design, performance and wake characterization of a scaled wind turbine with closed-loop controls [2]". The G06 was primarily designed to perform wake and wind farm control studies in complex wind farm configurations and complex terrain. The challenge was to ensure excellent aerodynamic performance and instrumentation while having a compact model, which allows setting several columns of at least five models in a section of 4m by 14 m at an atmospheric boundary layer wind tunnel. [3]

Two G06 prototypes with manual pitch and less instrumentation, which had already been running in the Dallas Wind Tunnel and the TUM wind tunnel for wake characterization purposes, were disassembled in the lab. The first step was to reassemble one again for two purposes. The first one is that it is always easier to assemble something that has already worked, and the assembling process can help to get a better understanding of the model, and thus make assembly of the new machines easier. The second one is that it is a more straightforward machine, which can be used for testing the suitability of the designed yaw mechanism in the wind tunnel. Given that only the optimal operation point is interesting, no loads or pitch measurements are needed for this experiment; it was a more effective way to proceed.

However, Nanos' work went further, and he designed a new version with active collective pitch control and strain gauges in the shaft. This version was a prototype before the final design and was available in the lab. Finally, some modifications were done, and the parts were manufactured and received but never assembled. Work was resumed from this point by updating the 3D CAD files, making an inventory and assembling all the pieces. The assembly process is documented in Chapter 4.

The final design did not resolve how to implement a yaw system, which is an essential feature of the model if farm optimization experiments are to be performed. Due to the small size of the tower and nacelle, a similar solution to the ones implemented for the bigger models in the Wind Energy Institute (G1 and G2) turns out to be very difficult if not impossible. Chapter 3 will explain and compare the different proposed solutions and then explain in more depth the best suiting solution, which has to match the specifications while being easy to implement and at a reasonable cost. Chapter 5 will explain in detail the implementation of the chosen yaw system.

1.1 Wind Energy development

Wind power is one of the fastest-growing renewable energy technologies. Usage is on the rise worldwide, in part because costs are falling. Driven by the goal to be more independent from fossil fuels, the wind energy industry has grown significantly over the last decades. While in 1985, typical turbines had a rated capacity of 0.05 MW and a rotor diameter of 15 metres, today's new wind power projects have turbine capacities of about 2 MW onshore and 3–5 MW offshore. Commercially available wind turbines have reached 8 MW capacity, with rotor diameters of up to 164 metres. The industry started to grow in 1997 when the installed capacity was 7.5 GW, and the rally started, tripling the capacity (to 24 GW) in only four years (2001). The average capacity of wind turbines increased from 1.6 MW in 2009 to 2 MW in 2014, which turned out to double the wind electricity production between 2009 and 2013. Between 2013 and 2018, there has been a steady growth of around 50 to 60 new GW installed per year. [4]

Looking at the bigger picture, in the last two decades, the global installed wind-generation capacity onshore and offshore has increased by a factor of 30 (almost 100 times since 1997), jumping from 24 GW in 2001 to 743 GW by 2020, according to the Global Wind Energy Council (GWEC) latest data (see Figure 1.1). Not only has the number of projects increased, but the technology has matured during all this period, which can be seen in the fast evolution of the size of the rotors (see Figure 1.2), mainly motivated because the wind caught by the turbine increases with the square of the length of the blades. The rapid growth in the accumulative installed capacity and the fast evolution in size and capacity of the commercially produced wind turbine systems demonstrate the wind industry's vital role in the energy transition.
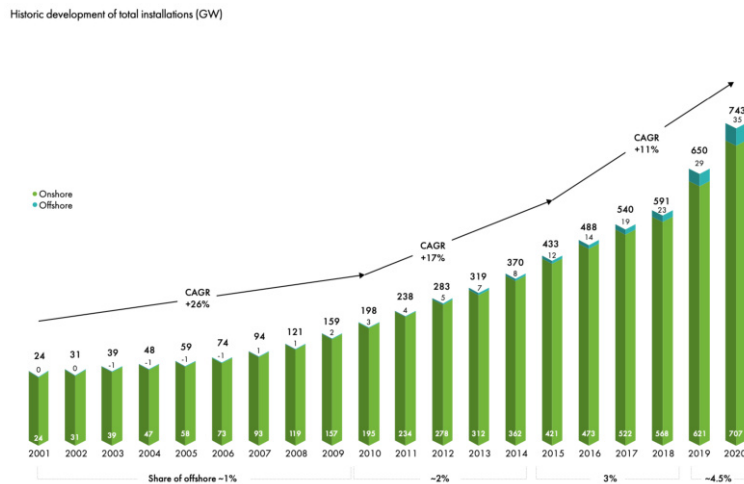
Figure 1.1: Historic growth of accumulative installed capacity [5]

The European Wind Energy Association estimated that 15–17% of the European Union's electricity demand would be met by wind energy by 2020. By 2016 wind energy already accounted for 16% of the electricity generated by renewables worldwide. Nevertheless, the peak does not seem to have been reached yet. Institutions and professionals agree that the future of wind energy is bright. One example is the International Renewable Energy Agency (IRENA), whose new report "Future of the Wind" says the deployment of wind power is accelerating worldwide. By 2050, the agency says, wind energy could account for 35% of global energy needs. However, for that to happen, the current capacity of wind energy would need to increase tenfold to 6,000 GW, including 5,000 GW on land and 1,000 GW offshore. [7]

The spirits are more optimistic than ever after 2020 was the best year in history in terms of year-over-year (YoY) growth (93 GW) despite the pandemic disrupting the global supply chain and project construction, showing an incredible resilience. In the onshore market, 86.9 GW were
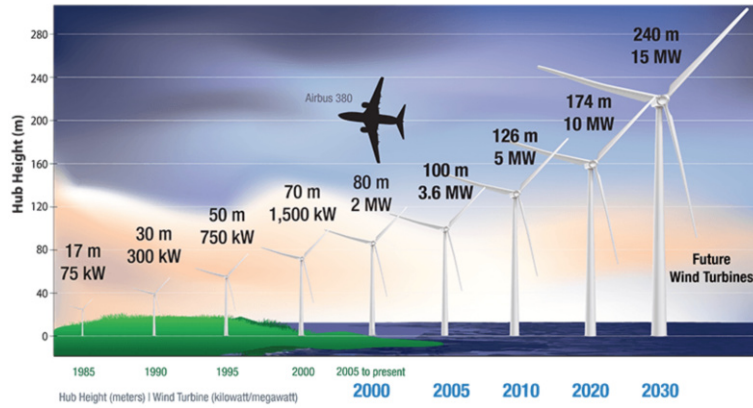
Figure 1.2: Rotor size evolution [6]

installed (53% increase respect 2019). China and the USA stood out as the main contributors to the change. Latin America also grew a 76% respect the previous year's installed capacity. Regarding the total offshore installation of 6.1 GW, China installed half of this share while Europe (especially the Netherlands, Belgium and the UK) showed steady growth.

These numbers are depicted in Figure 1.3. The world's top five markets in 2020 for new installations were China, the US, Brazil, Netherlands and Germany. These five markets combined made up 80.6% of global installations last year, collectively more than 10% greater than 2019. In terms of cumulative installations, the top five markets as of the end of 2020 remained unchanged. Those markets are: China, the US, Germany, India and Spain, which together accounted for 73% of the world's total wind power installations.
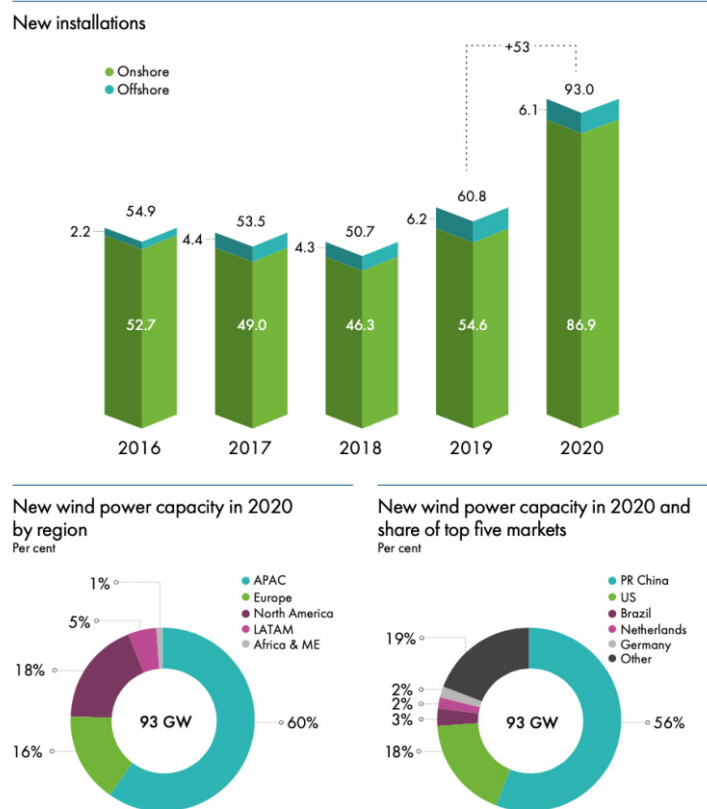
Figure 1.3: New installed capacity in 2020 [5]

The objective for 2050 is ambitious but realistic. It could be fulfilled considering that until now, objectives were always met (like in 2016 and 2020) and the still to be exploited tremendous potential of offshore wind power. The graphs show that a trend to move wind farms into offshore locations has already started. The total share of offshore capacity evolved from 3% in 2014 to 10% in 2020, and the rate of new installation per year from 2% to 4.5% respectively.

The reasons behind this movement are the following. Not only do offshore facilities offer less noise restriction, which allows them to operate at higher wind speeds, but there is less social resistance than against onshore farms. Besides, there are fewer logistical or transportation constraints, given that there is no limitation by inland infrastructure restrictions. Furthermore, there is also a high potential for reducing the levelized cost of energy (LCOE). This constant strive to lower the LCOE poses excellent challenges to engineers in designing and constructing wind turbine systems. Larger wind turbine systems with bigger rotor span experience a more substantial effect on the inhomogeneities of the incoming wind. Compared to onshore wind turbine systems, offshore systems face harsher conditions and higher load conditions during operation. Thus research and simulations are vital to exploit this potential, which has yet much to offer.

GWEC Market Intelligence expects over 469 GW of new capacity to be added in the next five years. The outlook for new installation in the following years is shown in Figure 1.4, being the objective to keep on with the rate of the year 2020. The global outlook remains positive with an expected growth of 4%, even though the installed capacity marked in 2020 a new high. At the beginning of the next five years, growth will continue to be driven by government policy, including FiT, PTC, ITC, Green Certificates, and renewable or technology-neutral auctions and tenders. New installations are expected to drop slightly in 2021. However, it is still possible to make it the second-best year in history, taking into account the ongoing installation rush in the world's two largest markets, China (offshore) and the US (onshore), driven by the cut-off of FiT and the deadline to qualify the total PTC value respectively. The role of offshore, which is expected to grow a 31.5% and new markets in development like Chile, Vietnam, Saudi Arabia and Colombia will be crucial to reach these goals. [5]
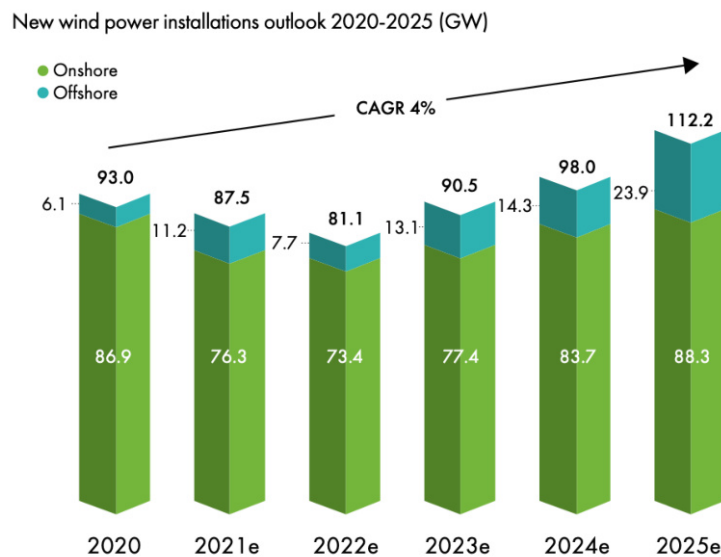
Figure 1.4: New installed capacity outlook 2020-2025 [5]

1.2   Wind tunnel testing using scaled wind models

The development of new wind turbine technologies focuses mainly on three different approaches: computer simulation, wind tunnel testing and field testing. Each of them has advantages and disadvantages. While field-testing provides the most reliable information, without validation, it tends to be the most time-consuming and costly technique. That is because of the opportunity cost of the turbines not running at their nominal power for the test time. A further drawback is that the test performers cannot freely choose the environment and test conditions. Besides the information obtained is difficult to extrapolate to other wind farms or locations, since the test conditions are difficult to know at each moment.

These problems trigger the need for computer simulations and wind tunnel testing, even if it is true that both of them have to deal with the limits of the model representing the field environment. In computer simulations, more complex, accurate models increase the computational cost. In contrast, the limits in wind tunnel testing are set by the mismatch between the non-dimensional parameters of the scaled model and the full-scale system.

Wind turbine sub-scaled models need to replicate the active control pitch, torque and yaw system of accurate models to obtain valuable data that can be scaled up to the real models. There are many different types of experiments, which can be performed in a wind tunnel. However, the most common investigation goals are: wake characteristics, wind turbine systems in normal and extreme conditions for certification, pitch effects, torque and yaw controllers, the interaction of the wind turbines in a farm and wind farm control strategies.

Over the last decade, wind tunnel tests conducted with small wind turbine models have gained increasing attention from the research community [8], being this the reason driving the development of the G06 model. Many authors have studied wakes, including the characterisation of the effects of the turbine operating conditions, inflow profiles, thermal stability and the testing of plant control strategies. Some of the most relevant studies about this topics are mentioned next.

Chamorro and Porté-Agel were pioneers in investigating the spatial distribution of the velocity deficit and the turbulence intensity, which are important factors affecting turbine power generation and fatigue loads in wind energy parks [9].

Hu et al. conducted an experimental study to characterize the dynamic wind loads and evolution of the unsteady vortex and turbulent flow structures in the near wake of a horizontal axis wind turbine model placed in an atmospheric boundary layer wind tunnel. Additionally a high-resolution digital particle image velocimetry (PIV) system is used to achieve flow field measurements to quantify the characteristics of the turbulent vortex flow in the near wake of the wind turbine model. [10]

Iungo et al. focused on wake meandering and spatial linear stability analyses of a wind turbine wake are performed on a base flow obtained with time-averaged wind tunnel velocity measurements [11]. Viola et al. investigated further the hub vortex stability, by neglecting the effect of turbulent fluctuations on the development of the coherent perturbations. A stability analysis taking into account the Reynolds stresses modelled by eddy-viscosity models, is performed to predict accurately the frequency of the hub vortex instability observed experimentally. [12]

Bottasso et al. expanded the classical scope of wind tunnel models by enabling applications ranging from aerodynamics to aeroelasticity and control. Focus is laid on the optimization of the open-loop pitch profile used during emergency shutdowns, the control in wake interference conditions of two models, and active load alleviation by higher harmonic individual blade pitch control. [13]

Howard et al. worked with complex inflow conditions and the effects on downwind turbines

of complex terrain and multi-turbine arrangements [14], objective for which the G06 turbine has been designed.

The effect of pitch and yaw on a wind tunnel scale has also been investigated in for instance Yang et al. [15], while Schreiber et al. studied the calibration and validation of a scaled modelled for wind farm experiments. The FLORIS approach is adapted and wake measurements are obtained for the calibrations of the wind farm setup [16]. Yaw effect on the wake deflection has also been studied by Schottler et al., finding that the wake deflections three rotor diameters downstream are equal while at six rotor diameters downstream insignificant differences are observed. [17]

Campagnolo et al. highlight the importance of using a robust formulation and plant flow models of appropriate fidelity and the existence of possible margins for improvement by the use of dynamic controllers. A set of wind tunnel experiments is performed, where three scaled wind turbines are exposed to turbulent inflow and dynamically changing wind directions. [18]

Bastankhah and Porté-Agel studied also interaction of scaled turbines with a turbulent boundary layer. The role of miniature models is highlighted for example in their study with the WiRE-01 model in [19]. The following section will cover in more detail state of the art regarding small scale wind turbines.

1.3   Yaw mechanism design in wind turbines

1.3.1   State of the art

Even though there is an extensive list of experimental work regarding experiments with scaled with turbine models, as showed in the previous subsection, the vast majority of them focus only on the results of the experiments. However, the wind turbine models are typically only superficially described. The goal of Nanos' work was to contribute to the literature with a more detailed description of the methodology behind the design of scaled models and provide some assessment of their characteristics.

Bottasso and Campagnolo are one of the authors in the literature who describe a wind turbine model with more detail, concretely speaking the G2 machine, a 2m diameter rotor machine, which was mainly operating in the Politecnico di Milano Wind Tunnel because of its extensive test section of 3.84x13.84 m and 36 m length. They later developed a smaller model (1.1 m diameter rotor) but still big enough to dispose of closed-loop individual pitch, torque and yaw control: the G1 model.

Nanos' challenge was to reduce further the scale while not losing as much instrumentation and wake behaviour as possible. Inspired by the G1, he designed the G06 model, which no longer has a closed-loop individual pitch but a collective one and a yaw system prototype was designed by Ruiz in [20]. In Nanos' publication [2] not only are the wake and aerodynamic performance of the G06 model characterised with wind tunnel campaigns but also the design methodology of the rotor, actuators and sensors are described in detail.

Other models described in the literature have a similar size to the one of the G1 but do not cover the design procedure in detail and, specifically, the design of the yaw system. The development of a scaled model with a rotor diameter of 0.58 m is presented in Schottler et al. [21], who used a blade element momentum (BEM) formulation to design the rotor and implemented closed-loop active pitch and torque control. BEM is also used in Lanfazame et al. [22] to evaluate the effects caused on miniature wind turbine blades by the low chord-based Reynolds flow conditions (Winslow et al. [23]). The authors designed, manufactured, and tested two rotors, one 0.45 m and one 0.225 m in diameter.

Bastankhah and Porté-Agel [19] published a study featuring one of the smallest instrumented models available on the literature, a 0.15 m rotor diameters with fixed pitch. The model blades employ a cambered plate because of the low chord-based Reynolds, resulting in a maximum power coefficient of 0.4 for a reasonably low tip speed ratio (TSR) equal to 4, which probably limits the realism of the wake immediately downstream of the rotor disk when compared to current full-scale designs.

Keeping in mind that small size wind turbines started becoming popular among the research community because of the capability of carrying out wind farm optimisation experiments in wind tunnels, where yaw is on the essential control variables, it is clear that a yaw system is needed for the G06 model. Yaw mechanisms have not been implemented in any of the mentioned small size models. Therefore this thesis will focus on documenting the whole design process of a yaw system for a small scale wind turbine, finishing the work done by Nanos in [2], and developing also further the preliminary design of Ruiz [20].

1.3.2 Objective of the project

The thesis's objective is to assemble one of the existing designed G06 models at the TUM Wind Energy department and implement a suitable yaw mechanism. Although the model's design was finished by E.M Nanos and the parts were manufactured, the model had never before been assembled. Therefore the first part of the thesis consists mainly of lab work and documentation for the future assembly of the other turbines. For the second part (the yaw mechanism design), the objective was to propose different solutions and compare them to find the best specifications-price ratio. The best solution will undergo a detailed designed phase.

Even if for the assembly part there is no innovation going beyond state of the art, the difficulty is primarily continuing the work of someone else and learn the different skills needed for the proper operation of the turbine: lab work, wiring maps, calibration, finding solutions, designing pieces, wind tunnel testing and an ordered and efficient way of working. Many doubts and assembling problems arise when doing it for the first time; solving and writing them now will be very useful for assembling all future turbines. The yaw mechanism design and implementation of such a small turbine is intrinsically state of the art because there are few publications of wind turbine scaled models where the design of the yaw system is explained. The following paragraph summarises more deeply the problem:

Yaw systems for scale wind turbines do not follow any design method but are own hand-made systems designed by a given company or research centre to be able to perform in scalable conditions to the ones of the actual model, which they are replicating. The G06 is a very compact and powerful machine, which makes the design of a system more complex. For space reasons, it is almost impossible to scale down the system designed for bigger machines (G1, G2) in the TUM Wind Energy department, which is located in the tower.

For this reason, it was necessary to at least come up with new solutions, which can provide the exact specifications (mainly yaw rate and positioning accuracy) and enough torque to counter the yaw moment in both static and dynamic situations. Ruiz [20] had already come up with a solution in her thesis, which could, in principle, meet these specifications. This idea (named as "Handmade rotatory stage") was further developed and redesigned with detail in Inventor to prove its viability and price.

Even though this proposal is a good starting point, it is far from being a final design which can be implemented. That is why, other designs were proposed and compared in price and viability with it. The brainstorming for the new designs can be summarised in three big groups: the purchase and implementation of an actual high accuracy rotatory stage, the adaptation of a

similar system to the one in the G1 machine and lastly the use of a right angle gearbox.

The research question that this work pretends to answer is, whether it is possible to scale further down a yaw system for a turbine with a 0.6 m diameter, while being still robust, fast and able to provide the same specifications as for bigger models. Besides, another question to be answered is, whether it is possible to implement such a system without distorting the scale of the model or inducing non desired effects on the wake, which would make the yaw measurements not valid.

1.3.3   Steady yaw aerodynamics

To extract the maximum wind power, the rotor axis of the wind turbine must be aligned with the wind direction. Misalignment, also known as yaw error, has three main consequences over the wind turbine. The first one is the reduction of the extracted power according to the cubic power of the yaw angle cosine (since power depends on the third power of the wind velocity). The second one is a cyclic disturbance of the angles of attack of the airfoils, caused by the crosswind, and the third one is the fatigue damage caused by vibrations induced by the excitation of low damped edgewise modes. [24]

In actual operating conditions, the wind turbine's rotor axis is often not aligned with the principal wind component since the wind is continuously changing direction. The control system cannot track these rapid, small changes, and the rotor spends most of the time in a yawed condition (even if it is small). Not only is this situation less efficient than the ideal non-yawed rotor (and should be taken into account for energy production calculations), but the continuous change in the angle of attack on each blade causes fluctuating loads and, therefore, fatigue damage. Besides, the angle of attack variation means that the blade forces cause a thrust in the axial direction and moments about the yaw (z) axis and the tilt axis. [25]

Nevertheless, yaw systems are a powerful control variable for three main purposes. One is to regulate power over rated wind speeds by reducing the rotor swept area (which is not common but has been proved to be feasible [26]). The second one is to increase the overall energy production of a wind farm by deflecting the wake and getting better energy yield in downstream turbines. This purpose is the principal motivation for wind tunnel testing with yaw mechanisms, which can replicate the behaviour of real machines. The last role of the yaw system is to prevent the twisting of cables between the nacelle and the tower.

The interest in predicting yaw behaviour lies primarily in improving the lifetime of the turbine, reducing fatigue damage and maximizing the total energy output of a wind farm. The most general theories are: the momentum theory applied for a turbine rotor in steady yaw, Glauert's momentum theory, the vortex cylinder model of the yawed actuator disc (Coleman) and the Øye simplification of Coleman's theory [25].While the first theories propose complicate models including wake expansion phenomena and can only be solved numerically, there exist some simplified models which can give an estimate of the actual yaw behaviour. The final equations of the mentioned theories will be shortly commented, and emphasis on Øye's equation will be given; thus, a good approximation of the yaw moment for the G06 can be obtained.

On the one hand, the theories mentioned above are typically used rather for simulations to increase the working life of big machines than in the design of scald models for wind tunnel purposes. The resulting differential equations are complex, and obtaining actual velocity data for field studies is almost impossible. The reason is that even for uniform induced velocity over the rotor disc (when it is aligned with a steady wind), once the rotor is misaligned, the induced velocity varies both azimuthally and radially, which makes its determination much more difficult. In wind tunnels, these effects are not seen as the wind is, unless specific experiments, coming

invariably from the same direction. [27]

On the other hand, the research and understanding of these theories are essential to developing a solution for the G06 yaw system. The state of the art of yaw mechanism design for small scale wind turbines is unknown since each company or research centre have their designs, whose purpose is basically to replicate as realistic as possible the behaviour of the real yaw system in a sub-scale manner and with the correct scale factor according to the dimensional analysis key theorem, the Buckingham π theorem, which has also been applied to several wind tunnel tests [28]. It is pivotal to remark that the design of the system will be a new concept as it will highly possible have to be placed on the base of the tower and not on the inside (like in other scale machines) or the nacelle (like in real wind turbines) because of space restrictions.

The equations of the models used to predict these effects will now be derived shortly. Even if it was necessary, needed data for the resolution of these equations is not handy and would have to be performed before in a wind tunnel study. Therefore they will not be used to dimension the yaw system of the G06, but the Øye simplification can give an approximate value of what average yaw moment to expect.

Yaw dynamics can be approached from the momentum theory taking into account the yaw angle. Even though it is a simple analysis, it is not the most accurate one. For the yawed rotor, the application of the momentum theory is in many cases not accurate since it is only capable of determining an average induced velocity for the whole rotor disc. Since the blade circulation changes with azimuth position, it is not appropriate to apply it in the yawed situation.

Looking at Figure 1.5 and applying Bernoulli's equation to both the upwind and downwind regions of the flow, the thrust (C_T) and power (C_P) coefficients (Equation 1.2 and Equation 1.3) depending on the yaw angle γ can be derived. This is only possible by assuming that the rate of change of momentum in the axial direction is equal to the mass flow rate through the rotor disc times the change in velocity normal to the rotor plane.
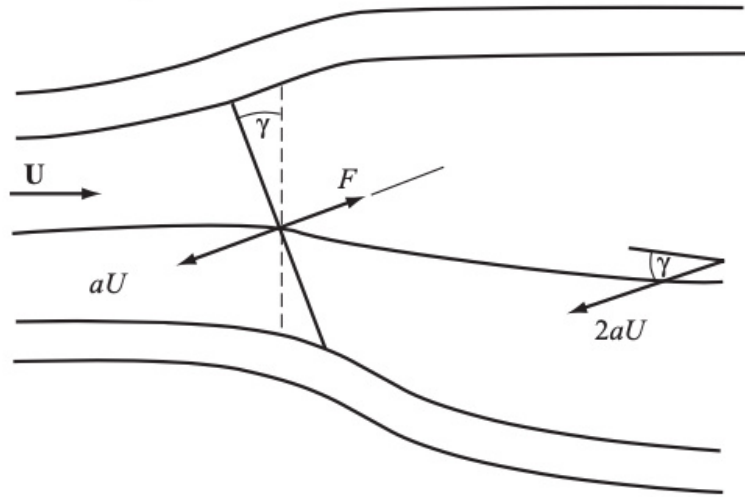
Figure 1.5: Yaw wake [25]

$$F = \rho A_d U_\infty (cos\gamma - a)2aU_\infty \qquad (1.1)$$

$$C_T = 4acos(\gamma - a) \qquad (1.2)$$

$$C_P = 4acos(\gamma - a)^2 \qquad (1.3)$$

Finding the maximum value with respect to a the Equation 1.4 and the distribution of Figure 1.6 are obtained. This equation, which depends on the cubic power of the yaw angle, is commonly adopted for power assessment in yawed flow as a simplification, but mainly due to the following reason, it is far from an optimal approach. Transverse pressure gradients which cause the wake to skew sideways contribute to the net force on the flow in the axial direction, influencing the axial induced velocity. Therefore, it is impossible to determine the induced velocity at each blade element position, implying non-satisfactory accuracy. The satisfactory calculation of blade forces is as essential as the estimation of power.

$$C_{Pmax} = \frac{16}{27}(cos\gamma)^3 \tag{1.4}$$
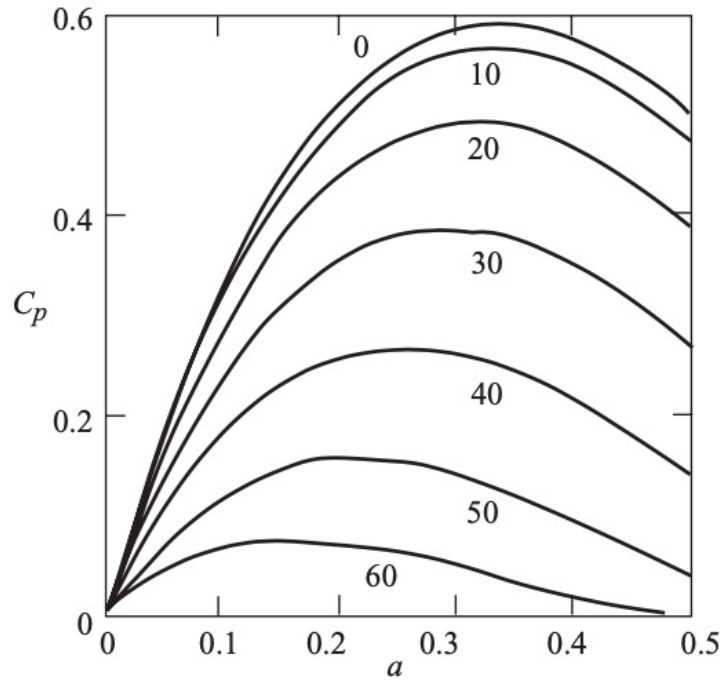
Figure 1.6: Power Coefficient Variation with Yaw Angle and Axial Flow Factor [25]

Glauert was primarily interested in the autogyro, an aircraft with a rotor to provide lift and a conventional propeller to provide forward thrust. The lifting rotor has a rotational axis that inclines backwards from the vertical, and by virtue of the aircraft's forward speed, air flows through the rotor disc, causing it to rotate and provide an upward thrust. Thus, the autogyro rotor is just like a wind turbine rotor in yaw when forwarding flight. The yaw angle is large at high forward speeds, but the yaw angle is zero in a power-off vertical descent. It gave rise to a more accurate definition of the average induced velocity. [25]

The definition of the average induced velocity (Equation 1.5) can be obtained by looking at the autogyro velocity triangle (see Figure 1.7). L stands for the lift and V for the forward speed of the aircraft.

$$u = \frac{2L}{\pi(2R)^2\rho V} \tag{1.5}$$

The final expression for the induced velocity is shown in Equation 1.6, where the value of K must depend upon the yaw angle and R is the radius of the rotor disc. To derive these equations, first some derivations are made from the properties of the velocity triangle, and then the following
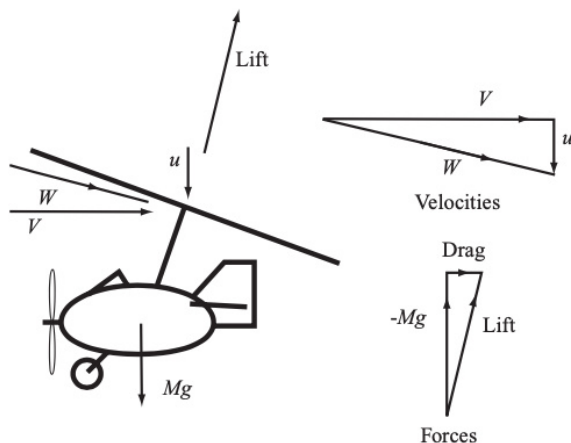
Figure 1.7: Autogyro velocity triangle [25]

assumptions are made. It is considered that the rate of change of downward momentum is equal to the lift, and it is taken into account that the rate of work done by the drag must be equal to the rate at which kinetic energy is created in the wake since the ambient static pressure in the wake of the aircraft is the same as the pressure ahead of the aircraft.

$$u(r, \psi) = u_0(1 + K\frac{r}{R}sin(\psi)) \tag{1.6}$$

where ψ is the blade azimuth angle measured in the direction of rotation, 0° being when the blade is normal to the flight direction (or when the wind turbine blade is vertically upwards), and u_0 is the amplitude of the non-uniform component which is dependent on the yaw angle.

One instrumental concept that emerges from Glauert's autogyro theory is that he predicted that the induced velocity through the rotor would not be uniform. The flow through the yawed rotor is depicted in Figure 1.8, and a simplification of the contributions to the velocity normal to the plane of the rotor along the rotor diameter parallel to the flight direction is shown. [25]
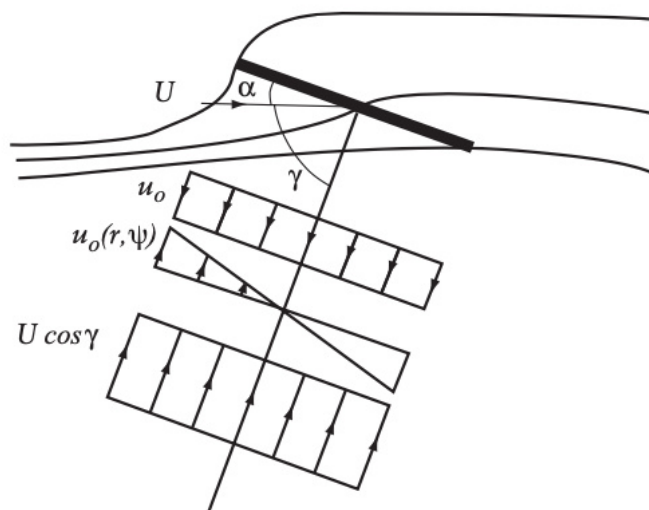
Figure 1.8: Velocities normal to the yaw rotor [25]

The vortex theory or Coleman approach has demonstrated that it is equivalent to the momentum theory and gives much more detail about the flow field. The wake of a yawed rotor

is skewed to one side because the thrust force (F) on the disc is normal to the disc plane, and so has a component normal to the flow direction. Therefore, the force on the flow is in the opposite sense to F, causing the flow to accelerate both upwind and sideways. The centre line of the wake will be at an angle χ to the axis of rotation (axis normal to the disc plane) known as the wake skew angle. [25]

The analysis was first performed by Coleman to understand helicopter rotors but can be applied to wind turbines reversing the signs of the circulation and induced velocities. The induced velocity component parallel to the skewed axis of the wake is uniform over the disc with a value aU_∞, as can be deduced from Figure 1.5.

The expansion of the wake imposes a complex analysis, as shown in Figure 1.9. In addition to the uniform induced velocities of Figure 1.5, the expansion of the flow gives rise to velocities in the y and z directions, respectively (directions in a vertical plane at the skew angle χ to the rotor plane, Figure 1.9).
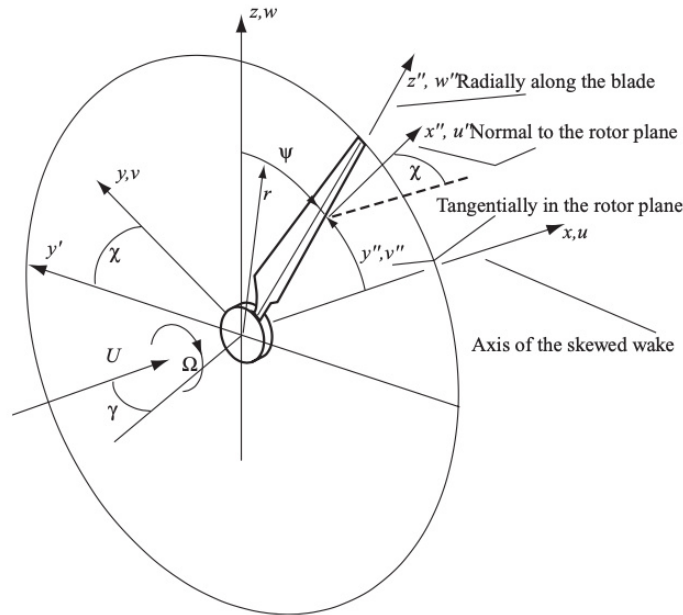
Figure 1.9: Yaw rotor wake without wake expansion [25]

Coleman et al. obtained an analytical solution for the flow expansion velocity in the y direction that involves complete elliptic integrals; the solution is not very practicable because numerical evaluation requires calculating the difference between two large numbers. [29]

Simplification of the analytical solution leads to Equation 1.7 for the horizontal flow expansion velocity which removes that difficulty but it is not in closed form. However, it can only be solved numerically.

$$\nu(\chi,\mu) = \frac{-2\mu sin\theta aU_\infty}{\pi} \int_0^{\frac{\pi}{2}} \frac{sin^2 2\epsilon}{\sqrt{(1+\mu)^2 - 4\mu sin^2\epsilon}} \frac{1}{[(\mu + cos2\epsilon)^2]cos^2\chi + sin^2 2\epsilon} \, d\epsilon \qquad (1.7)$$

where $\mu = r/R$, ϵ is a parameter arising from the elliptic integrals, which is eliminated from the function by the definite integral, and aU_∞ is the average induced velocity. An important feature of Equation 1.7 is that the flow expansion velocity is proportional to the average axial flow induction factor.

1.3.4 Simplified theories

Several refinements to the Glauert and Coleman theories have been proposed by other researchers, mainly addressing helicopter aerodynamics, but some have been explicitly directed at wind turbines. In particular, Øye undertook the same analysis as Coleman and proposed a simple curve-fit to Equation 1.7, obtaining Equation 1.8. Øye equation is not accurate at the outer edge of the flow expansion region but gives a fair average estimate. [25]

$$F_\phi(\mu) = \frac{1}{2}(\mu + 0.4\mu^3 + 0.4\mu^5) \tag{1.8}$$

To estimate the yaw moment in Chapter 3, the results of the measurements of a wind turbine at Delft University of Technology were used by comparing some parameters. The tests were carried out using a small wind tunnel model so that steady yaw could be maintained in a steady wind with no tower shadow and no wind shear. The setup of the experiment is the following: [30]

- Two bladed rotor of 0.5 m diameter with a uniform chord length of 80 mm.

- The blade root was at a radius of 180 mm, and the blade twist was 98° at the root, varying linearly with radius to 48° at 540 mm radius and remaining at 48° from there to the tip.

- The blade aerofoil profile was NACA0012.

- The rotor speed was kept constant at 720 rpm, and the wind speed was constant at 6 m/s. Tests were carried out at 108°, 208° and 308° of yaw angle.

The results used for the calculations can be seen in Figure 1.10a. Even though the Delft turbine model is different to the G06, by doing a dimensional comparison of the differences, the order of magnitude of the aerodynamic yaw moment of the G06 can be estimated.

(a) Measured Yaw Moment   (b) Averaged induced velocity factors
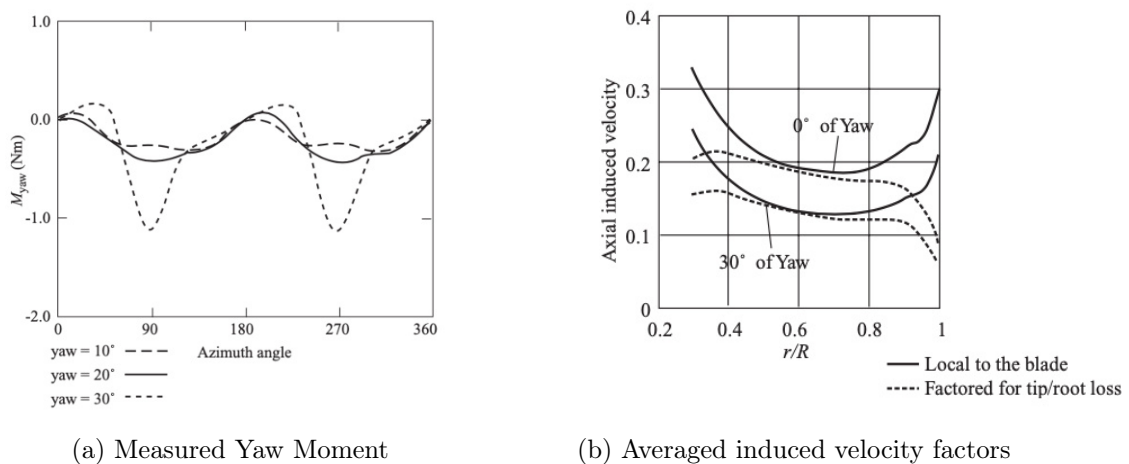
Figure 1.10: Measurements on the Delft Turbine, (Snel and Schepers, 1995) [30]

The G06 model

The following section will describe the current state of the last version developed of the G06, summarising the work done by Nanos in "Design, performance and wake characterization of a scaled wind turbine with closed-loop controls". The G06, in a nutshell, is a model intended to be used in complex terrain studies and deep array wind farm control tests. All the information of this Chapter has been taken from Nanos' publications: [1], [2] and [3].

Being compact and keeping a high level of instrumentation are opposite sides of the same coin and equilibrium had to be found. The output of the design is a three-bladed wind turbine with a rotor diameter of 0.6 m equipped with active pitch and torque control. In its design, it was possible to change the yaw angle with a base attached to the wind tunnel manually, but no active yaw system was designed. Table 2.1 summarises the main turbine parameters. The yaw mechanism design and implementation will be covered in the following chapters.

Table 2.1: G06 characteristics

Number of Blades	3
Rotation	Clockwise
Rotor diameter	600 mm
Hub Diameter	55 mm
Hub height	640 mm
Airfoil profile	RG-14
Rated power	65W
Active pitch control	Yes (collective)
Active torque control	Yes
Active yaw control	In progress
Sensor	Torque, shaft and tower loads

2.1 General description

Figure 2.1 shows the model prototype with active collective pitch already installed. This prototype was the last improvement left by E.M.Nanos. Two models without active pitch were running in two different wind tunnels.

The model features a 0.6 m three-bladed clockwise rotating rotor with a hub height of 0.64 m. It is equipped with load sensors on the shaft and at the tower base. Collective pitch control is

performed by an actuator and bevel gear system integrated into the hub, while yaw control was at this point possible only by turning manually over a second base. Two ball bearings support the shaft in the nacelle, which carries a slip ring to serve the pitch actuator and shaft load sensors; an optical encoder placed immediately behind the slip ring provides the rotor azimuthal position. A high accuracy torque-meter is placed behind the aft shaft bearing, while the torque actuator is placed at the very end of the drive train. More details on the various model sub-systems are given in the following sections.
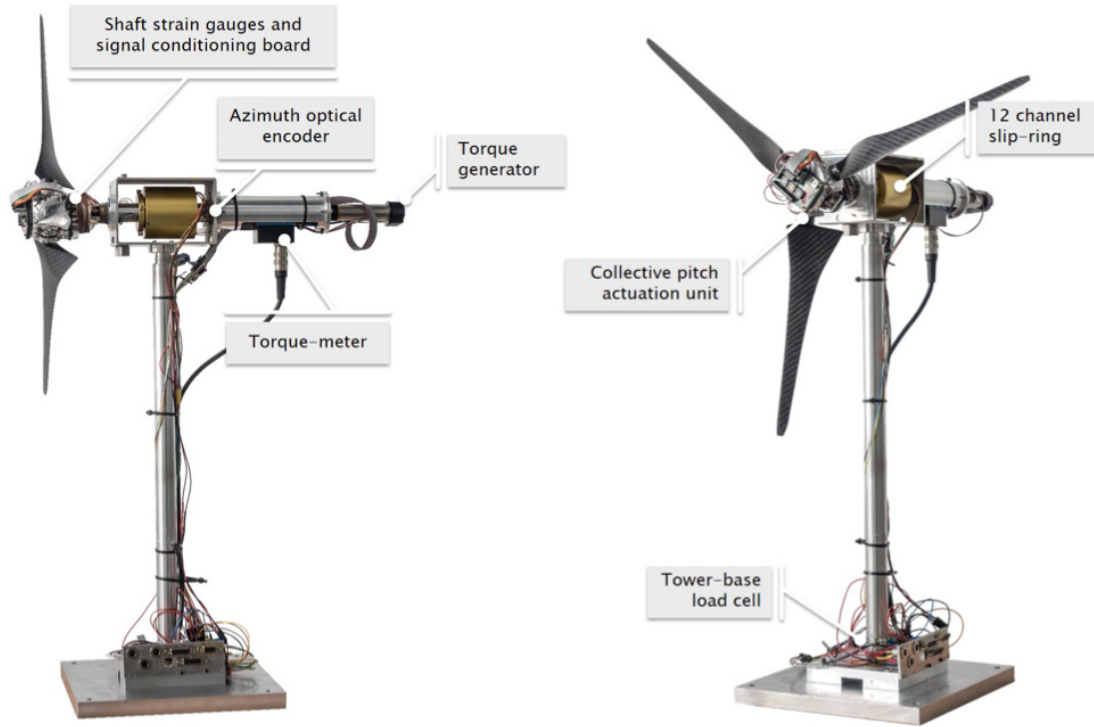
Figure 2.1: G06 prototype side and front view [2]

2.2   Actuators

2.2.1   Pitch mechanism

Given the relatively small size of the G06, an individual pitch control system would increase costs and complexity. Considering also its typical use cases, a collective pitch control system was chosen for this model. The pitch mechanism is realized through a bevel gear system, featuring a crown and three pinions as shown in Figure 2.2. The crown is connected through a flexible coupling with a Maxon gearhead, and each pinion is connected with its respective blade. The gearhead has an 84:1 ratio, and a Maxon 30 W DC motor drives it.

According to the manufacturer, a 1.3° backlash is to be expected for the gearhead. Given that the bevel gear ratio is 27:15, this gearhead backlash translates into a 2° play at the blade pitch angle, which is unacceptable. To eliminate this backlash, each blade is attached to a torsional spring. The spring constant and its position ensure that it is always under tension within the pitch angle operational range. The applied torque is always higher than the aerodynamic pitching moment on the blade. Consequently, the loading direction on the gearhead is always the same, resulting in a solution that presents no backlash of the blade pitch motion. [2]

The pitch motor is controlled through a two-channel encoder, thus only relative angular displacements are possible. The absolute pitch rotation of the blade is obtained by Hall sensors. There is a groove at each of the threaded blocks, whose function is to prevent the bearings of the blade shafts from falling, where the Hall sensors are placed. The magnets are glued to a hole on the bottom part of the blade bevel gears.

To verify the suitability of the actuator, the pitch actuation system dynamics were modelled in Simulink. The maximum continuous pitch rate is 550°/s. Considering that the time scale factor between the G06 and the full-scale reference is nt =1/240, this corresponds to a full-scale pitch rate of approximately 2.3°/s. This value is smaller than the typical maximum operational pitch rate of full-scale turbines, which is approximately in the range of 6 to 9°/s. Aeroelastic simulations of the DTU 10 MW turbine were conducted in the full-load regime (region III) with a turbulence intensity of 10% . The analysis of these simulations indicates that the pitch actuation exceeds 2.3°/s for only 5% of the time. Based on these results, the speed of the pitch actuator was deemed acceptable. [2] One new hub with the pitch mechanism was assembled for the thesis, and its assembly will be covered in Chapter 4.
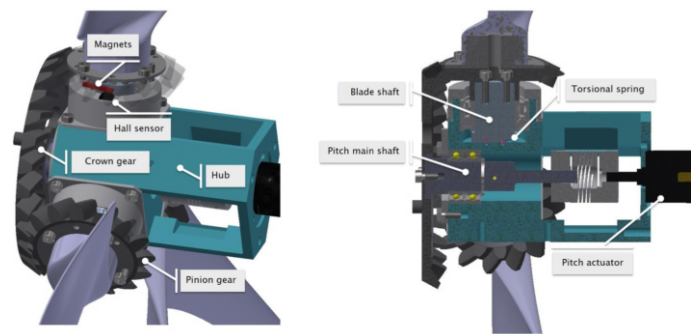
Figure 2.2: Hub section including pitch actuator system [2]

2.2.2   Torque mechanism

The torque actuator provides either torque or a speed operation mode, depending on the application. In torque mode, the actuator plays the exact role of the generator in a real wind turbine, whereas in speed mode, it provides the torque that is necessary to spin the rotor at a desired angular velocity. The actuator is a Maxon DC 120 W motor, equipped with a gearhead with a 4.4:1 gear ratio, produced by the same manufacturer. The motor is controlled through an analog Maxon ESCON Module 50/5 controller, allowing the user to select between the two modes (torque or speed) of operation. [2]

When the motor works as a generator, current flows from the motor to the controller and from there to the power supply. The motor controller is connected in parallel with an 8 Ohm resistor capable of dissipating up to 100 W of power to dissipate this flow of current.

There are no big difference in this mechanism between the prototype and the final version of the G06, but a change in the control board to be used. The machines running in the wind tunnels were using a small compact ESCON50/5-438725 to save some space. This board is more compact, but the connections are more complex and difficult to understand, which can lead to connection errors. Given that the yaw mechanism will anyway need more space, it was decided that the board being used in the G1 and G2 (ESCON50/5-409510) will also be used for the G06. This change also helps to achieve the goal of unifying all the cables of the different machines and Bachmann connections as much as possible.

2.2.3   Yaw mechanism

The yaw mechanism was intended to be a separate turning base on which the G06 is mounted and controlled through the same control hardware and software as the other models of the TUM family of scaled wind turbines, but the control was never implemented. According to Nanos, the small size of the G06 model, integrating the yaw mechanism into the tower —as done for the G1 and G2 turbines— would increase the tower diameter. An excessively out-of-scale tower creates a wider wake and has a mismatched vortex shedding, affecting the turbine wake.

The design of a yaw system was never finished, but a conclusion could be drawn: it is preferable to design some turning table or similar system, which is capable of moving the tower from the bottom without distorting the model scale.

2.3   Sensors

The G06 shaft is equipped with three full strain gauge bridges. Two of them are sensitive to shaft bending loads, and one is sensitive to torsional loading. The bending loads can be used to balance the rotor and detect shear inflow on the rotor disk. The torsion loads, which are caused by the aerodynamic torque, are used for the evaluation of the rotor performance. Each bridge is connected to a conditioning board mounted on the hub. A slip ring transfers signals and power to/from the conditioning boards to the control unit. In addition to the strain gauges, a high precision commercial torque-meter is placed between the main shaft and the generator. [2]

Two additional full bridges are placed at the base of the tower. These bridges are sensitive to the bending loads on the tower. Based on the bending loads, one can calculate the rotor thrust using its corresponding arm value. Both shaft and tower bridges are calibrated before each experiment using known loads, measuring the voltage output and correlating loads and output with linear regression.

2.3.1   Force and torque sensors

The G06 is equipped with strain sensors to measure bending and torsional moments on its shaft. To this end, three full-strain gauge bridges are located immediately in front of the first bearing (Figure 2.3a); two bridges are sensitive to shaft bending, whereas the third is sensitive to torsion. Bending information is used to assess the turbine's loading, optionally after transforming the rotating signals into a fixed frame of reference. Torsional loads are used for the evaluation of the rotor performance by measuring the aerodynamic torque. Each bridge is connected to an amplifying board mounted on the hub.

Signals and power to/from the conditioning boards are transferred to the control unit through a 12-channel slip ring. In addition to the strain gauges, a high-precision commercial torque-meter (Lorenz Messtechnik GmbH) is placed between the aft bearing and the generator. The torque-meter has a higher precision and sampling frequency than the strain gauges, but its readings are affected by the friction in the bearings and the slip ring. This friction, which depends on various factors and may change over time because of temperature and wear, can be estimated by the difference between the readings of the strain gauges and the torque-meter. [2]

Two additional full bridges are placed at the base of the tower to measure fore-aft and side-side bending (Figure 2.3b). The thrust generated by the rotor can be estimated from the former bending moment. The total fore-aft moment Mo measured by the strain gauges is the sum of the moments due to the rotor thrust (MT), the tower and nacelle drag (MD), and the nacelle weight (MG).
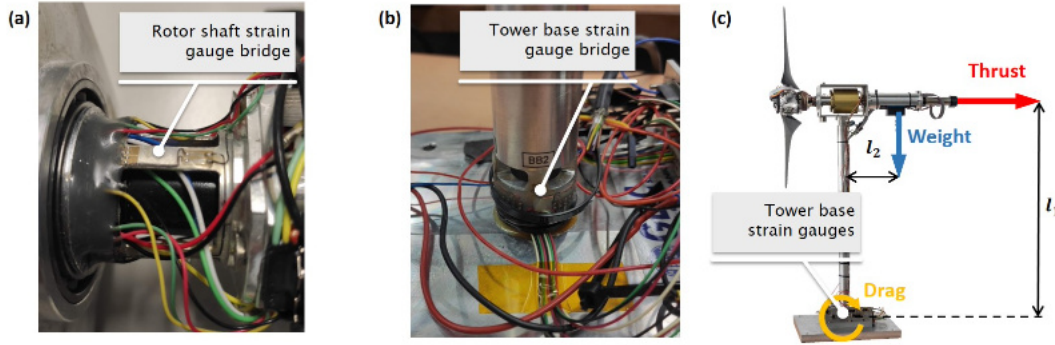
Figure 2.3: G06 load sensors [2]

MT is calculated as the thrust times its arm (l1), which is assumed to be applied at the rotor centre. The values of MD and MG are determined offline with reliable measurements. For calculating MD, the blades are removed, and the model is placed in the wind tunnel, where measurements at various wind speeds are taken. For calculating MG, a single measurement without wind is sufficient, which corresponds to the weight of the turbine applied at its center of gravity at a distance (l2) from the nacelle. The shaft and tower bridges are calibrated before each experiment using known loads, measuring the voltage and correlating loads and output via linear regression.

2.3.2 Positioning sensors

Two kinds of position sensors are used in the model: Hall sensors and rotary optical encoders. Both the torque and pitch motors have their own internal optical encoders, which the respective internal controllers use.

The pitch motor rotates the blades to a specific angular position but can only be commanded through a relative angular displacement. A Hall sensor obtains the absolute orientation of the blades. As shown in Figure 2.2, the Hall sensor is stationary and placed on the casing of the blade bearings, while magnets are placed on the bevel gear and rotate together with the blades. A calibration procedure determines the relationship between Hall sensor output and blade pitch angle. Using an adapter, an inclinometer is mounted on the blade. The blade is then rotated at several different pitch angles, and the readings of the Hall sensor output and the inclinometer are recorded. Before the model can be used, a "homing procedure" is performed where the blades are moved to a predefined known position, thereby providing the desired reference. [2]

A third optical encoder is placed on the main shaft to measure the rotor's rotating speed and its azimuth position, which is necessary for interpreting shaft loads and performing phase-locked flow measurements. Instead of using a Hall sensor, in this case, the calibration is performed manually by placing the rotor at a known azimuth position.

2.3.3 Measuring uncertainty

For the tower and shaft loads, given the sensitivity of the strain gauges and the expected strain within the operational regime, the uncertainty is estimated to be 1%. Similarly, the uncertainty of the torque measurement obtained from strain gauges is estimated to range between 2% and 3%, depending on the operating point. The manufacturer gives a value of 0.05% for the torque-meter and below 1% for the Hall sensor. Given the tiny dimensions of the collective pitch mechanism

assembly and all the uncertainties that this implies, a tolerance of $\pm0.3°$ can be estimated for the blade pitch angle. Uncertainties in the model's dimensions (blade length, tower height, etc.) and the measurement of the rotor angular velocity are considered negligible. [2]

2.4   Control

The G06 is equipped with active pitch and torque control. G06 has strain gauges on the shaft measuring the bending loads and aerodynamic torque from the sensor point of view. The latter can also be measured with a commercial torque-meter. Pitch angle is determined using Hall sensors, while the rotating speed of the rotor and its azimuth position can be measured employing an optical encoder. Finally, the bending moments on the tower are measured with strain gauges placed at the root of the tower. The rotating frame's power and signal transmissions are transferred to the stationary frame through a brushed slip ring.

The G06 is operated by a Bachmann M1 (Bachmann, 2020) programmable logic controller (PLC), which runs in real time the supervisory logic and the pitch-torque-yaw controllers.

Two analogue acquisition modules and one counter module are used to acquire the sensor readings (strain gauges, encoder) and the wind speed. All signals are gathered at a frequency of 250 Hz, except for the torque-meter and shaft bending moments sampled at 2.5 kHz. All sensor readings are provided as inputs to the supervisory controller, which is real-time executed by the M1-CPU unit with a clock time of 4 ms; the control pitch, torque and yaw demands are sent to the actuator control boards via an M1-CAN module or by analogue output. The real-time controller is organized into several applications written in the C programming language, each handling specialized tasks such as communicating with the actuators, recording data, or calculating actuator demands according to a control algorithm and the state of the machine (idle, power generation etc.). [2]

The objective is that the control hardware and software will be the same for all models of the TUM scaled wind turbine family. The G06 counts currently with a similar structure to the one of the G1, and the idea is to adapt it further, so only some parameters in the control software change slightly. Each model is uniquely identified by its ID, which allows the software to select the appropriate model-specific parameters, such as friction tables, controller gains etc. This unified framework simplifies software maintenance and development and shortens the preparation time for the experimental setup.

Yaw system design

The smaller the scale, the more difficult it is to develop solutions that can adequately replicate the mechanism driving an actual turbine. The compact size of the G06 is a challenge to develop a yaw system. First, the system implemented in the next bigger size model (G1) is difficult, if not impossible, to implement due to space restrictions in the G06. A similar solution would have been the most straightforward way since it would have just meant to acquire a smaller motor-gearhead-brake set and use a similar adapted control like in the G1 by changing the dictionary of the CAN in the PLC (Bachmann).

For this reason, it was necessary to come up with new solutions, which can provide the exact specifications (mainly yaw rate and positioning accuracy) as well as enough torque to counter the yaw moment in both static and dynamic situations. Ruiz [20] had already come up with a solution in her thesis, which could in principle meet these specifications. Her idea was further developed and redesigned with detail in 'Autodesk Inventor' to prove its viability and price. This design is referred to as a 'Handmade rotary stage' since its working principle resembles one of high accuracy rotary stages mainly used for positioning purposes in industry, CNC machines and 3D printers.

Implementing an actual high accuracy rotary stage was the second idea for the system. Different manufacturers were contacted in order to study the viability and price of this option. The conclusion was that these systems are far above our specifications and are used for many industrial accurate purposes. Therefore they are an expensive alternative, and the control systems they offer are not directly compatible with the Bachman PLC structure used for the TUM Wind Energy wind turbine models. Buying only the table without the control is not that expensive, but no easy way to implement them in this before mentioned structure was found.

This situation led to the investigate the viability of the handmade rotary stage. Nonetheless, by designing the pieces in detail and asking different opinions (in the Zentralwerkstatt of the Physics Department TU, and companies online) it was demonstrated that its manufacturing for minor units was not much cheaper than a high accuracy industrial rotary stage. Besides, both positioning accuracy and small backlash could not be ensured. In other words, it involved a high risk for the savings it could entail. Not only that, but any manufacturer was willing to fabricate a personalised customer tooth of the two gears needed for the design.

Variations of the G1 yaw system were also taken into account to have a price reference. However, they were quickly discarded because of the before mentioned space reasons and the structural limitations coming up when trying to make room for all the components. Both implementing the same system beneath the tower's base (what increases the height too much) and cutting the towers down to increase the diameters or reducing the tower thickness were considered.

The last proposal was to use a right angle gearbox, which is a compact and efficient way to perform a horizontal-vertical conversion of the motor's torque. The idea came from the fact

that the Handmade rotatory stage would be a good solution if the components performing this torque translation were more accurate. This mechanism appeared to be one of the preferred solutions for this kind of applications. It is a price/accuracy competitive solution, which also allows implementing the existing control system of the Maxon Motors in the lab since it is compatible with DC motors.

Regardless of the chosen system, a new geometry and distortion of the model scale, will be introduced. Therefore the influence on the wake must be checked on the wind tunnel, before purchasing all the components. The idea is to perform some wake measurements with a similar shape as the one to the system and with a 3D printed airfoil to see if it is possible to reduce the effect on the wake to negligible levels.

If a yaw system impacts the wake on a similar order of magnitude of the one produced the by yaw condition itself, the measurements are not valid. Thus this test is decisive to check the viability of the designed system. After the experiment, the system was ordered and assembled. In the following sections, all these solutions will be explained in detail, and their advantages and drawbacks will be compared.

3.1   Calculations

The design objectives are compared with the ones of G1 and summarized in Table 3.1. The specifications are very similar and even a higher torque could be demanded because the G06 has a higher wind nominal speed, and thus higher loads.

Table 3.1: Yaw system specifications

Parameter	G1	G06
Yaw rate (rpm)	2	2-4
Positioning accuracy (°)	0.2	0.1
Yaw Moment (Nm)	6	8
Safety Factor (-)	3	3
Rotor-yaw axis distance (m)	0.12	0.066

To calculate the needed yaw moment, two different approaches were followed. While the Equation 3.1 calculates the torque the motor set would have to provide to overcome the yaw moment, Equation 3.2 is a model a bit more complex (extracted from Ruiz calculations to design the handmade rotatory stage [20]) which consists in 5 terms: friction, aerodynamic forces, inertial momentum, imbalance and backlash.

$$M_{yaw} = Thrust_{max} * d_{rotor-yaw-axis} * SF \tag{3.1}$$

$$M_{G1} = 15\,N * 0.12\,m\ * 3 = 5.4\,Nm$$

$$M_{G06} = 10.46\,N * 0.066\,m\ * 3 = 2.08\,Nm$$

Looking at these results, it makes sense to design the G06 system to overcome at least a 2 Nm torque since the G1 was designed for 6 Nm. This can be confirmed by calculating the moment with the second approach too.

$$M_{yaw} = M_f + M_w + M_p + M_i + M_{backlash} \tag{3.2}$$

As commented in the introduction chapter, resolving the equations to calculate the aerodynamic moment (M_w) is quite challenging, but Ruiz already made an approximation with the following approach. The aerodynamic yaw moment is produced because of the blades not having the same angle of attack, so there is a part in the rotor with higher angle of attack, which creates a restoring moment trying to align the rotor back with the wind. Equation 3.3 is obtained from Øye´s simplification equation, considering besides that the normal coefficient (C_n) is constant along the blade, making the integration much simpler.

$$M_z = \frac{1}{2}\rho V_{rel}^2 c C_n sin(\psi)\frac{R^2}{2} \tag{3.3}$$

where ρ is the air density, V_{rel} the rated wind speed of the turbine, and c the chord of the blade. The total yawing moment is the sum of the one of each of the three blades, which is evaluated at the azimuth position ($\psi = \pi/2$). If it is considered that blades two and three have a similar angle of attack as blade one, and thus equal normal coefficient, the yaw moment can be expressed as in Equation 3.4.

$$M_w = F_{n,1}sin(\frac{\pi}{2}) + F_{n,2}sin(\frac{7\pi}{6}) + F_{n,3}sin(\frac{11\pi}{6}) = F_{n,1} - 0.5F_{n,2} - 0.5F_{n,3} = \Delta F_n \frac{R}{2} \tag{3.4}$$

This equation, combined with the information from the Delft study (see Figure 1.10a) and the definition of the thrust variance (Equation 3.5), can give an estimate of the aerodynamic yaw moment shown in Equation 3.6 by performing a dimensional conversion. Looking at the $C_{l-\alpha}$ curves it is observed that $C_{l,G06} = C_{l,Delft}$ and that the moment is equal to 1 Nm.

$$\Delta F_n = \frac{1}{2}\rho V^2 c R \Delta C_n \tag{3.5}$$

$$M_{w,G06} = M_{w,Delft} \frac{V_{G06}^2}{V_{Delft}^2} \frac{R_{G06}^2}{R_{Delft}^2} \frac{c_{G06}}{c_{Delft}} \frac{C_{n,G06}}{C_{n,Delft}} \tag{3.6}$$

$M_{w,G06} = \frac{10^2}{6^2}\frac{0.3^2}{0.6^2}\frac{0.02}{0.08} = 0.17\,Nm$

This result shows that the aerodynamic moment is in a lower order of magnitude than the one of imbalance for example, which is around 2 Nm, meaning that even if the approach for calculating the exact aerodynamic yaw moment is not the best, it is not that relevant since its contribution to the total moment is negligible.

The imbalance moment can be calculated as the centrifugal force times the distance from the rotor to the tower (0.066m). Taking into account the nominal rotational speed of 2700 rpm and supposing a 10g mass imbalance at a position r= 40mm between the hub and the blade, the result of Equation 3.7 is obtained.

$$M_i = F_c d = M_R \omega^2 r d \tag{3.7}$$

$M_i = 0.01 * (\frac{2700\pi}{30})^2 * 0.04 * 0.066 = 2.11\,Nm$

The sum of this two moments is very similar to the total one obtained with the first approach. Nonetheless, the backlash term has not been taken into account. While the friction and inertia terms are included in the safety factor, it is difficult to calculate the right moment needed for backlash. Typically good practice is to set a spring or mechanism which exerts twice the total torque in the opposite direction to prevent backlash. Given that assumption, the final design torque would be at least 6 Nm, like in the G1. Depending on the proposed design and the backlash of the mechanism, this torque design was set between 6 to 8 Nm.

3.2   Possible solutions

3.2.1   Rotatory stage

A market study of different positioning companies products was carried out. A rotatory stage solution was initially a good idea because of its compact size and accuracy, despite being the most expensive possibility since they are high precision devices.

The first problem was that it was the lack of the market's available information. It was impossible to get the specifications of the products without investing some time talking with companies. All the companies are very reserved with their technology and prices, which are not available in catalogues, but only after a meeting with the customer an offer is made. Three different German companies were contacted: "Aerotech", "Busch", and "Föhrenbach". The price of the lowest gamma (worst accuracy) product was only for the table around 3000 €, extra costs are the stepper motor, wires and the control system, which can be even more expensive than the table itself. The main parameters of the three offers are summarised in Table 3.2, and the offers are available in the Annex.

Table 3.2: Rotatory Stages offers

Parameter	Aerotech	Föhrenbach	Busch
Yaw rate (rpm)	2-10	2-10	2-100
Positioning accuracy (°)	0.05	0.05	0.04
Yaw Moment (Nm)	3.5	5.6	32
Price (€)	7247	9302.23	9366.49

"Aerotech" recommended to use their model AGR75, according to the data sheet it has a 180 arcsec positioning accuracy, a maximal rotational speed of 60°/s (10 rpm) and maximal acceleration of $720°/s^2$. The maximum torque is 3.5 Nm, which could suffice the next model can provide 12 Nm with the rest of the parameters being the same. They specify on their website that the table need to use an "Aerotech" controller. The specification from the "Busch" product were very similar, but the smaller table on their catalogue can provide 32 Nm and it is a bit more expensive. This option was discarded.

A further issue of these manufacturers (and many others in the market) is that their product has already implemented their own control system and cannot be programmed by the customer since they are not compatible with external hardware. Only the third company ("Föhrenbach") offered to sell the table without the motor and the control system, replace it with a stepper motor from another company, and implement our control, which is principle would be compatible with our CAN bus.

That could be an easy to implement solution if the rotatory stage did only not with stepper motors. These motors use different control boards, so the ones currently used by "Maxon Motors" do not work because Maxon does not have any stepper motor in their catalogue. That means that the Bachmann code and the CAN would have to be reprogrammed from scratch to use this new control. "Föhrenbach" recommended the company "Nanotech" for the external stepper motor and its control. The final price was 2,564.45 € from "Föhrenbach" plus 394.9 € from the "Nanotech" stepper motor and control board (see Table 3.3), adding up to a total amount of 2959.35 €. Figure 3.1a shows how the proposal would look like. A coupling plate between the rotatory stage and the tower would have to be designed, by the company or handmade and was estimated to cost between 100-200 €, with the plate the final height would be around 6 cm.

Table 3.3: "Nanotech" Stepper motor budget

Component	Description	Price (€)	Quantity
C5-E-1-09	Motor controller board	221,70	1
Z-K4700/50	Kondensator	4.3	1
Z-K-PADP-12-500-S	Encoder cable	9.2	1
NTS-120W-24V-5A	Switch mode power supply	50.1	1
NEMA 23 AS5918S2804	Stepper motor	100.90	1
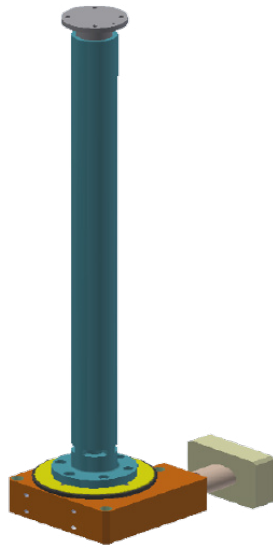
(a) Model perspective
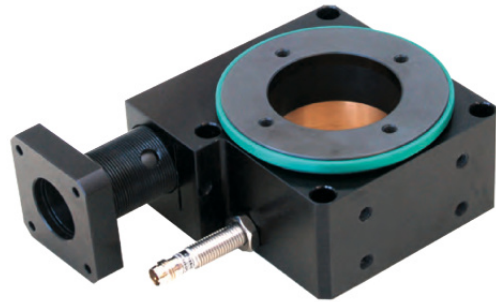
(b) Föhrenbach RT2A075

(c) Stepper motor control: C5-E-1-09

Figure 3.1: Rotatory stage best proposal

The most relevant parameters of the model are extracted from the data sheet (which is available in Annex 7) and summarized in Table 3.4. With the gear ratio (i=25), the efficiency of the system (0.3) and the maximal torque at the shaft (0.75 Nm), a maximal output torque to the plate of 5.6 Nm is obtained. As in all the other rotatory stages evaluated the maximal loads that can be applied to the plate are quite higher than the ones the G06 would transmit at is nominal working point. Small backslash is also observed, being the 5.6 Nm enough to counter the aerodynamic torque if no anti-backslash system (like springs) has to be implemented. However,

the maximal frictional torque of 8 Ncm seems to be small and maybe a braking system would have to be implemented.

Table 3.4: RT2A075 technical data

Parameter	Units	Value
Ratio worm gear drive	-	i=25:1
Max.no-load moment	Ncm	8
Torque tranmission efficiency	-	0.3
Max torque at the shaft	min^{-1}	0.75
Positioning accuracy mechanical	°	0.05
Reversing backlash	°	0.035
Parallelism	μm	15
Wobble error	arcsec	6
Weight without motor	Kg	1.2
Protection class	-	IP50
Allowable axial load on the plate	N	440
Allowable radial load on the plate	N	80
Allowable tilting moment	Nm	18

Even though the "Föhrenbach" proposal with a external motor seems to be viable, the idea of having to implement a totally new code just for the G06 yaw system because of the new board was the main drawback. Furthermore extra costs must be considered, for assembling the motor of "Nanotech" on the "Föhrenbach" table, and also for the braking system, which is maybe necessary and would be different to the one of the G1. Besides, "Nanotech" did not recommend to control the rotatory stage with their board, so this solution was also not convincing.

The offer from "Busch" is far above our application needs. Conversations with more companies started but went in the same way as with "Busch", even bigger more powerful tables and thus higher prices. The conclusion was that this technology is too accurate and for more demanding applications than our yaw application. There is no availability of devices with the same function and worst performance, which could be more affordable.

3.2.2   Handmade rotatory stage

This proposal was taken from the preliminary design of Ruiz in her work [20]. The underlying idea of the design is to replicate the working principle of a rotatory stage but to build it with mechanised pieces. The working principle is the following.

The motor torque is increased by the gearhead ratio and will move the pinion shaft since a coupling connects it to the gearhead. The pinion will then move the bigger bevel gear where the tower is connected, and the bevel gear ratio was set close to 3. The turbine is then moved from below. Inside the big bevel gear, there are two bearings to allow the movement with respect to the base without friction. A groove for spring works to prevent backlash between the bevel gear and the pinion inside the gear. The motor's torque needed increases considerably because of this moment produced by the spring.

The motorset proposed consists of a Maxon RE35 Motor, equipped with the gearhead GP32C, one coupling and a brake AB20, adding up to a quantity of 954.81 €.

The model was created from scratch in Inventor in order to study its viability and price. Figure3.2a shows the system seen from the front, where all the parts are visible (the two bevel gears, the base, the ring to prevent the big bevel gear from falling, and the motor support). In Figure3.2b a cross section allows to see how the system would be assembled. The big bevel gear with the spring two bearings has to be inserted inside the ring, and then the base is screwed.

(a) Front view

(b) Cross section view
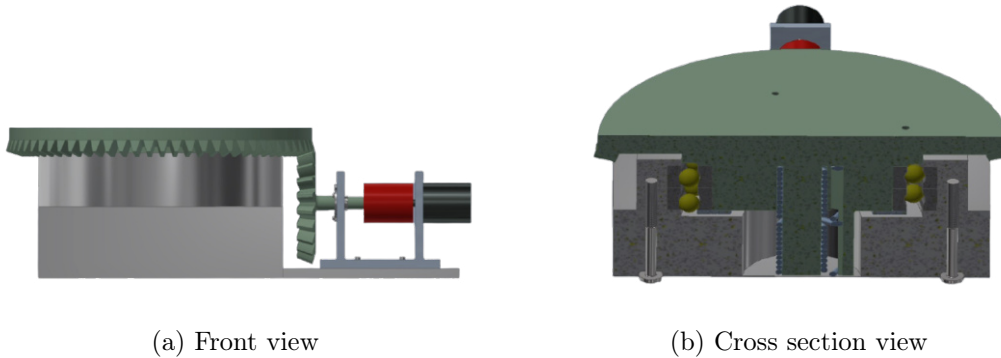
Figure 3.2: Handmade Rotatory stage CAD model

The most problematic piece is the big bevel gear, whose not standardised teeth are difficult and expensive to fabricate. An offer of 700 € was made by the "Zentralwerkstatt of the Physics Department TU", not having the bevel gear included, which was not possible to be manufactured. Other offers were obtained with different companies online tools, being the cheapest one from "Xeometry" 1429,39 € (see Figure 3.3). This offer includes the big bevel gear, but it was not ensured that the tooth will be the same one designed. There is another offer attached in the Annex.

In the best case scenario, the system's total price would be 2384.21 €, provided that the tooth is successfully manufactured. Prof.Stahl from the FZG TUM provided a list of companies specialised in gears and teeth manufacturing, and none was willing to fabricate the before mentioned teeth.

One further issue of this proposal relies on the fact that to have an accurate final movement, the different pieces need a perfect synergy between them. When the different tolerances of the components start to pile up, the overall operation of the system is affected. Designing all the pieces with good tolerances supposes also increasing the price considerably, without any guarantee that the final results will be the one expected since any mismatch between any part can increase the backlash considerably. At the end of the day, the pieces could be more expensive than the rotatory stage itself to ensure reasonable accuracy. Even so, a non-backlash continuous movement is not ensured.

Even if the rotatory stages evaluated in the previous subsection offer much better performance than the requirements needed, the difference of price between both proposals does not pay off when comparing it with the difference of accuracy between the handmade system and the guaranteed performance of the industrial systems. Not only that but the size of the system would also be bigger (see Figure 3.4) and would thus have a negative impact on the wake.

Pos.	Description	Quantity	Price per 1	Total
10.	Part name : Bevel gear part 1 Bounding Box: 83.64mm x 83.1mm x 71.5 mm Process: CNC Machining Material: Aluminium EN AW.2007 Surface roughness: Standard (3.2 um Ra)	1	223.17 €	223.17€
30.	Part name : Ring Bounding Box: 200 mm x 200 mm x 35 mm Process: CNC Machining Material: Aluminium EN AW.2007 Surface roughness: Standard (3.2 um Ra)	1	121.70 €	121.70 €
40.	Part name : Base Bounding Box: 360 mm x 250 mm x 60 mm Process: CNC Machining Material: Aluminium EN AW.2007 Surface roughness: Standard (3.2 um Ra)	1	311.20 €	311.20€
50.	Part name : Motor support Bounding Box: 90 mm x 60 mm x 40 mm Process: CNC Machining Material: Aluminium EN AW.2007 Surface roughness: Standard (3.2 um Ra)	1	154.11 €	154.11€
60.	Part name : Bevel gear part 2 Bounding Box: 243.61 mm x 243.55 mm x 102.03 mm Process: CNC Machining Material: Aluminium EN AW.2007 Surface roughness: Standard (3.2 um Ra)	1	489.27 €	489.27 €

Figure 3.3: CNC cost of handmade rotatory stage pieces. "Xeometry" offer

Figure 3.4: Size comparison Handmade Rotatory stage vs RT2A075

3.2.3   G1 system variations

The yaw system of the G1 is active, fixed and electrically driven. It was designed to resemble the working principle of a full-scale wind turbine machine, allowing the model to control the yaw error and its effects by moving the rotor into or out of the wind direction. An electromagnetic braking system was incorporated to serve not only the purpose of preventing gear backlash problems but also adds safety features to the scaled wind turbine model during wind tunnel testings.

The desired rotational movement of the nacelle with respect to the tower is realised by the mechanical drive concept based on a gearhead-motor assembly, which is equipped with an electromagnetic brake and an encoder at the gearhead output. The yaw mechanism of the G1 is depicted in Figure 3.5, being the main components of a Maxon drive set RE25 + GP32C, which is connected through a coupling to a shaft hanging between two ball bearings and a brake.

Furthermore, one mounting plate is used to mount the encoder with a disk to account for the homing position. Fixed within the hollow tower, the gearhead-motor assembly is connected the shaft of the nacelle mounting plate via a bellow coupling. The shaft of the nacelle mounting plate is aligned and connected to the screw-on portion of the tower by two ball bearings. [31]

An electromagnetic brake and a circular optical disk are installed along the shaft near the nacelle mounting plate. One of the purposes for installing the electromagnetic brake is to prevent gear backlash problems. A transmissive optical encoder module is installed on the screw-on portion of the tower shaft. Four holes and an alignment hole on the mounting plate allow the rectangular metallic housing of the nacelle to be screwed on.

The space constraints on the G1 is the following. The inner diameter of 40.3 mm of the tubular tower limits the component that could be placed within the tower. With a maximum diameter of 32 mm and an overall length of 92.9 mm, the gearhead-motor assembly fits in the hollow section of the tower.

The same system would work and meet all the requirements for the yaw of the G06 if there was enough space to mount it. Given that space was already the most restrictive constraint for the 40.3 mm inner diameter of the G1, it is impossible to mount that system on the G06, which has an external diameter of 28 mm and an internal one of 12 mm. Even if it appears the difficulty of this solution is high, some modifications for the implementation were considered, being the primary motivation for trying it, the fact that implementing the same system would be the most reliable and easy solution for the G06 because it has already been working correctly in the G1 and the control is well-known (only updating some parameters would be needed).
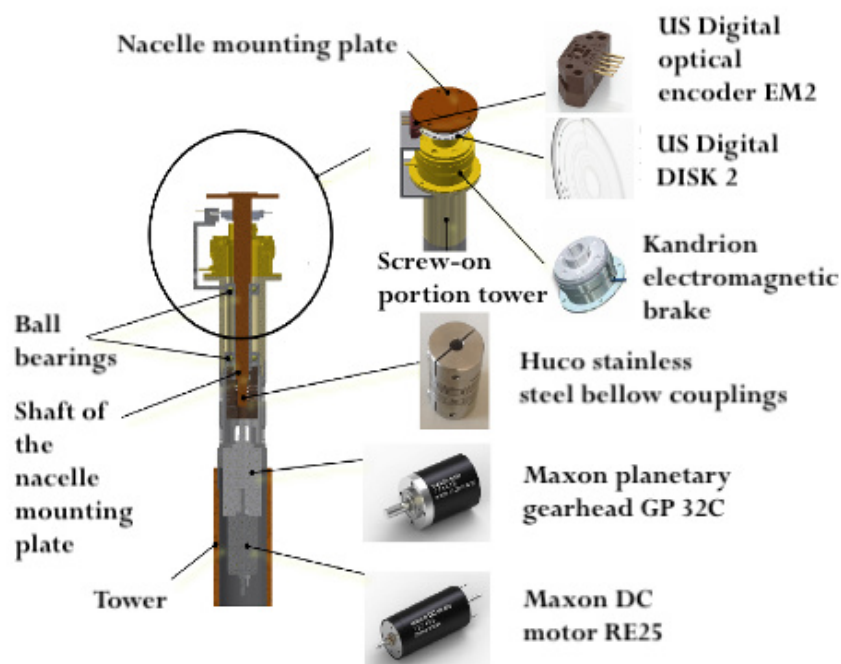

Figure 3.5: Yaw system G1 [31]

The first try was to check if with a smaller motor it could work, the smallest possible to provide enough torque would be the same RE25 but with a GP26 gearhead. Even so a hole would have to be made in the tower as shown in Figure 3.6. Being the external diameter 28mm, only a 2mm circular section would be left, which seems to be infeasible because of how weakened the structure would be in that part and the drastic change in the natural frequencies of the model it would cause.

Figure 3.6: Variation G1: Integrate inside the tower

Discarding this option, the following proposal was to try to allocate the motor set outside the tower and transmit the power through a small internal axis allocated inside the tower. Allocating it below the tower, as shown in Figure 3.7, would save the need of implementing some component to transform the horizontal torque into a vertical one, and the extra cost of the small axis would be negligible. The problem is that the axis would be too thin and too long (5-10 mm diameter and 538 mm long), and therefore experimenting too much deflection. Slenderness higher than five is not recommended for shafts working under torsional stresses for buckling reasons. Furthermore, the extra 33.1 cm are not acceptable.

The last evaluated option was to either use the G1 towers and get rid of the G06 thinner ones or adding the thicker section with space for the motor set in the upper part and cut down the towers and solder the thicker remaining part. Regarding adding the thicker section above the G06 tower, taking into account that the G1 motor set is 33.1 cm long and the tower 53.8 cm, it would mean an increase of its length of a 61% (Figure 3.8a), which because of scale reasons is not acceptable. To maintain the desired length of the tower, it would have to be cut to a 20.7 cm height as shown in Figure 3.8b. This raises the question of whether it is worth it to modify the towers or use the ones of the G1 directly.

The cost of replacing the G1 towers with the ones of the G1 per turbine, would be the sum of the following costs:

Figure 3.7: Variation G1: Shaft inside the tower

(a) Adding G1 tower section

(b) Cutting G06 tower down

Figure 3.8: Variation G1: Tower modifications

- Cost of throwing away the 6 G06 towers in the lab, with a unitary cost of 600 €.

- Cost of the strain gauges already installed in the towers, 200 € extra per tower.

- Cost of the G1 tower and the maxon motorset (920€), in total around 1200 €.

That adds up to 2400 € per turbine, plus the total cost of getting rid of 6 towers (3600 €). Even if this would be the easiest solution in terms of not changing anything from the already designed system, it has three major problems. The first one is that in terms of price is not much cheaper than any of the other proposal, besides the time of delivery of the G1 towers could be high and finally the reason because of which Nanos did not use the G1 towers for the G06. That is the distortion of the down-scaling of the model and the loss of proportions. Not only that effect is to be taken into account, which could be not that problematic -given that the drag coefficient of a cylinder is one and a thicker cylinder should not have such a significant effect on the wake-; but the effect on the natural frequencies of the model would be affected by the new extra mass. The G06 tower was designed smaller and softer in order to have natural modes below the rotor frequency. Therefore, this solution was discarded.

3.2.4   Right angle gearbox

After realizing that trying to allocate anything inside the tower or outside was not a good solution, new alternatives to the principle of the rotatory stage, converting a horizontal movement into a vertical one, were searched. The solution that came up was to use a right angle gearbox with a Maxon motor to use the same control system used in other models in the lab.

Right angle gearboxes are used to create drive trains that can transmit torque 90° while also being suitable for space-saving. Their advantages are their compact design, compatibility with other types of gearboxes, and quiet and accurate for their compact size. Not only is this solution cheaper than the rotatory stage one, but it can meet the requirements of torque and backlash similarly. A standard motor can be used instead of the stepper motor that rotatory stages need, which would suppose designing a new control algorithm.

The best product found in the market was the TK+ series of the company "Wittenstein". It is a compact one stage (see later reduction ratio) high accuracy right angle gearbox. The TK+ has a high frictional torque, which prevents backlash and makes a brake non-necessary but at the same time requires an intermediate reduction of the rotational speed of the motor to have enough torque to be able to move the gears inside. For that purpose, a high quality, low frictional torque gearhead is needed. "Wittenstein" offered his CP series, which have comparable prices to the gearheads from Maxon and are designed for this kind of situations, having high efficiency and low frictional torque while reducing backlash.

Not only that, but the connectivity between the TK+ and the CP was also a good point for choosing it over gearheads from Maxon or other companies. The motor set of the proposal is composed of the following components: Maxon Motor, coupling piece between Maxon-CP, CP, "Wittenstein" coupling between CP and TK, TK, a support to screw fix part of the TK and one adapter mechanism between the TK and the tower. How those components are assembled can be seen from right to left in Figure 3.9. The drawings of the TK and CP are available in the Annex 7.

The price of the TK is 1683 €, and the CP costs 130 €. The Maxon Motor set becomes cheaper, as the brake is no longer needed and the EPOS boards in the lab could be used, being reduced from 768,55 € to 350-400 €. Assuming that the manufacturing of the coupling pieces and the steel support (which was proposed to be made of steel in order to be softer and try not to increase the frequencies of the model too much) would cost around 400 to 600 € according to the "Zentralwerkstatt", the final price is around 2500-2800 €. That is a competitive price compared
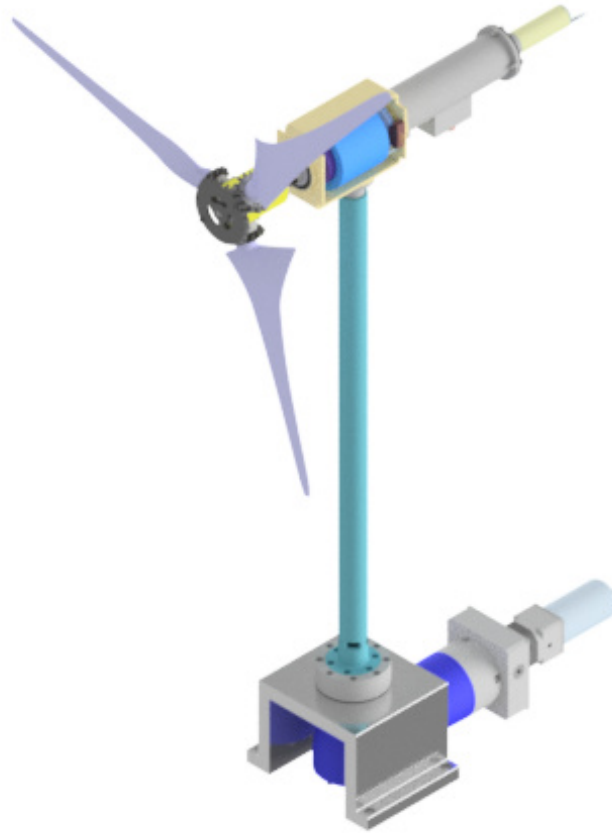
Figure 3.9: Right angle Gearbox

to the other solutions while being able to use the Maxon control and ensure low backlash.

The backlash of the system can be calculated by looking at the technical data. According to Table 3.5 it is less than 5 arcmin for the TK and 12 for the CP (which is divided by the reduction ratio of the TK). So the maximum backlash would be 5.12 arcmin plus the torsional stiffness, which is 2.35 Nm/arcmin. If there were applied 2 Nm, the maximum play would be 10.72 arcmin, equal to 0.17°, which is below the 0.2° set as objective. Other crucial parameters are the 0.2 Nm of frictional torque of the TK. Looking at the most powerful Maxon Motors of the RE35 series, the highest nominal torque is 107 Nmm, not being able to move the TK. That is why a first reduction stage around 5-20 is needed to surpass it. The CP has a frictional torque of 50 Nmm, which can be achieved with these motors.

As a first estimation, the Maxon Motor RE35 was chosen with nominal torque 107 Nmm, nominal speed 2290 rpm and 83% efficiency and a reduction ratio i=100 for the TK+ and i=10 for the CP were selected, so preliminary calculations were performed with their technical data.

In the following calculations, the torque at the output of the TK and nominal rotational speed are obtained by taking into account the frictional losses. The resulting 16.92 Nm have some margin above the 9.6 Nm estimated for the worst-case scenario with gears and high backlash. Considering the low backlash of the system, this scenario is even more impossible and 6 Nm should be enough. With that total reduction rate, the system could rotate at 2 rpm close to the nominal point of the motor, preventing overheating.

$$M_{CP} = (0.107 * 0.83 - 0.05) * 10 * 0.97 = 0.38 \, Nm$$

$$M_{TK} = (0.38 - 0.2) * 100 * 0.94 = 16.92 \, Nm$$

$$\lambda = \frac{2290}{1000} * 0.97 * 0.94 = 2 \, rpm$$

Table 3.5: TK+ and CP technical data

Parameter	Description	Units	TK+	CP
i	Gear ratio	-	100	10
T_{2a}	Max. Torque at shaft output	Nm	20	20
T_{2B}	Max. Acceleration torque	Nm	20	13
T_{2N}	Nominal torque	Nm	15	6
n_{1N}	Nominal rotational speed	min^{-1}	5500	43000
n_{1Max}	Max. rotational speed	min^{-1}	6000	9000
T_{012}	Frictional torque	Nm	0.2	0.05
j_t	Max. backlash	arcmin	< 5	< 12
C_{t21}	Torsional stiffness	Nm/arcmin	2.3	0.5
F_{2AMax}	Max. axial load	N	2400	240
F_{2RMax}	Max. radial load	N	2700	170
M_{2KMax}	Max. tilting moment	Nm	251	4
η	Efficiency	%	97	94
L_h	Lifetime	h	> 20000	>20000
m	Weight with standard plate	kg	3.2	0.5
L_{PA}	Operation noise	dB	64	59

3.3   Evaluation of the proposals

For the approval of one of the proposed systems, the following methodology was followed. First, all the options were compared, and a decision matrix was used to rank the four options. After choosing one of them, a final solution with more detail was proposed, taking into account all the modifications and changes that must be done to the G06 model to implement it, as well as the final offer of the manufacturer. Finally, a similar geometry to the one that would be implemented must be tested in the wind tunnel to check that the wake will not be affected by modifying the geometry and scale of the model. Table 3.6 summarizes the main criteria to be considered from the different proposals.

3.3.1   Solution selection

A decision matrix was used to rank the different proposals, in which five criteria were evaluated and given relative importance: specifications (20%), control implementation (20%), price(25%), height (25%) (related to the effect on the wake) and reliability (10%). The final result is shown in Table 3.7.

Table 3.6: Proposals overview

Proposal	Price (€)	Yaw rate accuracy (°)	Extra-height (cm)	Torque (Nm)
Rotatory stage	3000	0.05	6.4	5.6
Handmade rotatory stage	2500	>0.9	11.4	14.6
G1 tower	3000	0.2	0	3.94
Right angle gearbox	2800	0.08	11.2	16.92

The first criterion evaluates how accurate and close to the defined requirements each of the solutions is, while the second one how easy it is to connect with the control infrastructure of the TUM wind turbines family. The price was normalized to obtain a mark from 0 to 10 and the size of each of the systems, as well as the height of the system. The reliability factor measures the risk of each of the proposals not working as expected.

Table 3.7: Decision matrix

	Criterion 1	Criterion 2	Criterion 3	Criterion 4	Criterion 5	
Weight	20%	20%	25%	25%	10%	100%
OPTIONS	Specifications	Control	Price	Effect on the wake	Reliability	Weighted score
Rotatory stage	9	2	6	8	8	6.5
Handmade rotatory stage	2	8	7	1	2	4.2
G1 variations	5	10	5	10	5	7.25
Right angle gearbox	8	8	8	5	9	7.35

In terms of specifications, both the right angle gearbox and industrial rotatory stages are the best solutions. In contrast, a handmade rotatory stage could, for example, give some backlash and positioning problems. Besides, the rotatory stage would suppose a new control system, while the right angle gearbox is compatible with a Maxon Motor, making life much easier, even if using the G1 yaw system and tower does not require any effort in terms of control.

When it comes to the price, the rotatory stage and the right angle gearbox are very similar, and the final cost will depend on how much the extra pieces cost. For the right angle gearbox, there are two coupling pieces to be designed and a new basis, while for the rotatory stage, only a coupling plate has to be designed. The G1 variations suppose wasting material that has already been paid. The final cost of the handmade stage depends on the tolerances set for the pieces, which could significantly increase the cost. Besides, maybe the teeth of the big bevel gear is not doable.

The final decision is between the proposed G1 variations and the right angle gearbox (mainly replacing the towers for G1 towers, since the other proposal was discarded). Not only is the right angle gearbox a bit better on all of the parameters, but it also prevents the creation of a wider wake and vortex shedding, which was the reason because of which E.M Nanos designed the G06 tower.

Furthermore, there is another advantage of the right angle gearbox over keeping the G1 system to take into account, that is the significant improvement of the performance of the G1 system. The right angle gearbox system would be more powerful and able to perform more demanding movements, which is interesting for the wind farm studies to be performed with the model. Therefore the right angle gearbox was selected as the final solution and will be designed with more detail and tested on the wind tunnel to prove that its effect on the wake is acceptable.

3.3.2   Proposed solution

Some modifications to the model have to be done to implement the right angle gearbox, and some pieces have to be designed and manufactured. The first is a new support, which must house everything inside (TK+, CP, motor, control boards and cables) while giving a solid foundation for the TK+. The new pieces to be created are a coupling between the tower and the rotating part of the TK+, which will transmit the output torque to the tower, and a coupling between the motor and the CP since they are from different companies. The design of these components will be covered more in detail in Chapter 5. The final data sheets of the components after the parameters design with the Simulink model are available in Annex 7.

Not only must there be space for the yaw system within the airfoil profile, but also a similar connector plate to the one on the G1 has to fit inside, given that it is pretended to use the same connection cables as in the G1. The final proposal, including all the components inside the airfoil is shown in Figure 3.10a.

Even if at this point it was only a proposal, having a precise estimate of the size of the system was important to design an airfoil profile for the wind tunnel that could house everything and is not smaller than the one which will be used at the end to be at the conservative side. It was checked that everything could fit on the ground surface, as shown in Figure 3.10b. The profile selected was a NACA0030 with a 50 cm chord, which had a low drag coefficient and had an acceptable width/chord ratio, preventing the airfoil from getting too long. It was printed in 3D with a 4 mm thickness.

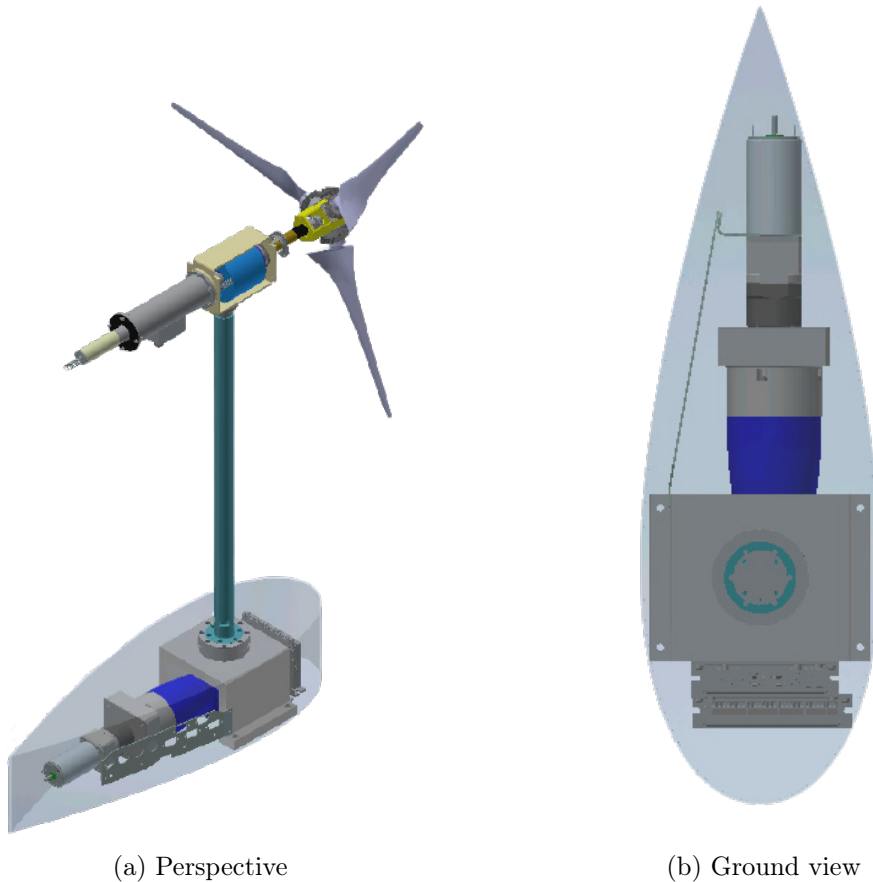(a) Perspective   (b) Ground view

Figure 3.10: Final design of the yaw mechanism

3.3.3 Aerodynamic check on the wind tunnel

Even though the right angle gearbox seemed to be a robust and compact solution, it was still necessary to check whether the effect of such a geometry on the tower's base is negligible or if it is inducing turbulence and deflection on the wake of the same order of magnitude as the one the yawing movement of the turbine induces. If the effect is in a similar order of magnitude, the yaw system is unsuitable since no wake measurements of the yawing turbine can be performed. That it why a wind tunnel experiment was performed in the TUM boundary layer wind tunnel in order to study this effect on the wake.

The experiment's goal is to prove that the extra height and shape of the proposed solution at the bottom of the tower is not pulling the wake down too much, and that it can even be further improved if the whole system is covered with an airfoil profile. For this purpose, a NACA0030 profile dummy was printed in 3D to cover the structure, and the shape of the TK+ and the support structure was simplified to the one of a 5.2 cm diameter and 12 cm height cylinder. These dimensions and the ones of the dummy profile were set a bit bigger than the actual ones needed to be on the safe side, just in case future modifications are needed.

Figure 3.11: G06 turbine setup for the Wind tunnel experiment with NACA0030 dummy printed in 3D

In order to have an order of magnitude of the expected results on the wind tunnel, the problem was approached theoretically, performing some drag calculations. This is because drag and turbulence on the wake are directly correlated. Therefore the smaller the drag generated with the new geometry, the more negligible the effect on the wake. Drag force per meter length is calculated as shown in Equation 3.8.

$$D = \frac{1}{2} C_D \rho V^2 l \; (N/m) \tag{3.8}$$

Taking into account the characteristic length (l), which corresponds to the height of the G06 tower (28 mm), the height of the G1 tower (48 mm) and the chord of the 3D printed NACA profile (490.5 mm); as well as their corresponding drag coefficients: 1 for the towers and between 0.1-0.14 for the NACA (see Figure 3.12a); drag force can be calculated. The conclusion that can be drawn from the results, summarized in Table 3.8, is that the drag caused by the airfoil is in the same order of magnitude as the one of a G1 tower, which is around two times the one of the G06.
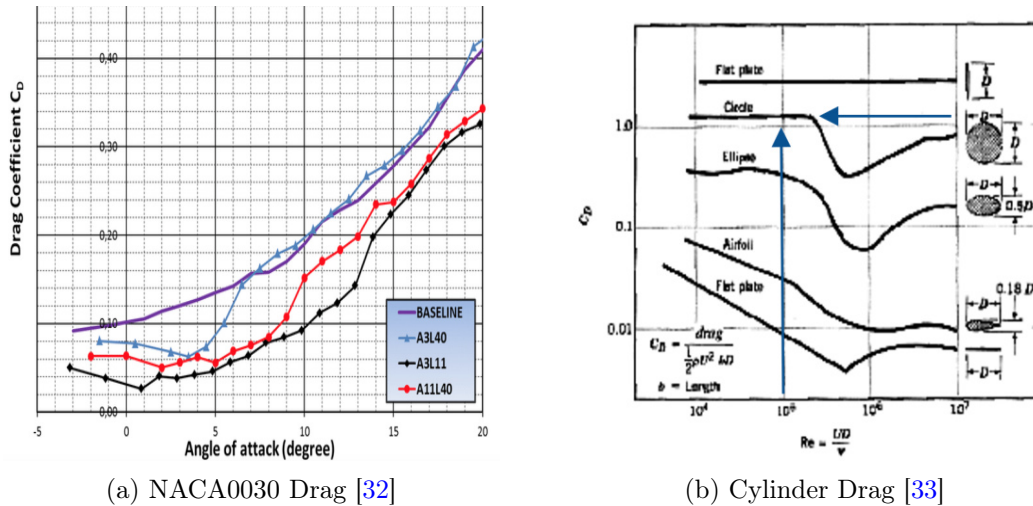

(a) NACA0030 Drag [32]   (b) Cylinder Drag [33]

Figure 3.12: Assumed drag coefficients

Table 3.8: Drag calculations

Parameter	G06 Tower	G1 Tower	Airfoil
Characteristic length (m)	0.028	0.048	0.490
Drag Coefficient C_D	1	1	0.1-0.14
Drag force per unit length (N/m)	1.89	3.24	3.34-4.67

If the experimental results in the wind tunnel back this affirmation up, the proposed yaw system would be as good as using the G1 towers in terms of wake disturbance and would affect less the natural frequencies and proportions of the model.

The experimental setup was the following. The same measurements were performed for two different settings: without (A, Figure 3.13a) and with airfoil (B, Figure 3.13b). In the pictures the turbine is 30° yawed, but the settings are the same for the 0° yaw case. These measured points were disposed in horizontal lines (at:1D, 1.5D, 2D, 2.5D and 3D) and vertical lines (at: 1D, 2D and 3D). The G06 model used was the one that had already been working in Dallas and TUM wind tunnel for the wake characterization, which has no active pitch control. Tower and

hub sensors we also not used as the only interest involved in the experiment is to measure the effects on the wake, being thus only torque control needed.

The turbine was set at its optimum point at 2250 rpm and $\lambda = 7.1$, the wind tunnel velocity to the rated one of 10 m/s. These conditions replicate the ones from the wake characterization study E.M.Nanos also realized at the TUM wind tunnel in [1], so the wake can be compared. The test matrix is summarized with the coordinates used for each of the lines and the number of points and resolution in Table 3.9.
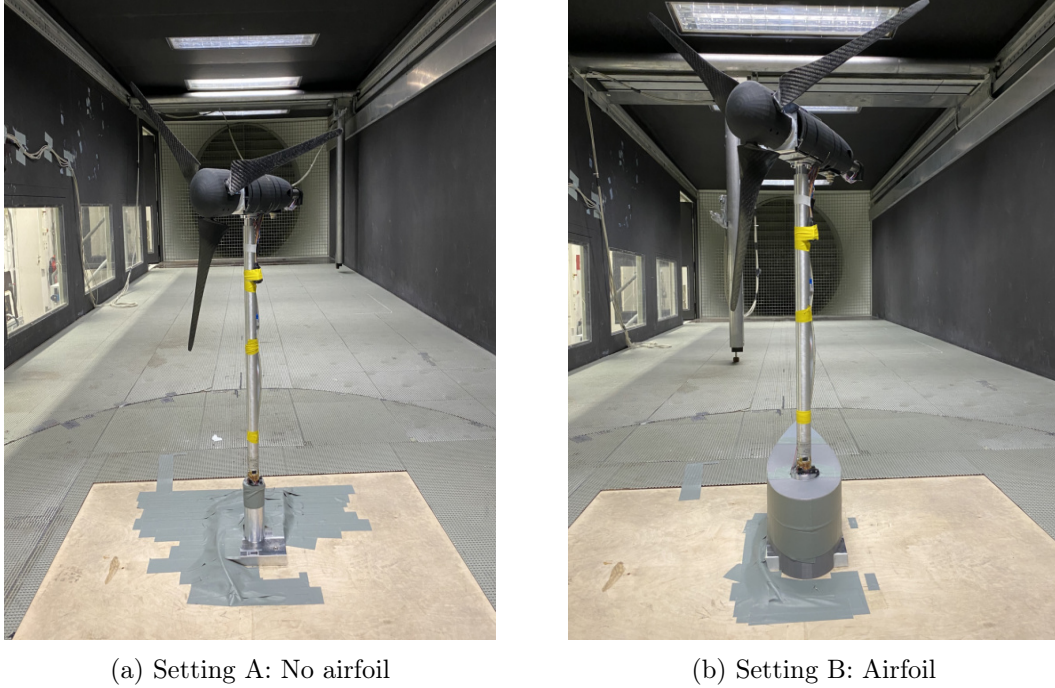

(a) Setting A: No airfoil   (b) Setting B: Airfoil

Figure 3.13: Settings for the wind tunnel experiment

Table 3.9: Test matrix

Code	Type of line	X distance (mm)	Number of points	Resolution (mm)	Y (mm)	Z (mm)	Yaw angle (°)
H1D	Horizontal	-3770	13	30	[908,1268]	-1429	0°
H1.5D	Horizontal	-3485	13	30	[908,1268]	-1429	0°
H2D	Horizontal	-3200	13	30	[908,1268]	-1429	0°
H2.5D	Horizontal	-2900	13	30	[908,1268]	-1429	0°
H3D	Horizontal	-2600	13	30	[908,1268]	-1429	0°
V1D	Vertical	-3770	21	30(13),50(8)	1088	[-1430,-1020],[-1020,-690]	0° and 30°
V1D-2	Vertical	-3770	21	30(13p),50(8p)	988	[-1430,-1020],[-1020,-690]	30°
V1D-3	Vertical	-3770	21	30(13p),50(8p)	1188	[-1430,-1020],[-1020,-690]	30°
V2D	Vertical	-3200	21	30(13p),50(8p)	1327.5	[-1430,-1020],[-1020,-690]	0° and 30°
V2D-2	Vertical	-3200	21	30(13p),50(8p)	1227.5	[-1430,-1020],[-1020,-690]	30°
V2D-3	Vertical	-3200	21	30(13p),50(8p)	1427.5	[-1430,-1020],[-1020,-690]	30°
V3D	Vertical	-2600	21	30(13p),50(8p)	1396.5	[-1430,-1020],[-1020,-690]	0° and 30°
V3D-2	Vertical	-2600	21	30(13p),50(8p)	1296.5	[-1430,-1020],[-1020,-690]	30°
V1D-3	Vertical	-2600	21	30(13p),50(8p)	1496.5	[-1430,-1020],[-1020,-690]	30°

The horizontal lines were only measured for a 0° yaw angle, and the vertical lines at both 0° and +30° yaw angle. Besides for the yaw measurements two extra vertical lines at +10 and -10 cm of the wake center were added at every distance. A scheme of the mentioned measured points is depicted in Figure 3.14. The horizontal lines were measured at the lowest height possible (8

cm above the floor), which lies a bit above the mid-line of the airfoil and 13 points with a 3 cm resolution were measured. The vertical lines were made out of 21 points with the same 3 cm resolution until the rotor and 5 cm resolution from the rotor height until two points above hub height. The dashed lines represent the lines that are exclusive to the yaw measurements.

The wake center (in the Y coordinate) was corrected for the centered vertical lines at 1D, 2D and 3D as proposed by Schreiber in [16], using Equation 3.9.

$$D_i(\Delta x, \gamma) = max[0, (D + 2\Delta x K_{e,i})cos(\gamma)^{k_{e,\gamma}}] \tag{3.9}$$

where Δx is the distance downstream of the wind turbine, D the rotor diameter, γ the wind turbine yaw-misalignment angle and $k_{e,\gamma}$ a parameter that describes the reduced wake expansion due to wind turbine yaw-misalignment. As the wake zones can have a negative expansion coefficient, the wake diameter has to be limited to positive values.
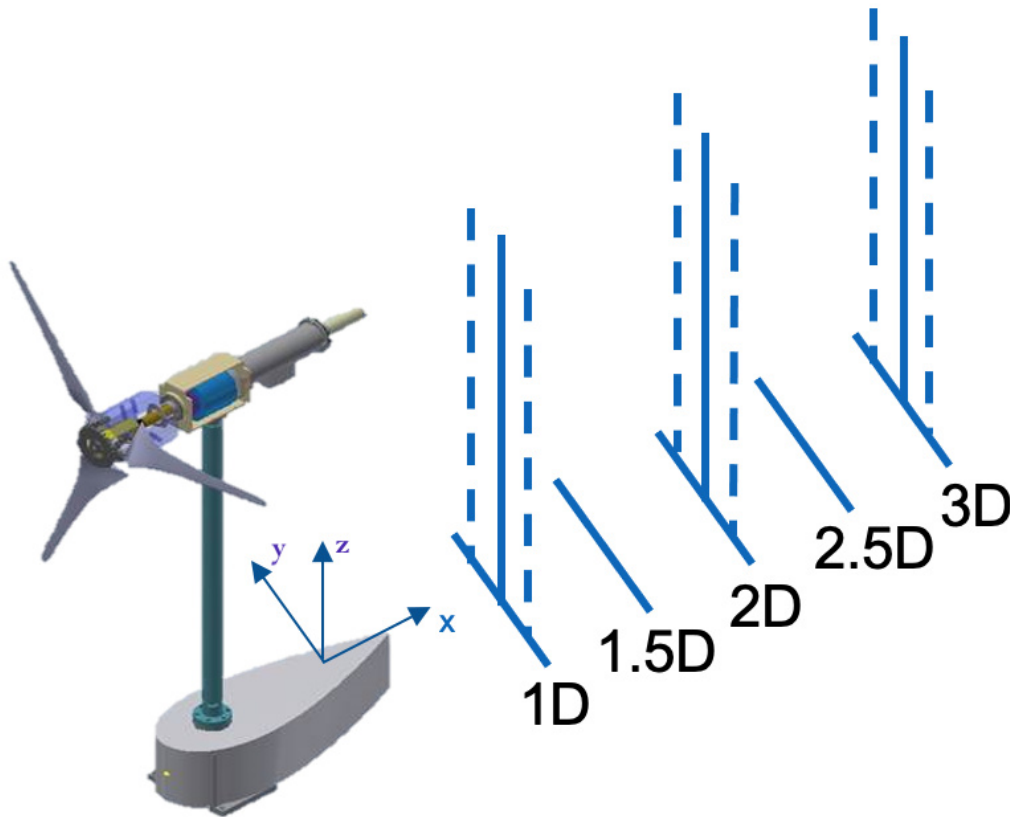

Figure 3.14: Wind tunnel measured points

The TUM wind tunnel has a height of 1.8 m, a width of 2.7 m and a length of 27 m. For both settings and yaw (9 vertical lines) and non-yaw (5 horizontal lines and three vertical lines), the wake was measured using a fast-response aerodynamic pressure probe (FRAP) and manufactured in-house at TUM (Heckmeier et al. [34]) at 5000 Hz sampling. The three gold-plated tungsten wires have a diameter of 5 μm with a length of 1.25 mm. The output binary files were post-processed and plotted with Matlab.

The results for the horizontal lines are shown in Figure 3.15. The absolute velocity u is normalised with respect to the 10.5 m/s wind tunnel velocity, and the radial direction Y is normalised with respect to the rotor radius. A schematic draw of the airfoil from the top is shown to have an order of magnitude of the distances. On red the airfoil measurements of setting B are visible, while blue represents setting A, with only the cylinder and the base.
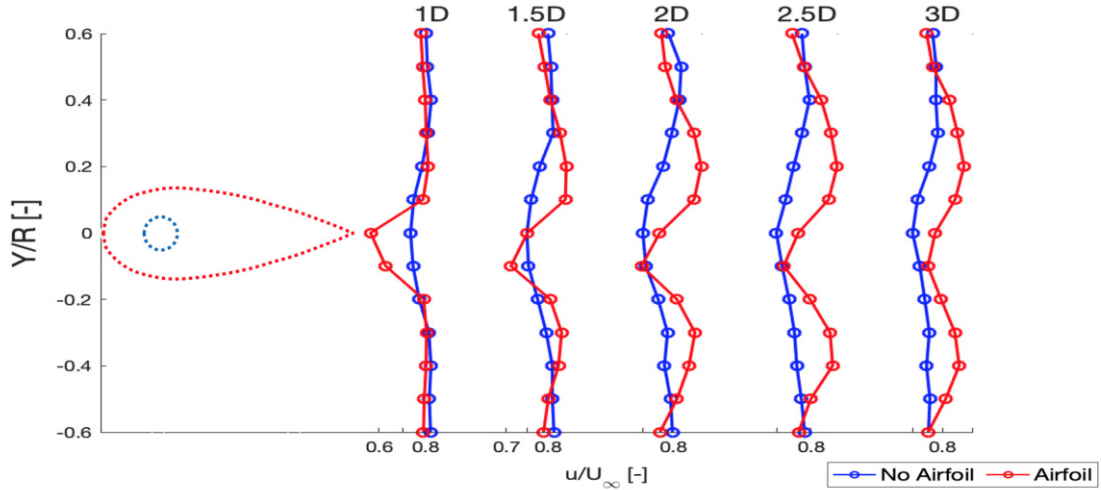
Figure 3.15: Horizontal lines behind yaw structure

The first interesting observation is the fact that the velocity deficit is similar or just slightly higher over the whole range, being it a bit higher just directly behind the structure for setting B. The airfoil setting shows a faster recovery of the wind velocity, especially from 2D on, while this deficit only occurs directly behind the airfoil because of the turbulence at the trailing edge, which is again similar to the profile without airfoil at 1.5D. Not only are the results with the airfoil a bit better, but both cases show that the wake is not being pulled down, which is a positive result since the effect of the geometry is only affecting the wake very close to it.

In Figure 3.16 it was zoom on in every X distance to be able to have a better look at the normalized velocities values at each distance. It can be seen that at 1D, the value range of the normalized velocity is between 0.55 and 0.82, while for bigger distances it remains in the 0.75-0.85 interval, apart from at 1.5D where the airfoil setting is still recovering a bit slower at the close to the symmetric plane at the radial direction (0.72 and 0.75 for setting B). The better behaviour of setting B in terms of speed recovery with increasing X distance is clearly visible.
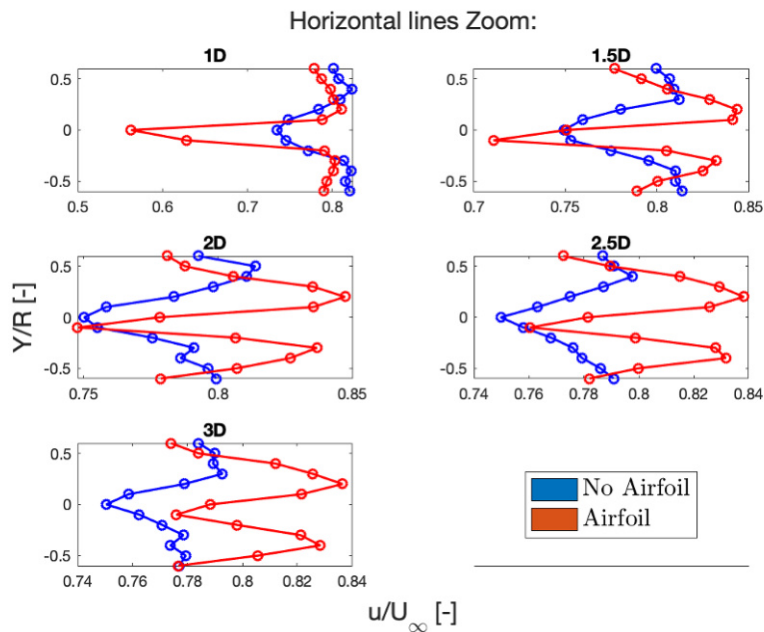

Figure 3.16: Horizontal lines behind yaw structure zoom

The next check is to see whether the negligible effect on the airfoil plane is also not affecting the velocity profile closer to the rotor. This effect can be seen in Figure 3.17, where the velocity was again normalised and the height in the z axis too again with respect to the radius of the rotor. A scheme of the turbine scaled to the graph is visible, and the rotor swept area is marked with two blue lines. The airfoil and the cylinder are also visible at the bottom.
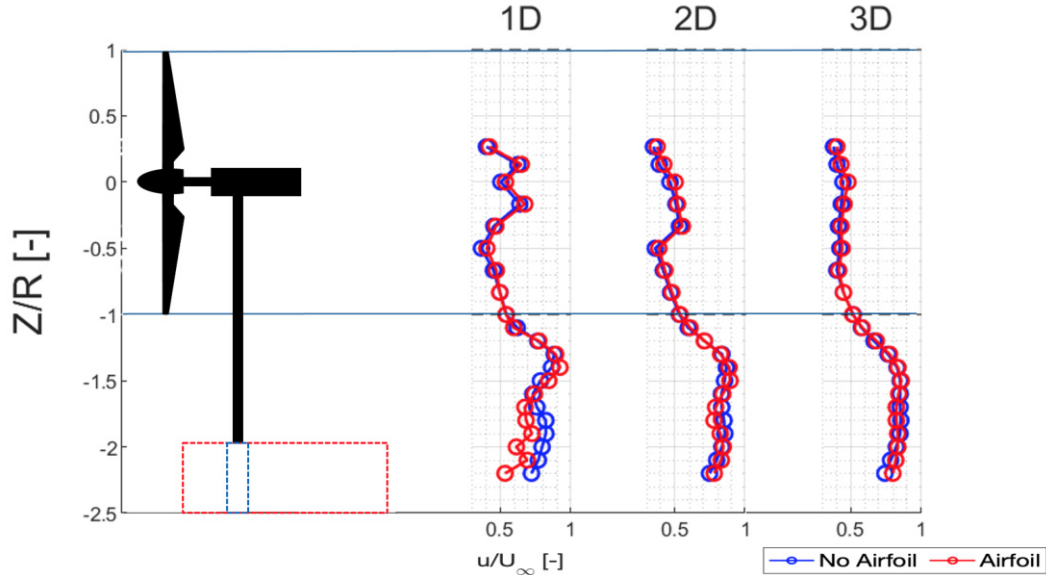

Figure 3.17: Vertical lines for no yaw

The results are even better than for the horizontal lines, not being almost any velocity difference at all distances in the rotor area even at 1D. This supports the fact that the geometry is only having a local effect on the wake just after it. Closer to the cylinder in 1D is the only place where a higher velocity deficit can be seen with the airfoil, which makes sense because it has to do with the effect seen on the horizontal lines.

For the vertical lines the results can be compared with the ones from E.M Nanos at the wind tunnel with the same operating conditions. At 1D see (Figure 3.18a) the velocities are very similar, and only uncertainty, slighter different setting and the small influence of the new geometry might be the reason for this small differences, while at 3D, as shown in Figure 3.18b the difference at the lower part is a bit bigger, but not higher than a 10%.
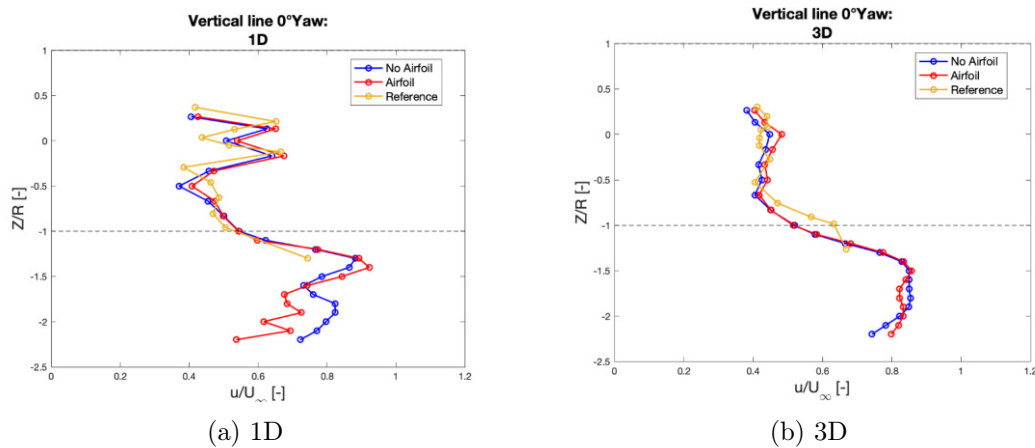

(a) 1D

(b) 3D

Figure 3.18: Vertical lines for no yaw compared with reference wake characterization of the G06 [2]

This study made no measurements closer to the floor, so no conclusions can be drawn from there, but the overall shape validates the measurements. The data for the reference was extracted from the wake characterization study of the G06 performed also in the wind tunnel of the TU with the same wind and turbulence conditions in [2].

The final check is to see the behaviour when the turbine is yawed to a maximum angle of 30°, for which nine vertical lines were measured at the same X distances, taking into account the deflection of the wake centre. With the same plot outlay, the following plots summarize the wind speed at the vertical lines at the wake centre, to the left side (-10 cm) and to the right side (+10 cm). Figure 3.19 shows a perfect match for the lines at the wake centre at 2D and 3D with only small differences visible at the lower part at 1D, the same thing as for the non-yaw case.
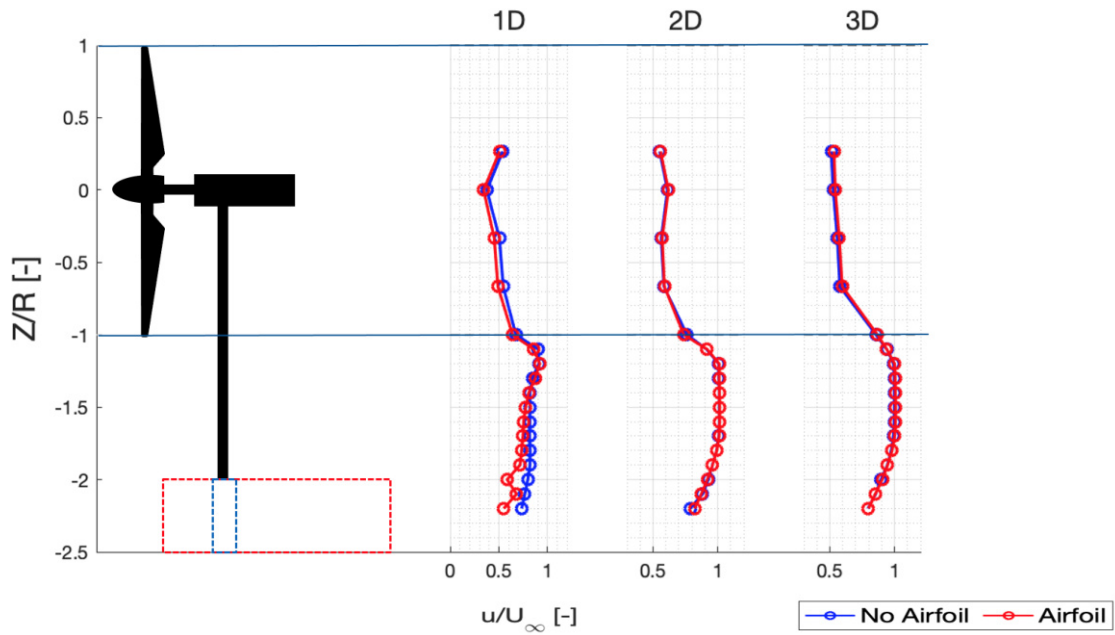

Figure 3.19: Vertical lines for 30° yaw, center line

For the left (see Figure 3.20) and right lines (see Figure 3.21) the same observation can be made since the only differences are in the wake shape but not in the effect caused by the geometry. The conclusion is that at these locations, even further from the yaw structure, the differences in velocity are even smaller and the match at the three investigated distances is better. The discrepancy at 1D also disappears at these lines, which coincides with the horizontal lines, being the differences in these points also smaller there.

To sum up, the experiment delivered positive results for the suitability of the yaw system. The following points summarize the most relevant observations and back up to proceed with the implementation of the right angle gearbox solution:

- The wake is only slightly affected at the bottom part by the airfoil cover. The velocity deficit is higher only in the centre. With increasing downstream distance this effect decreases and the velocity distribution of the two compared settings and thus the drag is similar. Consequently, the wake will not be pulled down.

- The airfoil structure only influences the lower part of the wake at the closest investigated distance of 1D. At higher distances also the lower part behaves similarly. The wake behind the rotor area including tip vortexes is matching very well for all distances.

- The excellent match is also existent if yaw is applied. If not on the center-line, even the differences in the lower part at 1D are not existent.

- The effect on the wake introduced by the airfoil structure is only marginal and corresponds well to the drag calculations. For this reason, the airfoil is a suitable solution hiding the yaw system without influencing the wake.
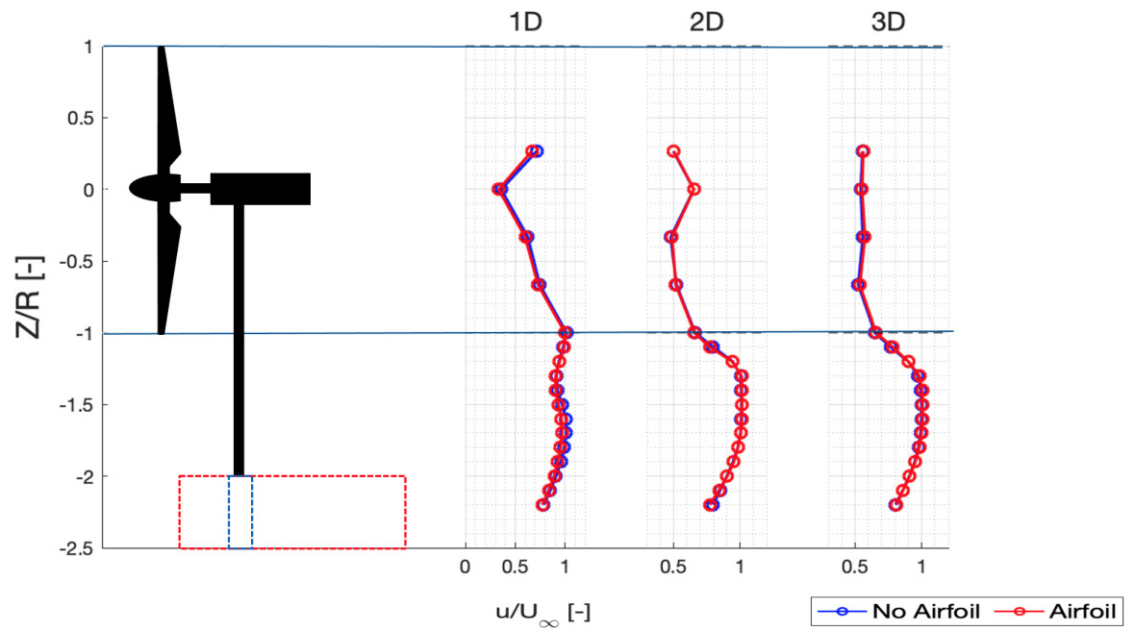

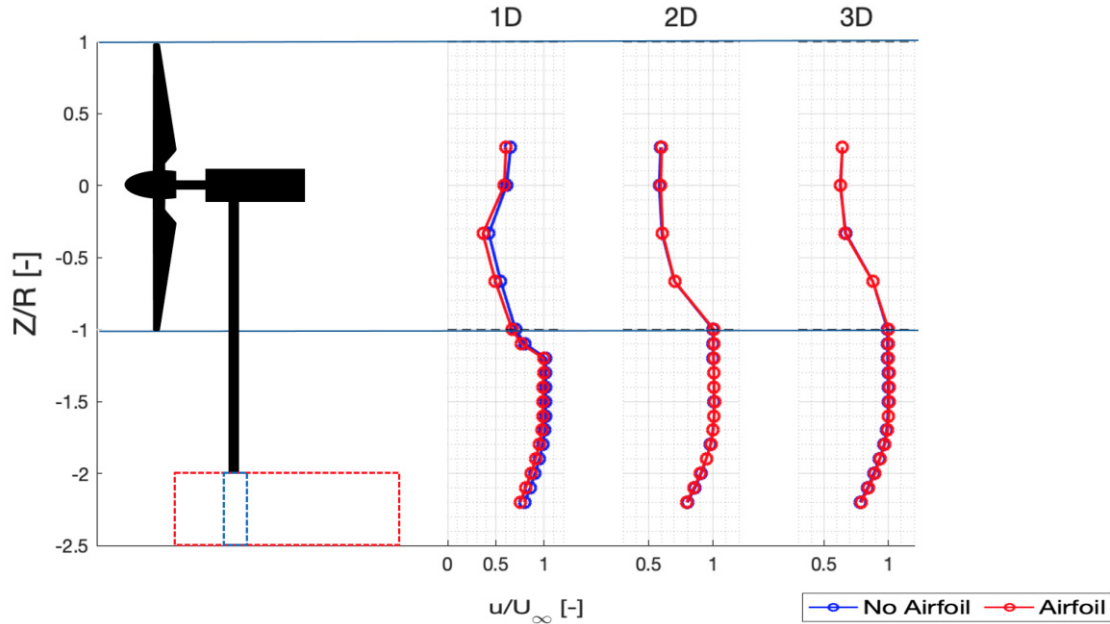Figure 3.20: Vertical lines for 30° yaw, left line

Figure 3.21: Vertical lines for 30° yaw, right line

Turbine assembly

The assembly of the turbine can be divided in four parts. The assembly of the blades, the hub assembly (which involves inserting the three blades shafts and implementing the pitch mechanism); the assembly of the nacelle (mainly the slip ring and generator) and the assembly of the tower and base, which is no longer the same one as for the G06 prototype because of the new yaw mechanism, and will be covered in Chapter 5.

The old CAD files from E.M.Nanos design have been updated, and a list of all the components needed to assembly one turbine has been made. All the components have been assigned a code (X.Y), where X stands for the group they belong to, and Y the number of the component. In the list it has been noted how many parts of each component are needed for the assembly of one turbine. Other codes stand for B (bearing) f.e or E (extra components).

This chapter aims to summarize all the knowledge obtain while assembling the turbine, to make easier the future assembly of new turbines. All the pieces of the model have been kept, organized and label in the G06 cluster in the lab, and it has been proved that there at least enough components available to assembly a second turbine. The main purpose has also been to transfer this knowledge to the next person, who will take over the G06 project.

4.1 Blade assembly

Table 4.1 contains the blade components, and the assembly is depicted in Figure 4.1. New blades with a new coupling were delivered, which made the assembly easier by getting rid of a piece called adjustable pitch (2.4). Now the blade can be directly screwed on the piece bevel gear (2.3), and long screws which went through pieces 2.1, 2.2 and 2.3 are no longer needed. The new blade base has different screw patterns, which allow to calibrate the pitch offset. The blade profile can be left apart until everything else in the model is assembled since it only has to be screwed to the holes in the bevel gear.

Table 4.1: Blade components

Code	Component	N°per turbine
2.1	Blade	3
2.2	Blade shaft	3
2.3	Bevel gear blade	3
B	Bearing 6180	2
E	Hall magnet	2

As commented, the blade assembly is the last thing for the assembly of the turbine. However, the blade shafts (2.2) have to be prepared to start the hub assembly. When the hub is assembled, the blade bevel gears (2.3) can be inserted into blade shafts. Then they have to be screwed with M2 screes and a pin indicating which is the correct angular position. The blade bevel gears can also be prepared by placing the two Hall Magnets in the slot placed for them, sticking them with glue. It is essential to take care of the correct polarity of the magnets.

Regarding the preparation of the blade shafts to proceed with the hub assembly, the main task is to mount two 6180 bearings in them. They have to be inserted to the very end, where the diameter changes. It is recommended to use the bearings tools in the lab or preheat the bearings slightly since the tolerance is quite tight, and they can be damaged if they are not being pushed parallel to the shaft axis.

The aim of the Hall sensors is to prevent pitch error between the blades and finding the homing position, besides backlash is prevented by placing a spring at the bottom of each of the blade shafts. The bottom of the shaft and the hub housing have a nine shape groove to allocate the springs.

Figure 4.1: Assembled Blade. From left to right, the blade shaft (2.2) with the two 6180 bearings inserted; the bevel gear (2.3) in black with the Hall Magnet and the Blade profile

4.2   Hub assembly

The components of the hub are listed in Table 4.2. The hub of the final G06 design has a collective active pitch mechanism, composed of a big bevel gear crown (3.10), three smaller bevels gear at each blade (2.3) and a 30 W Maxon motor controlled with an EPOS2 24/2-530239 board, which is placed at the front of the big bevel gear. The G06 hub resembles the G1 hub, but everything is more compact, and redundancies are eliminated because of the lack of space.

The motor connection to the board is pretty simple, only connecting the motor power supply and encoder. The board is supplied with 24V, which arrive at the hub structure through the slip ring and reach two power distributors, which supply power also to the strain gauges amplifying boards. Hall sensors of the three blades also deliver information to the control board. These connections are explained with more detail in the wiring maps (a simplification of the G1 hub) provided in section 4.4.

There are 3 strain gauges (2 for stresses and one measuring torsion) which are placed in the shaft connecting the hub and the nacelle. Each of the strain gauges is connected to an amplifying

Table 4.2: Hub components

Code	Component	N°per turbine
3.1	Hub housing	1
3.2	Pitch motor EC16-400161	1
3.3	Bevel gear blade	3
3.4	Springs	3
3.5	Bearing ring crown	1
3.6	Block bearings	3
3.7	Motor gearhead	3
3.8	Hub cover	1
3.9	Pitch shaft	1
3.10	Bevel gear crown	1
3.11	Coupling pitch	1
B	Bearing 628_9-2z	2
E	Hall sensors	3
E	Segel ring	1

board, which at the other side is connected to the slip ring. The assembly of the hub should start from the inner components and be quite accurate and organized since the space is limited.

First and foremost the blade shafts have to be placed on the three housing holes for the blades, inserting the springs inside. If this is not done first, it will be difficult to do it later, because it is needed to have a free surface to fix the housing while inserting the bearings inside. Besides it is a bit difficult to insert them properly while ensuring that the springs are in the right position. As commented before on the blade assembly, only the blade shafts with the bearings inside are needed at this point, the blade can be screwed at the end.

The right way to insert the blade shafts is fixing the housing with a clamp, put the shaft with the spring into the nine shape groove and check that the pin (which has to be inserted first) falls into the arc close to the nine on the bottom surface of the hole (see Figure 4.2a and Figure 4.2b) to understand the final result and the components inside.

Then use the bearing tools to insert the bearings and check after that the pitch movement is really constrained to that arc while the spring its opposing to the pitching movement. The block bearings (3.6) are to be screwed at the four holes after this step. They prevent the bearings from falling and have a hole to allocate the Hall sensors. Glue the Hall sensors there, connect three cables with shrink tube and use some tape to ensure that they do not fall. At this point leave the hub at this stage, and wait to connect the blade bevel gears and blade until the end of the hub assembly.

Once the housing has already the blade shafts inside, the insertion of the pitch shaft can start. The first thing to do, is to insert two bearings 628_9-2z until the bottom part of the pitch shaft (3.9), reaching the bigger diameter. They should be placed between that diameter change and the groove at the mid of the shaft, where a segel ring has to be placed to prevent them from moving backwards. Now it can be inserted into the housing. A suggestion is to place also first the amplifying boards of the strain gauges inside the holes on the housing before doing anything

else, since later there is no much space left to operate.

(a) Inventor outside

(b) Inventor inside

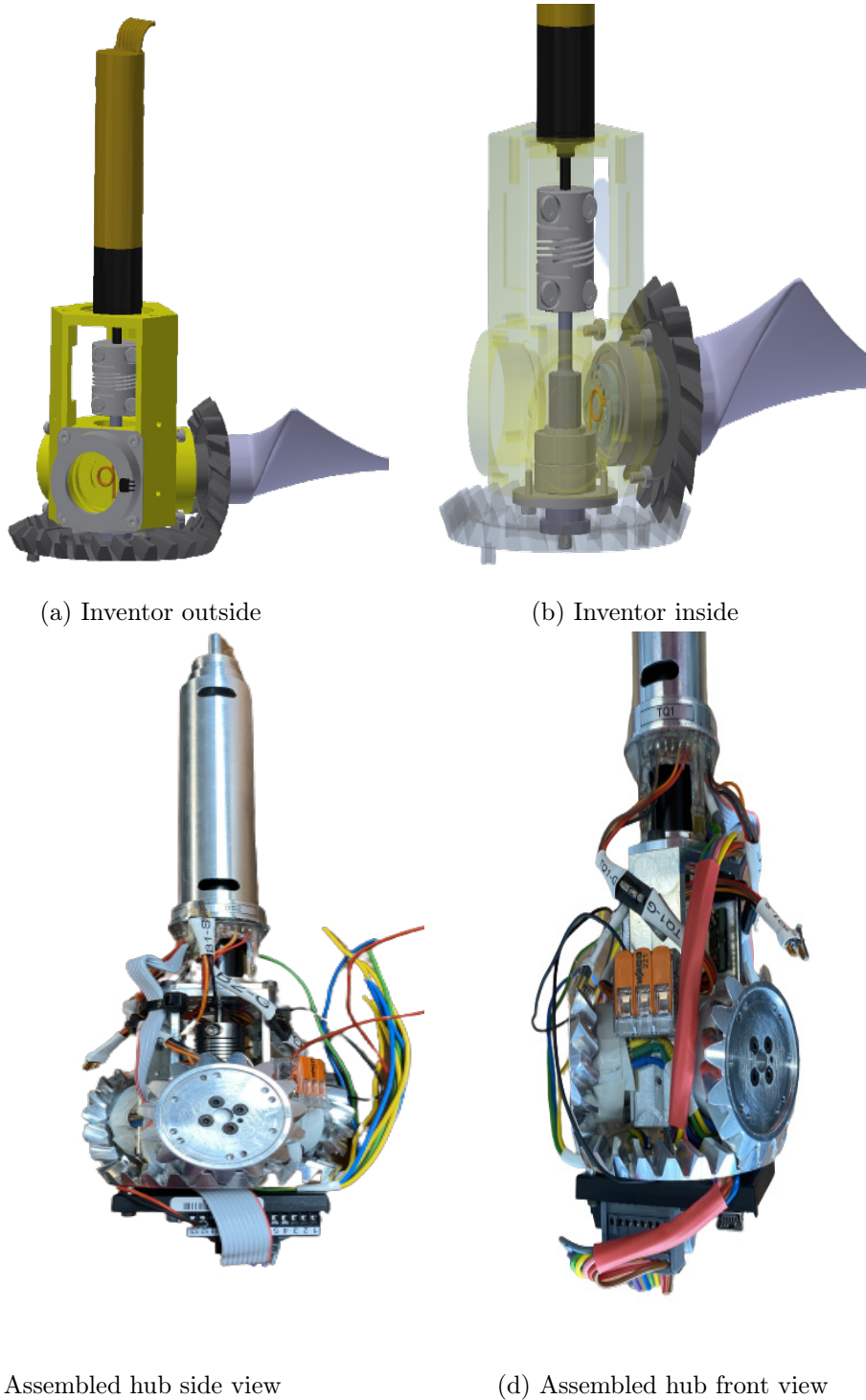(c) Assembled hub side view

(d) Assembled hub front view

Figure 4.2: Hub assembly

At this point, it is time to place the motor and gearhead inside the shaft, which connects the hub and the nacelle. The reason is that the motor cables have to go through the holes of the shaft. First, fix the motor with the holes on the upper part of the housing and mount the bellow coupling (3.11) in the inner region, touching the bottom surface. Tighten the coupling at the motor side and screw the shaft to the hub. Then insert the pitch shaft (with the two bearings inserted) inside the other side hole of the hub housing, which has enough tolerance to let it pass

through. The shaft must fit inside the bellow coupling, and finally, it must be tightened at this side too.

Once both shafts are inside the coupling and adequately tightened, the bearing ring (3.5) has to be placed on top of the housing and its function is to prevent the bearings from falling in this direction. The bevel gear crown can be finally placed on top of the pitch shaft, while fitting the tooth of the other gears, there are two small holes and a pin to fix it. The last step is to make all the connections to the board, for which there are holes in the bevel gear crown to slip the cables through. The amplifying boards are connected with their connector to the slip ring and the strain gauges at the other side. The results should look like the one shown in Figure 4.2c and Figure 4.2d.

Future work will also take care of the design of a hub cover, since the ones which were already designed were not thought to cover the active pitch mechanism and the EPOS2 board does not fit inside.

4.3 Nacelle assembly

The nacelle, whose components are listed on Table 4.3, consists of a support structure (4.1), where two ball bearings support the shaft (4.4). The shaft carries a slip ring (4.7) with 12 channels, which serves power to the pitch actuator and amplifying boards and pitch actuator. Six channels are used for the amplifying boards, 3 for the EPOS2 board controlling the pitch and the other 3 for the power and ground.

An optical encoder is placed after the slip ring to account for the rotor azimuth position (4.5 and 4.6). The support structure and the generator are connected with the torque-meter tube (4.3), which contains a high precision torque-meter (4.10) connected with two couplings to the main shaft. Finally the generator (4.11), a Maxon EC Motor is fixed to the generator ring (4.2), which is screwed on the back part of the torque-meter tube. The generator is controlled with an ESCON board which is hidden on the base support within the airfoil profile. The signals coming from the slip ring and the ESCON output are connected directly to the Bachmann.

To assembly the nacelle, the most important thing is to connect correctly the slip ring and check the continuity of the cables according to the wire maps, screw the support on the right position on the tower and connect the hub and the shaft (4.4) with the pitch actuator (as described on the hub assembly) to the support. The result of the assembly should look like the one on Figure 4.3.
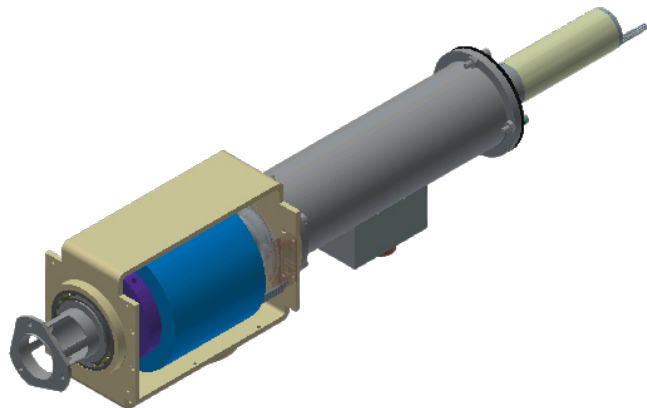

Figure 4.3: Nacelle. From left to right: 4.3, 4.1 (housing 4.6-4.9), 4.3 (4.10 inside) and 4.11

Table 4.3: Nacelle components

Code	Component	N°per turbine
4.1	Support	1
4.2	Generator Ring	1
4.3	Torque-meter tube	1
4.4	Shaft	1
4.5	Encoder	1
4.6	Encoder disk HUB	1
4.7	Slip ring TB2468	1
4.8	Ring bearing	1
4.9	KM3	1
4.10	Torquemeter DR2112	1
4.11	Generator	1
B	Ball bearings 61806	2
E	Bellow couplings	2

4.4 Wire maps

The wire mapping used for the generator to run the turbine in the wind tunnel for the yaw system validation; the one used for running the yaw mechanism in its performance check, and the one of the pitch mechanism of the assembled hub will now be specified.

The wiring maps were updated in the G06 files in the lab. The rest of them will not be included since there are no significant changes. The connections to the Cabinet are the same as the last ones E.M Nanos specified and only the connection to the ESCON of the generator changes because it was decided to use the same board as in the G1 (ESCON50/5-409510).

4.4.1 Generator

With the board change, the torque module is the same as in the G1. The generator has to be connected to the ESCON has shown in Figure 4.4. The generator windings (1-red, 2-black and 3-white) have to be connected to the J2 block as specified. The Hall sensors have to be connected to the module J3 in the correct order (1-red/grey, 2-black/grey and 3-white/grey; pins 4 and 5 are for the Hall sensor power supply and ground). A bad connection of the Hall sensors or the ESCON power supply can damage the board of the motor and must be avoided.

The pins in blocks J5 and J6 are the analogue and digital inputs and outputs, which go to the connector (3), which brings the information to the Bachmann cabinet module AIO288 as shown in Figure 4.5. The information provided is the rpm of the generator, temperature and current. For more information of each of the socket's pins of the ESCON, the Maxon website can always visited, looking at the corresponding ESCON model's Hardware reference document.

The cabinet was not used for the wind tunnel experiment, as it was not necessary to measure the turbine's performance data but only wake measurements. So what was done was to constantly measure the temperature and rpm o the motor with a voltmeter from the ESCON analogue

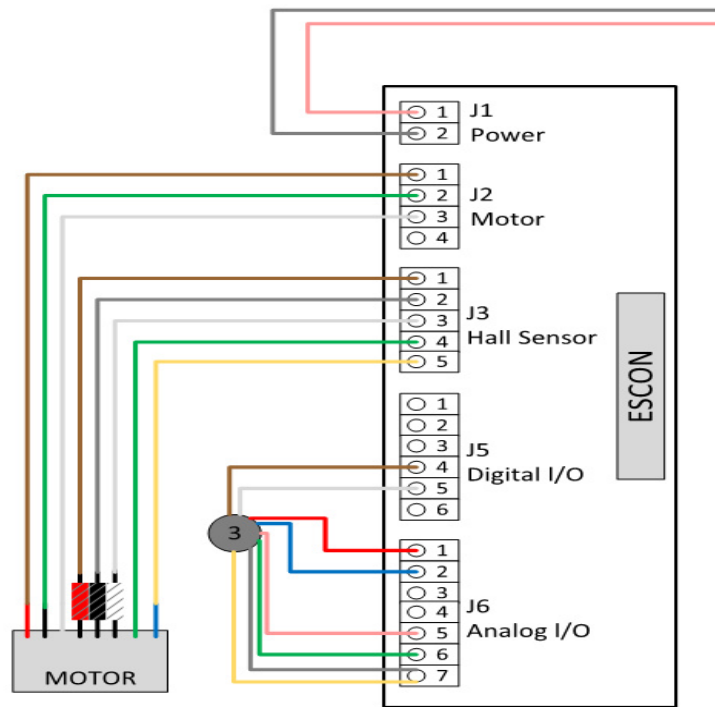output pins to check that it was working correctly at the nominal point.

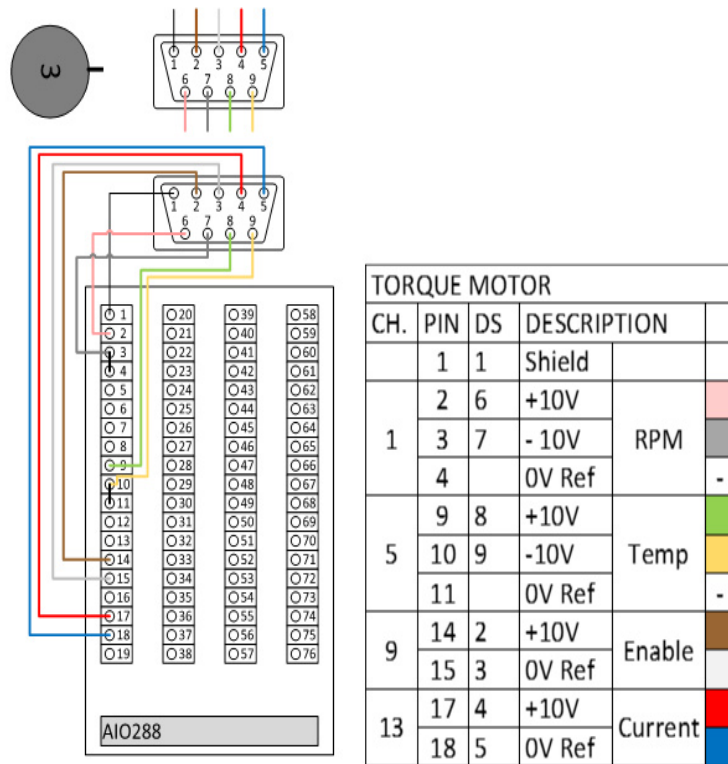Figure 4.4: Wire map: Generator-ESCON

TORQUE MOTOR					
CH.	PIN	DS	DESCRIPTION		
1	1	1	Shield		
	2	6	+10V	RPM	
	3	7	- 10V		
	4		0V Ref		-
5	9	8	+10V	Temp	
	10	9	-10V		
	11		0V Ref		-
9	14	2	+10V	Enable	
	15	3	0V Ref		
13	17	4	+10V	Current	
	18	5	0V Ref		

Figure 4.5: Wire map: ESCON-Cabinet

4.4.2   CAN

There are two CAN lines, one for the pitch, which is connected through 3 channels of the slip ring to 3 pins of the EPOS2 board in the hub, and another one for the yaw. The same CAN software of the G1 can be used, but the dictionary parameters have to be adapted to the needs of the G06. For the pitch, it will have to be taken into account that it is collective, and some parameters will have to be removed, making it even easier. Figure 4.6 shows all the connections.
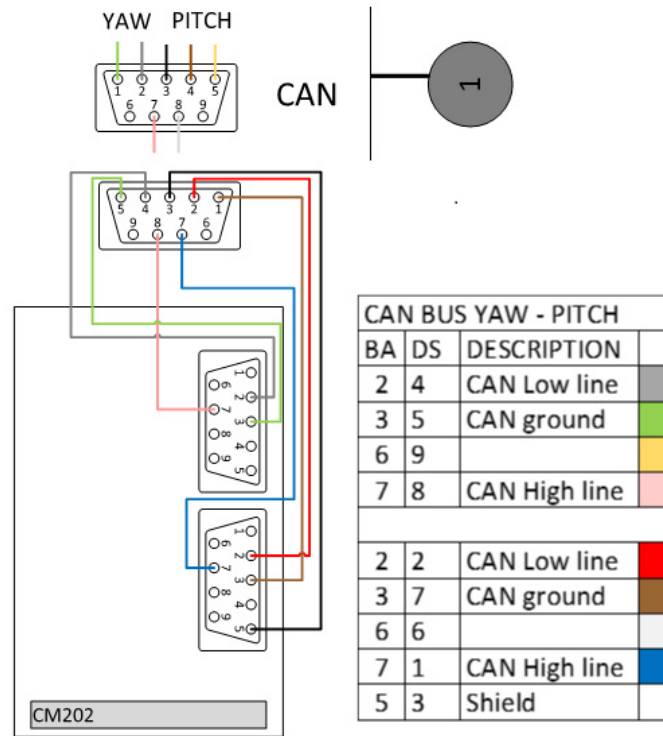

Figure 4.6: Wire map: CAN

Both EPOS (for pitch and yaw) deliver three cables to connector one, the low, high and ground line. There is also an optional shield pin. The pin assignment between the Bachmann connector and the CM202 module of the Bachmann is identical for both channels.

4.4.3   Pitch mechanism

For the collective pitch, the wiring is very similar to the one of the G1, but only one EPOS2 is used. There are still three amplifying boards, which are smaller and slightly different but the connections are very similar. Figure 4.7 shows a scheme of the connections used in the G1, where three EPOS2 boards are used (one per blade). For the G06 the connections are the same but just using one board.

The side of the amplifying boards that connects with the strain gauges already has a connector labelled with a 'G'. The ones going to the slip ring are labelled with an 'S' and also carry a connector, which probably has to be removed since each board has two cables going to two different channels of the slip ring and two going to the power supply, which comes from the slip ring and is distributed in the hub with a connector to share voltage in parallel.

The information from the amplifying boards goes through the slip ring to connector 2, which

connects to another AI0288 module in the cabinet set for loads. To this module also the tower loads are connected, but these connections are identical to the ones of the G1.
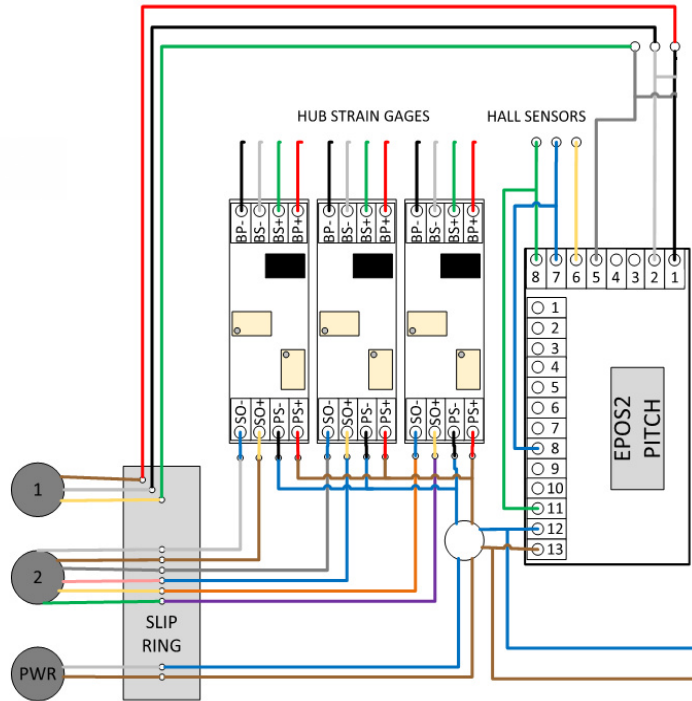

Figure 4.7: Wire map: Collective pitch

Implementation of the yaw mechanism

5.1   Components design

Once the yaw system was validated on the wind tunnel, a way of implementing the TK+ proposal together with the CP gearhead and the motor in a compact way within a similar airfoil profile must be found. Not only the old base of the G06 must be redesigned to contain the system, but two coupling pieces have to be designed to transmit the torque between the Maxon RE40 Motor and the CP and between the TK+ and the tower. This chapter will cover the design of these components, then justify the motor selection with a Simulink model and will finally summarise the test performed to check that the system is capable of performing the movements analysed in the simulations. The final drawings of all the components are included in the Annex.

5.1.1   Support structure design

The base of the tower has two main functions: withstand all the loads from the whole turbine and transmit them to the floor while being soft enough not to change the natural frequencies of the model too much. With the implementation of the new yaw system, the old aluminium square base has to be replaced. Furthermore, another critical function that it must accomplish is that the TK+ is fixed to it. The TK+ has a rotating protrusion with 64 mm diameter that has to go through a hole with a H7 tolerance, and a bigger 79 mm one that has to be fixed to the support structure with seven holes with a M4 thread.

The new base or support structure must be an optimum design between two constraints. On the one hand, it has to be big enough to cover the whole system, while there must be enough material or section to avoid a significant reduction in the natural frequencies of the model. Not only it has to be compact since it has to be covered with an airfoil, similarly to the one used for the experiments in the wind tunnel to test the suitability of the system; but it also needs to have a robust, thick enough flat surface where the fixed part of the TK+ can be screwed to ensure the proper transmission of the torque.

The design of the structure was an iterative process, which started at the same time as the design of the NACA0030 airfoil for the wind tunnel, given that it had to fit inside. Then it was tried to make it as small as possible, assigning only slightly bigger dimensions to the ones needed to fit the TK+, leaving the thickness as the final free parameter to iterate for reducing the impact on the frequencies.

The impact on the frequencies was studied in 'Autodesk Inventor' with the nodal analysis environment tool. The updated 3D model for the assembly of the G06 was used to check the natural frequency of the system. Due to the complexity of the model, that leads to convergence issues, it had to be simplified. The nacelle and the hub were assimilated to a cube with similar dimensions, same mass and inertia.

Figure 5.1 depicts this simplification of the model, where the calculated model frequency of 25.89 Hz can be seen. The estimated measured frequency on the G06 campaigns was between 18-20 Hz. Considering the simplifications and the deviation of the model characteristics, this value gives a good approach for studying the reduction of the system's natural frequency. Since only the percentage change in the frequency is interesting, this deviation from the obtained frequency is not meaningful for the study.
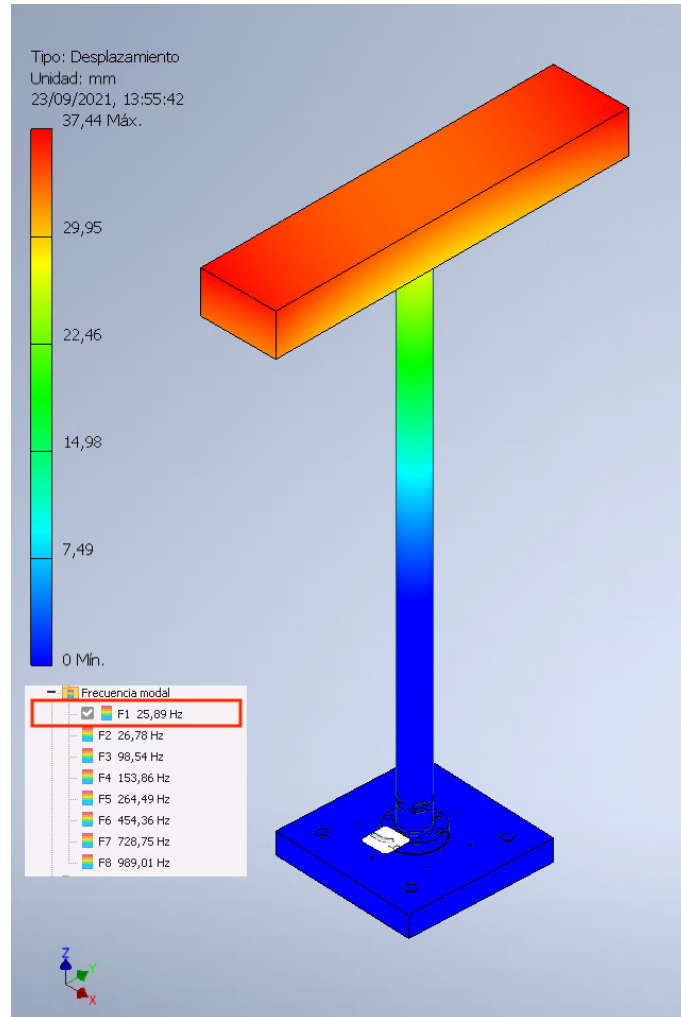
Figure 5.1: 3D model for the natural frequency study

The objective is to limit the frequency reduction to a maximum value of 1%, which corresponds to 25.63 Hz. Different thicknesses for both aluminium and steel were analysed to obtain the minimum thickness needed for that reduction. Even if the whole model is made out of aluminium, steel was considered to prevent because for the same frequency reduction, a more significant thickness out of aluminium is obtained, which could excessively increase the size of the support structure.

Figure 5.2 represents the obtained curves for different thicknesses of the support for the two materials. It can be seen that with steel, 15 mm is the first value over the 1% limit, while for aluminium, the minimum thickness is 25 mm. Given these results, it was decided to make the structure out of stainless steel with a 15 mm section.

The final height of the support structure with that thickness is 101 mm and thus lower than the one of the cylinder (120 mm) tested on the wind tunnel, so there is still some room for the coupling pieces. A aluminium base of 25 mm section, would not only left only 9 mm for
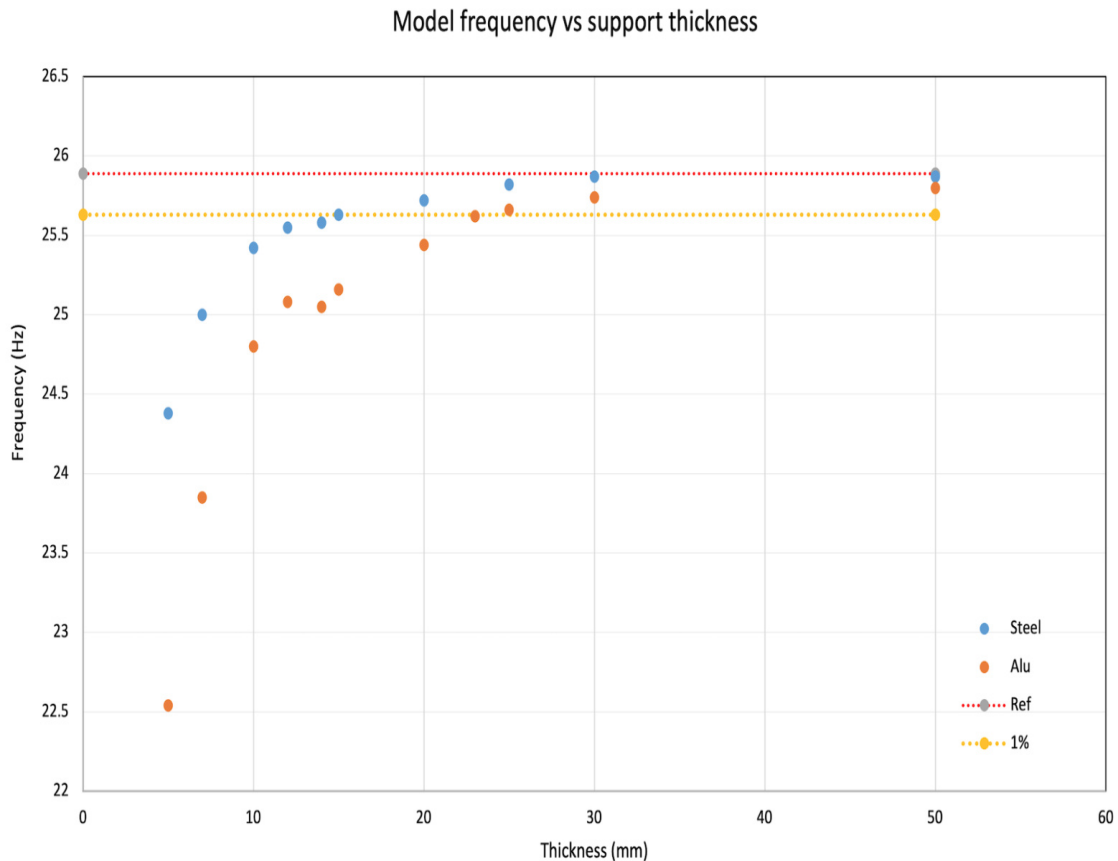
Figure 5.2: Steel and Aluminium thickness effect on the model's frequency

the coupling pieces, but would also have increased the length of the airfoil considerably since the chord increases significantly with the thickness of the airfoil. The drawing of the support is available in Annex 7.

5.1.2 Coupling pieces

While the TK and the CP are connected with an adaptor piece from the manufacturer company 'Wittenstein', two coupling pieces have to be designed to connect the tower and the rotating part of the TK+; and the motor and the CP shaft. These pieces are pretty critical since a lousy design could reduce the proper transmission of the torque considerably or damage the motor or the TK+ if, for example, the shafts are not correctly aligned.

The connection between the tower and the TK+ has to be performed through 8 M5 holes. Not only is it essential to obtain an efficient transmission, but the height has to be as small as possible to avoid surpassing the height of the airfoil tested in the wind tunnel. The first concept was to try to realise the coupling with only one piece, but it was impossible to do it compactly since the holes for the tower and for the TK+ were overlapping at a same diameter length. The final design consists of two pieces connected between them with a total height of 23.50 mm, which gives a total height of 124.50 mm. Both of them have a 70 mm external diameter and are connected with eight M3 holes.

Figure 5.3a shows the first part of the coupling, where the holes of the tower base are allocated, while Figure 5.3b has the holes needed to connect the rotating part of the TK+, which

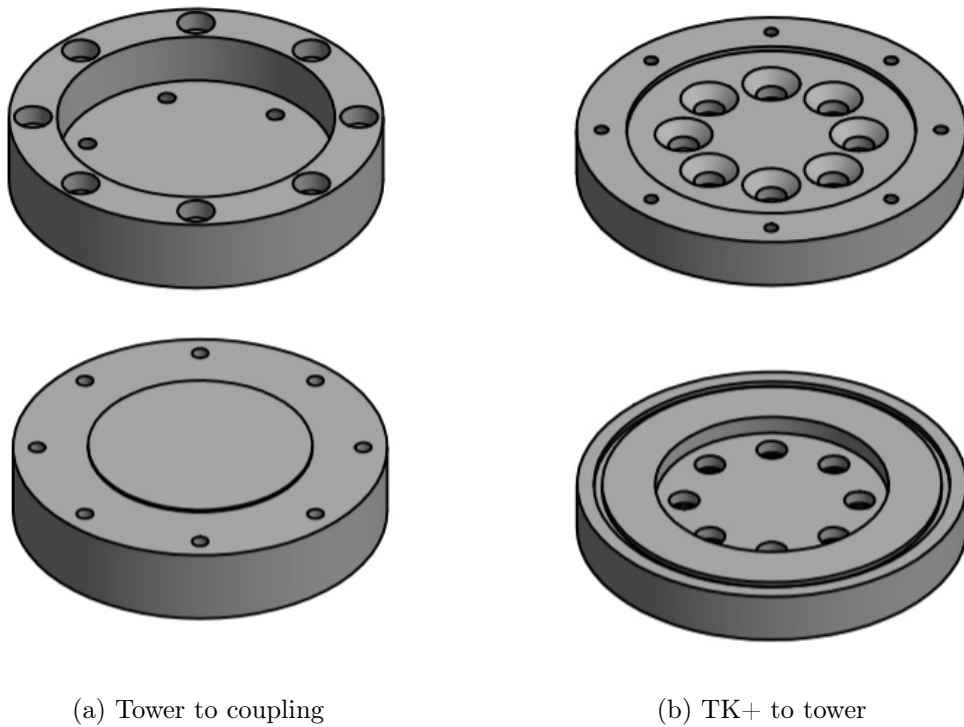(a) Tower to coupling   (b) TK+ to tower

Figure 5.3: Coupling tower and TK+

are made with a countersunk, so the surface in contact with the other piece is flat. These special screws were bought together with other high-quality screws and nuts in the shop 'Schrauben Preisinger', and they are appropriately labelled in the G06 cluster. At the bottom part of the coupling to the TK+ a small groove of 1 mm depth had to be made since there was some friction with a TK+ protrusion preventing the maximal torque from being transmitted.
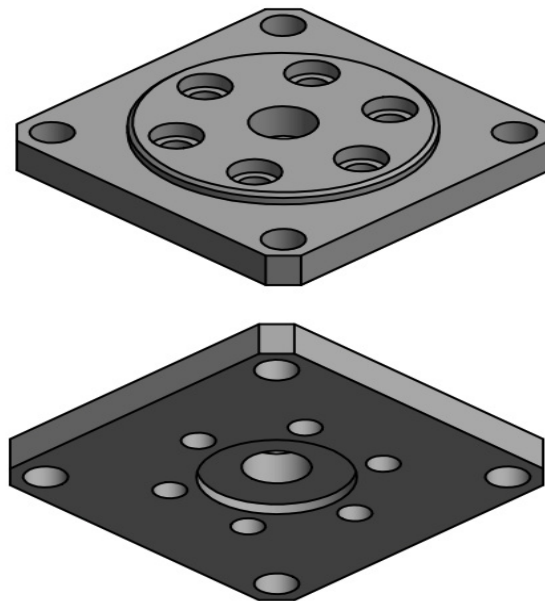

Figure 5.4: Coupling CP and Maxon Motor

Between each cylindrical connection, one piece always has a part acting as a hole and the other a step acting as a shaft to ensure concentricity. Figure 5.4 represents the piece designed

with the correct tolerances to align appropriately the shaft of the motor and the CP, which also follows this principle to achieve concentricity. At one side the motor is fixed, while at the other side a 31 mm diameter protrusion coincides with a hole in the CP to ensure concentricity.

The RE40 has a large diameter, which, when plugged into the piece is causing some friction with the head of the screws located at the four external holes, which are attaching the piece to the TK+. Due to this reason, screws had to be brought to the workshop, where some material was removed from their heads.

The final drawings of the pieces with the modifications for future versions are available in Annex7. Despite being manufactured out of an aluminium alloy, this turned to be very soft and the threads are easily damaged. It was agreed on producing future versions out of steel to prevent this from happening.

5.1.3   Assembling process

The yaw system has been designed with the objective that it is a separate block to the turbine, so any turbine can be placed at any moment on top of it. One system has been assembled and there is material to assemble another one. The necessary pieces are listed in Table 5.1.

Table 5.1: Yaw system components

Code	Component	N°per turbine
5.1	Support yaw	1
5.2	Tower coupling sup	1
5.3	Tower coupling inf	1
5.4	TK+	1
5.5	CP	1
5.6	RE40 with encoder	1
5.7	CP-RE40 coupling	1
5.8	Wittenstein coupling	1

The assembly starts fixing the G06 to the steel support, whit the 7 holes. This ones go trough in the manufactured support (5.1) and are ensured with anti-friction nuts, but for the future supports it is preferred that the TK+ is screwed in M4 holes.

When the TK is fixed, the CP can be connected to it with the coupling pieces that 'Wittenstein' provided (5.8). The CP shaft must go inside, and a tightening torque of 9.6 Nm has to be applied with the torque wrench. Before doing it, clean the shaft and all the surface that are in contact.

The next step is to connect the motor (5.6) to the CP (5.5, also cleaning all the surface first) using the designed coupling (5.7). First the motor has to be fixed to the coupling with small M2 screws, and then the other side of the coupling (which has a protrusion behaving as a shaft) must be inserted inside the CP, where a 31 mm diameter is located. The motor shaft has to go as deep as possible into the CP, and a tightening torque of 6 Nm has to be applied. Finally, check that the torque is transmitted through the whole chain of components.

Finally the coupling pieces for the tower have to be mounted. First the inferior (5.3) part has to be fixed to the TK rotating part with the available countersunk screws. Then the superior

piece (5.2) can be connected above or first screwed to the tower, and plug it together with the tower above the inferior coupling piece. Check that the torque is also properly transmitted through all the screw joints.

5.2   Motorset simulink model

When the right angle gearbox system was chosen as the final solution, a gear total gear ratio of 100 was proposed. Before ordering the motor, it had to be checked that this ratio (tau) is the most appropriate one and that it allows the system to handle the pretended yaw dynamics movements. The most demanding movements are sinusoidal signals. The G06 aims to improve the performance of the G1 yaw system, being the objective at least to follow a demand signal of 5° at 2Hz frequency.

The motor drive set will be composed of a Maxon DC Motor from the RE series (as it is in the G1), a gearhead from the company 'Wittenstein' (called CP), which has lower frictional torque and backlash and has better compatibility with the TK, which is the last component. The TK and the CP gearhead are connected with an adapter plate from the company, while the CP and the motor are connected with an in house designed piece. The Maxon Motor is controlled with the same EPOS2 board used in the G1. Even if more powerful boards are recommended for the selected motor, it is also interesting to check what capabilities can be achieved with the EPOS2 boards already available in the lab.

The parameters to be designed are the gear ratios of both the TK and the CP and the motor's power. In order to do that, a Simulink model was built to check the influence of those parameters in the tracking of the sinusoidal demand signal and that any variable (power, torque and current) is below the nominal one of each component. The data-sheets with all the final parameters of the motor and its encoder, TK+ and CP are included in the Annex. Looking at the high frictional torque of the CP, and with the aim of having a more powerful system, the iteration started with the RE40 model (supplied at 24V) instead of the proposed in the previous sections RE35 model. For a small difference in price, the power increased from 90 to 120 W and the nominal torque from 107 Nmm to 177 Nmm.

5.2.1   Description of the model

The model pretends to recreate all the phenomena affecting the performance of the motor set. Figure 5.5 shows the environment in which the yaw control model is embedded. A sinusoidal wave is compared to the reference, and goes to the control loop. Two scopes are used to look at the demand tracking and the control signals.

The control signals are mainly: the yaw performed (following the demanded signal), the motor's current, and the torque at the output of the motor and the gearbox (the final one applied to the tower). These signals have to stay under the nominal one, which are 3.17 A and 177 Nmm for the motor, and 20 Nm at the TK+. An example of the scope results is shown in Figure 5.6a for the demand tracking and in Figure 5.6b for the control signals. These results correspond to the design point of 2° at 2Hz sampled during 8s, with the parameters of the RE35. It can bee seen, that it is already working in its limit.

The control loop (yaw model) is depicted in Figure 5.7. It can can be divided into different blocks. The red block is the control of the model, in this case, a PI with auto-tuned gains. Even if these could be tuned more carefully to get better performance, they will be more or less similar to those obtained with the autotune wizard of EPOS Studio in the control board.
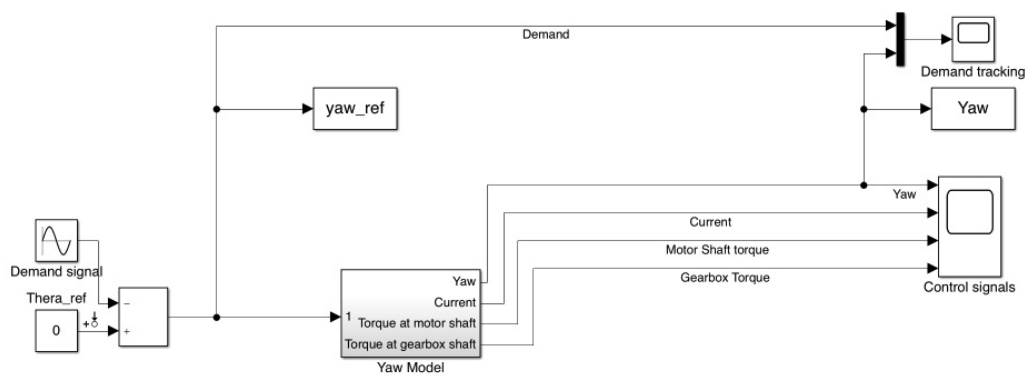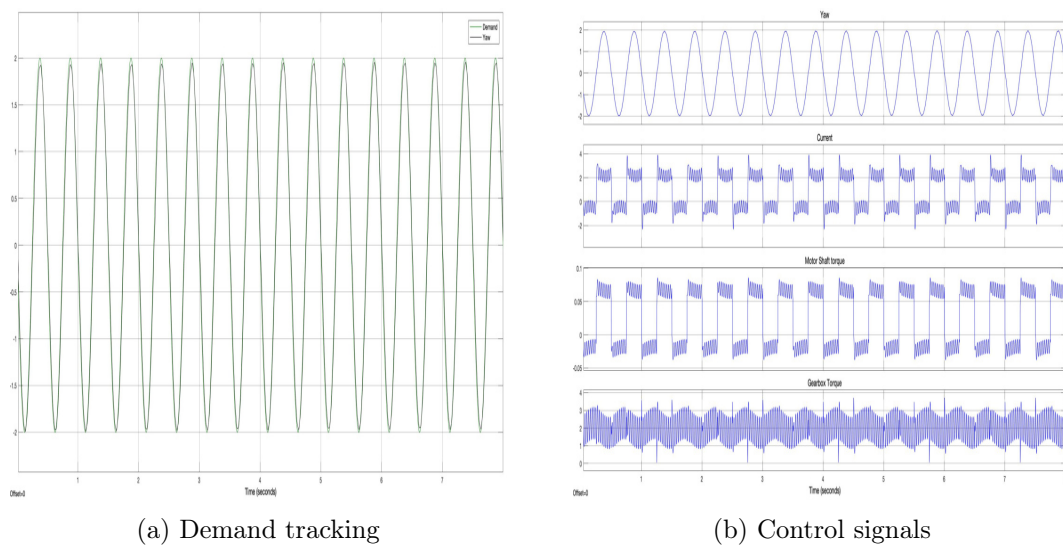
Figure 5.5: Simulink model of the motorset

(a) Demand tracking

(b) Control signals

Figure 5.6: Design point 2° at 2 Hz

In the blue blocks, the characteristics of the model (for instance, its total inertia, which was calculated with Inventor, taking into account the designed support) and the ones of the motor are highlighted. The characteristics of the motor are given in the datasheet: inertia, rpm-constant, torque-constant, inductance and resistance. The iterations started with the RE35 motor, which was not able to follow many movements. That is why it was decided to use RE40 and try to iterate with the CP and TK gear ratios.

The grey blocks account for the efficiencies and gear ratios (tau) of both the CP and TK, which have the most significant effect on the model since they affect the torque to the second power. In a physical sense, what happens is that if the total reduction rate is too high, the motor needs more torque to accelerate itself and cannot provide enough torque. In general words, the smaller the total tau, the better performance. On the other hand, if the torque reduction is too small, a more powerful motor is needed to provide the same torque to the tower.

Finally, external forces are modelled in orange. These are the aero-yawing moment, which was set according to the calculations to 2 Nm, the viscous forces, and the spring moment to prevent backlash. The last one is set to 0, as there is no spring and the backlash is pretty small. All these forces are inputs into the big block with an opposite sign of the total output torque at the TK (after the grey blocks). The frictional torque of the TK (0.2 Nm) was also modelled after a filter and before the block, where it is being subtracted from the torque after the CP.
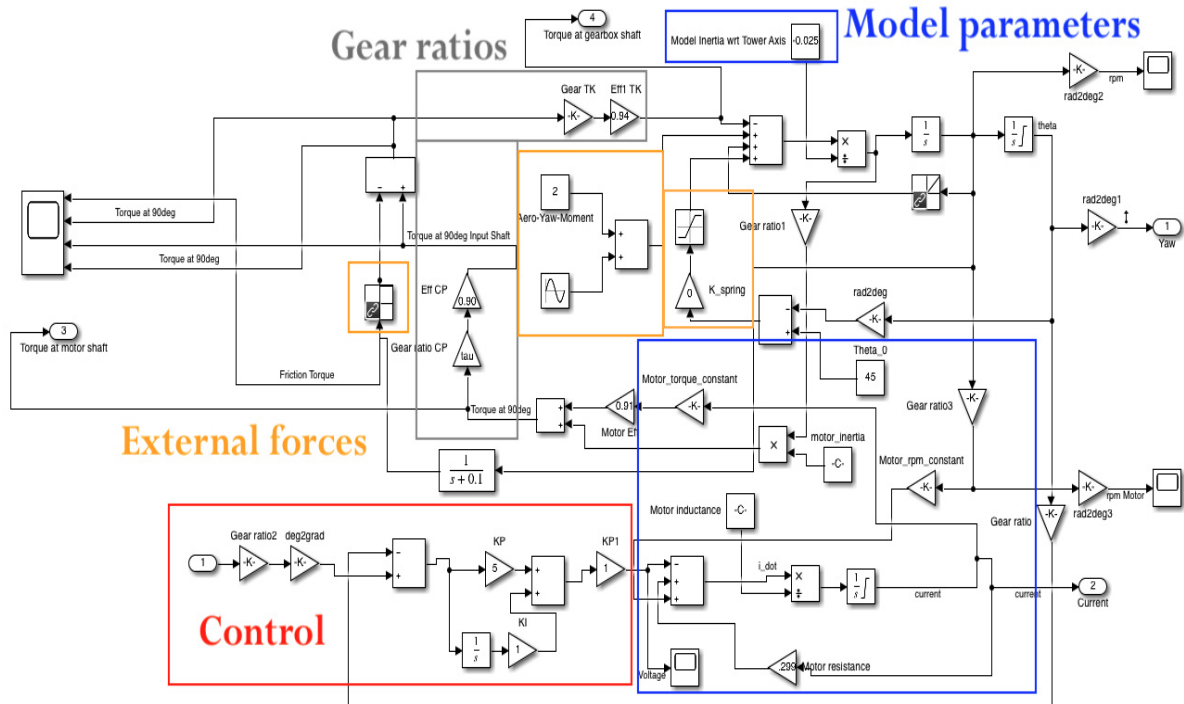
Figure 5.7: Simulink model of the motorset

5.2.2 Results of the simulation

First, the tracking of the demanded signal was tested for different amplitudes and frequencies. At 2 Hz it is possible, according to the model, to follow waves up to 10° of amplitude (highest amplitude value interesting for dynamic yaw) without any kind of phase shift appreciable. Taking into account that the design point was set to 2° at 2 Hz, this result suggests quite a good performance.

The system was tested further to check its limitations according to the modelling. Problems started to come up at 3Hz. Even though there is a good match between the setpoint of the signal (blue curve) and the real movement (green curve) up to 7°, as Figure 5.8a and Figure 5.8b show, at 10° (Figure 5.9c) the motor set can no longer follow the signal properly.

The performance at 5 Hz was also tested extensively, even playing a bit with the gains of the controller. Nevertheless, it was only achieved to follow the signal with a 2° amplitude (Figure 5.9a), but it is no longer possible for higher amplitudes as shown in Figure 5.9b and Figure 5.9c. Other extreme operation situations are 7° at 4 Hz (Figure 5.10a), which was possible at 3Hz, and the highest frequency that can be achieved at 2° is 8 Hz, being the tracking at 3° and 8 Hz impossible as shown in Figure 5.10b.

It is important to bear in mind that this model is only a tool to size the motor and the gear ratio of the CP and the TK+. It will be interesting to check if the system will actually be able to perform these movements since 8 Hz is such a high frequency, which will actually probably never be used. 5 Hz is actually quite an improvement from the 2 Hz maximal frequency of the G1.

Regarding the sizing of the model it was observed that the proposed total gear ratio of 1000 was too high, and the model suggested that the motor would not be able to decelerate at frequencies higher than 2 Hz. This was seen as a limitation, and given that the RE40 provides

(a) Amplitude 5°

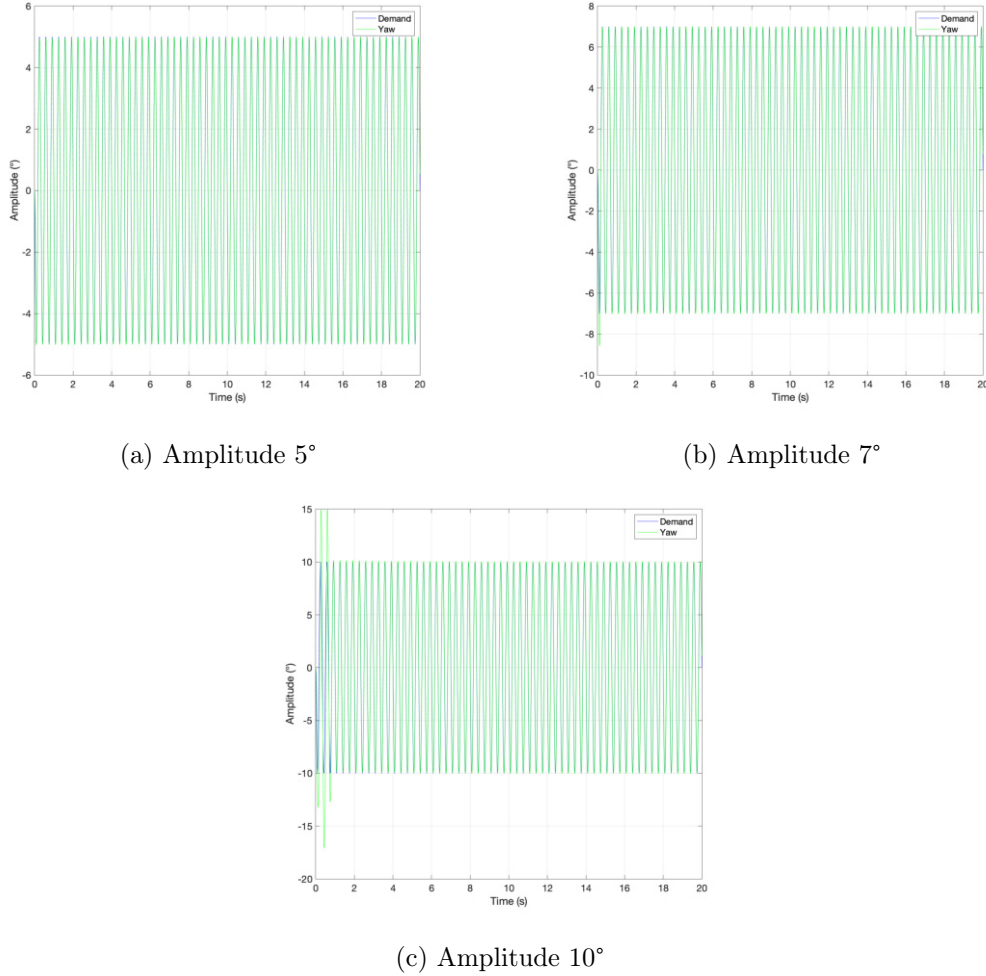
(b) Amplitude 7°

(c) Amplitude 10°

Figure 5.8: Results for 3Hz frequency

already a high torque and there is no problem to counter the aerodynamic yaw moment, it was decided to set a total gear ratio of 100.

All the simulations shown in the pictures were carried out with this parameter. It was divided as i=5 for the CP, and i= 20 for the TK+, which was the most balance share between both components. A lower total ratio would impose the need of increasing the power of the motor to obtain the presented movements and higher ones suggest that even at 2 Hz it could be problematic to track the signal. Therefore 100 seemed to be the optimal ratio.

Apart from checking the target and obtained movement, it is vital to check that the current at the control board and the torque at the motor and gearbox output do not exceed the nominal ones, which have also been predicted with the model. It is important to remark that the performance check will be carried out with the small EPOS24/2-530239, which has a nominal current of 2A but the idea in the future is that a bigger EPOS50/5 will be implemented, which can withstand up to 5 A and will therefore allow performing more demanding movements. The nominal torque of the motor is 177 Nmm, and the one of the TK+ is 15 Nm.

The scope of the operational points shows that the motor and the gearbox are far from their maximum operational points, so even if the frictional losses had been underestimated, there should be no problem with these variables. What constraints the signals which can be followed is the current flowing through the motor and the control board. The motor can work at is nominal point at 6A, but the big EPOS2 board only with 5A, higher currents would saturate
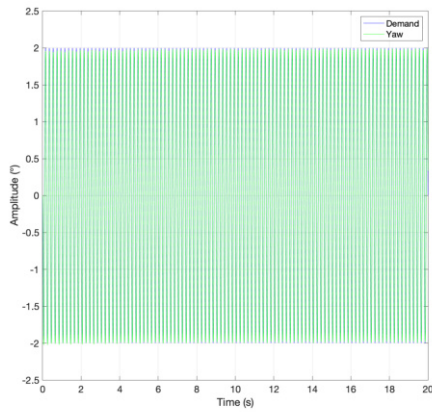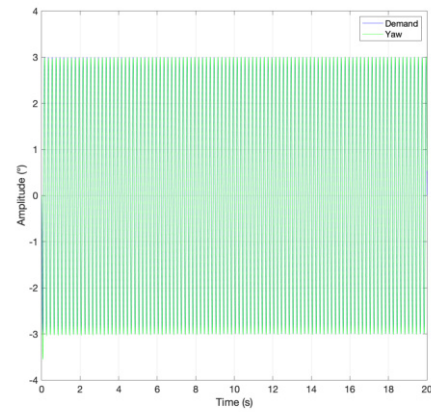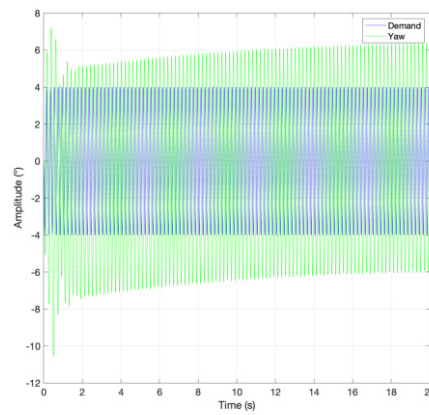
(a) Amplitude 2°

(b) Amplitude 3°

(c) Amplitude 4°

Figure 5.9: Results for 5Hz frequency
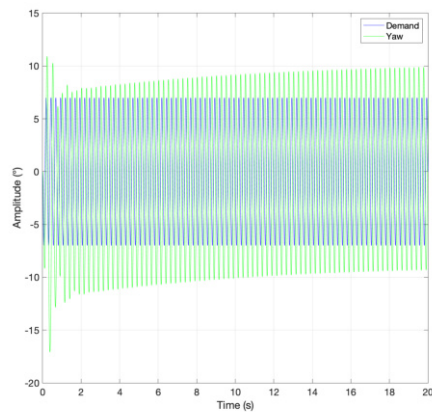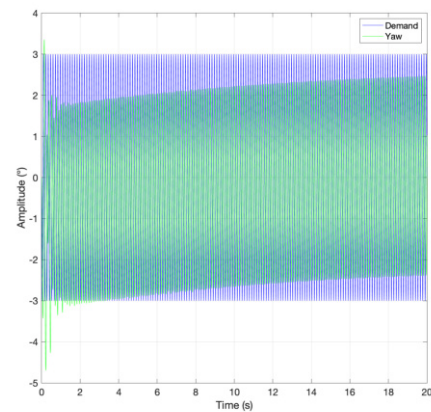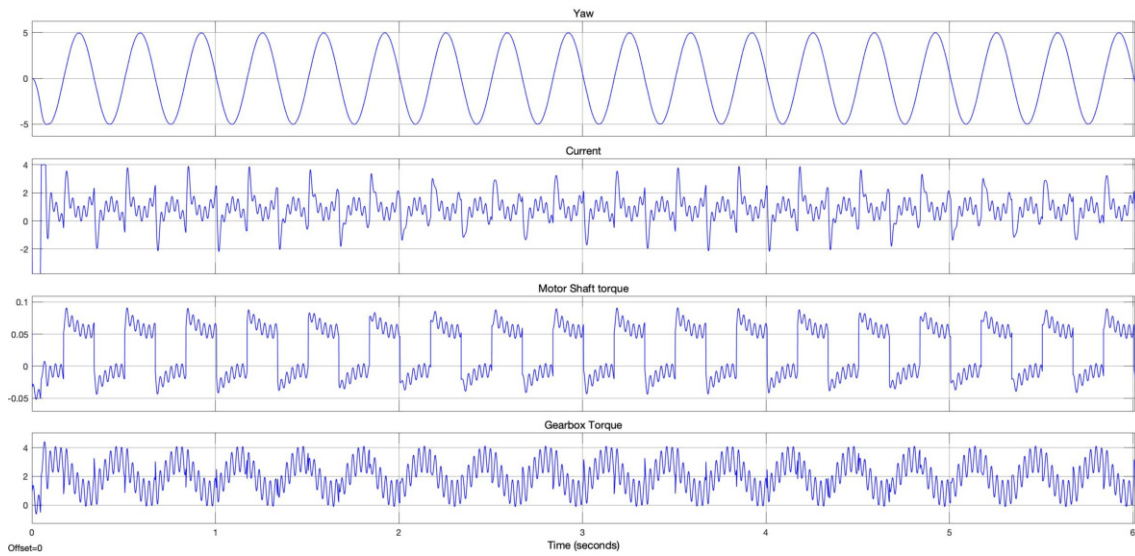

(a) Amplitude 7°-4Hz

(b) Amplitude 3°-8Hz

Figure 5.10: Results for other extreme cases

the system. At 2Hz there all the parameters are under the nominal values. The designed point was already shown in Figure 5.6b, where it can be seen that the motor and gearbox output are far away from their maximum operation points

At 3 Hz and 4 Hz, the critical amplitudes are 5° and 4°, respectively (Figure 5.11a and

Figure 5.11b), where the current starts to saturate in the second case, being this point the limit.
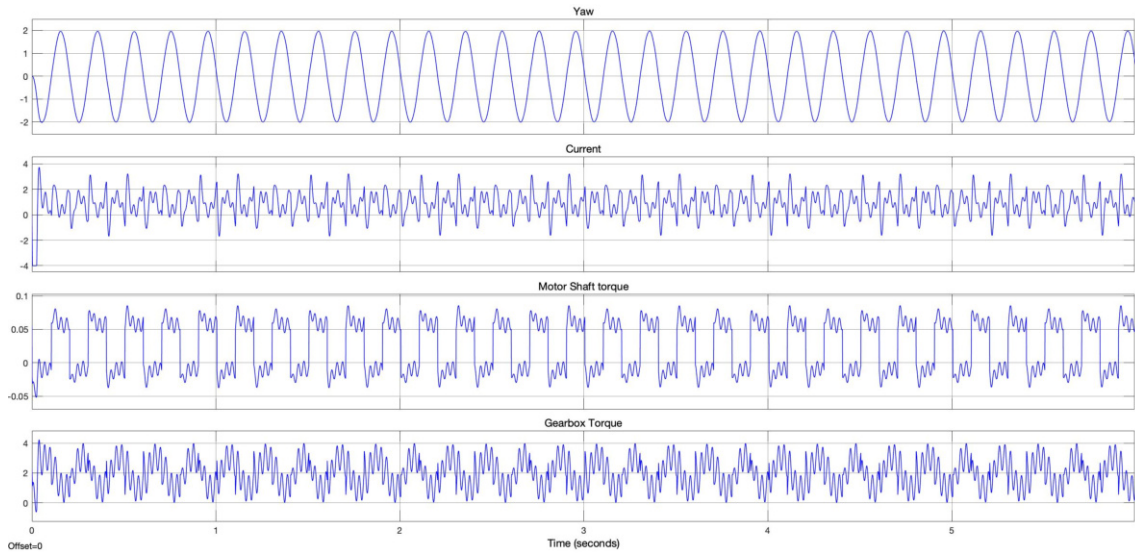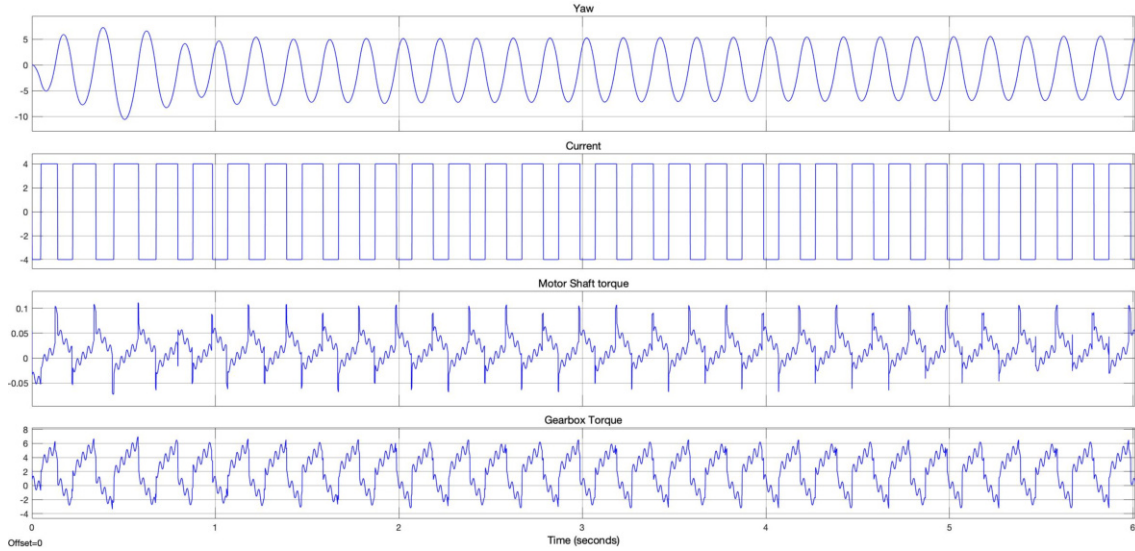

(a) Amplitude 5°- 3Hz
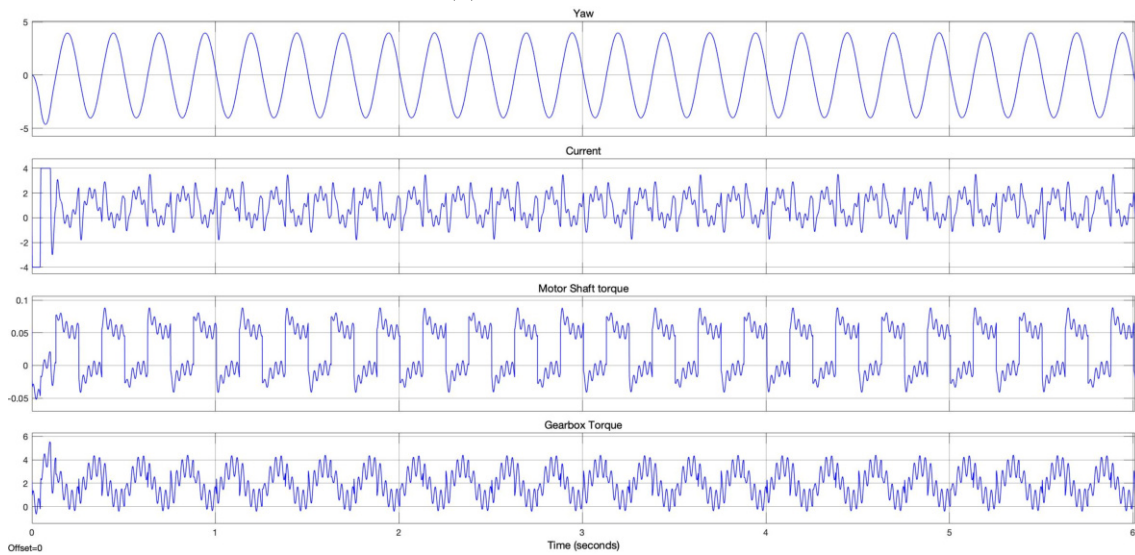
(b) Amplitude 4°- 4Hz

Figure 5.11: Control signals check at 3 Hz and 4 Hz

At 5 Hz, the saturation of the current can be observed as more amplitude is demanded (Figure 5.12a and Figure 5.12b), showing a square shape in the second one for a 4° amplitude.

(a) Amplitude 2°- 5Hz

(b) Amplitude 4°- 5Hz

Figure 5.12: Control signals check at 5 Hz

5.3   Performance test

To verify that the designed system can follow the demanded signals as expected with the Simulink model, the system was assembled, and dynamic yaw was performed for different amplitudes and frequencies. The experiment's setup will be first explained in detail in the following subsection, and the results will be later summarized.

5.3.1   Experimental setup

The first step to carry out the experiment was to assemble the motor, CP and TK+ as explained in the last Chapter. The motor uses a three-channel encoder that can provide only relative position, as the homing method has not been implemented. The setup can be seen in Figure 5.13. As it can be seen, the control board is supplied with a power supply with 24 V, and a 12 Ω resistor is connected in series. The resistor's role is to drain the current when the

motor is decelerating since the power supply cannot absorb it, which allows it to perform faster movements.

The control board used is the EPOS24/2-530239, as in the G1, which can only withstand 2A. This is a limiting factor, which prevents the system from performing more demanding movements, which require higher currents. The board has a safe mode, which activates when the temperature is too high (when operating in currents higher than 2A for a given time). The system was tested to the limit, but it was always because of the board that no more demanding movements could be achieved, constantly entering in this safe mode.
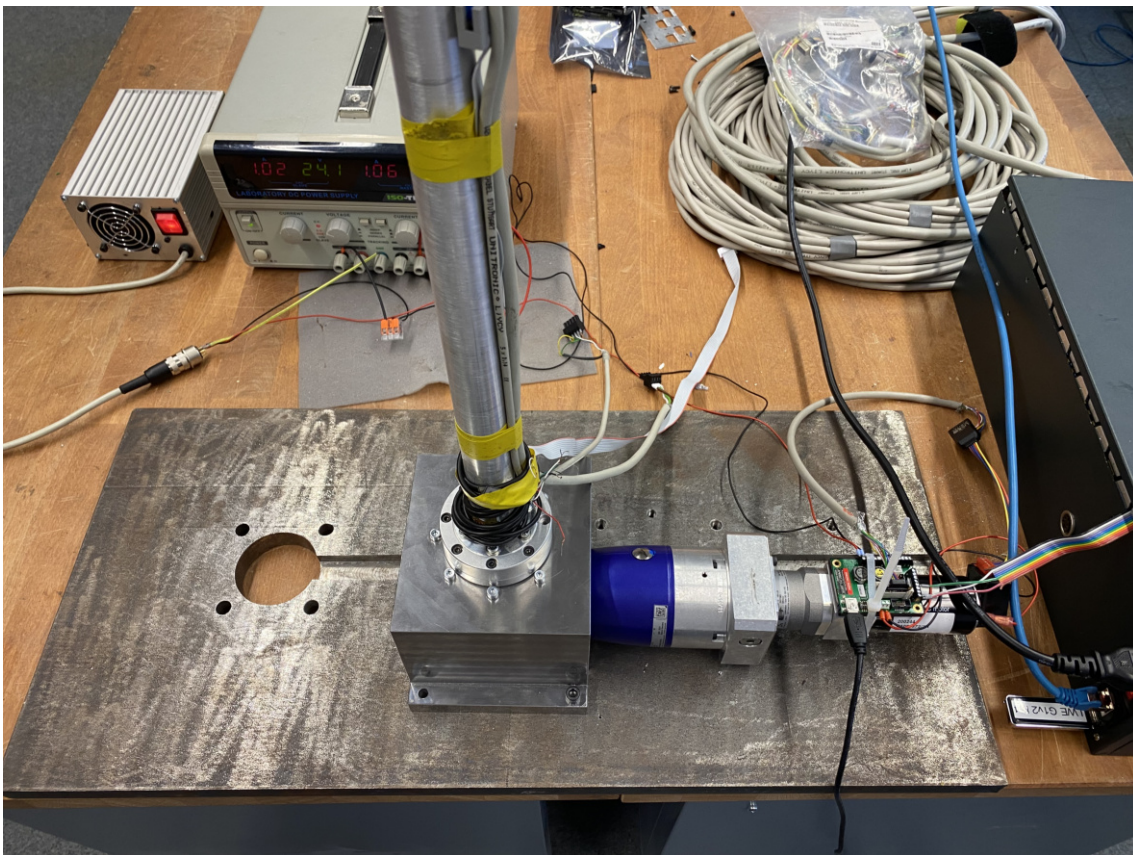

Figure 5.13: Performance test experiment setup

The board was connected to the Bachmann, and it was programmed with the code from the G1 yaw application. Some parameters were changed to adapt the code to the G06, such as the current and yaw angle limits and adjusting the motor pulses to yaw angle ratio, which was 0.009 for the G1 but 0.0018 for the G06 with the new motor. Furthermore, some of the communication delays were set to 0 to be able to move faster.

5.3.2 Experiment results

The first thing to check was to see if the system could move in both directions fast and accurately in static yaw conditions, and then a testing matrix for dynamic yaw was prepared. Even though the system was designed to follow a demand signal of 2° of amplitude at 2Hz, greater amplitudes (up to 30°) and their limit frequency were tested. The first positive conclusion is that the designed movement was easily reached even with the small board setup. All the measured points were also recorded on video.

The results for all the measured points (amplitudes 1 to 10, 15, 20 and 30° and increasing

frequencies until board safety mode) were saved with the Bachmann recording structure and post-processed in Matlab. Additionally, the current flowing through the motor was controlled with EPOS Studio, where it was checked that the current started to saturate in the boards some seconds before entering the safe mode and the turbine starting to rotate slower. The movements were recorded for 60 seconds.

One example of the problem with the board is shown in Figure 5.14, which correspond to a signal of 8° and 2 Hz. The demand was being correctly followed until the board prevents it to keep doing it after 18 s. This can be seen in the EPOS Studio scope, showing Figure 5.15a that the current (4A) was too high and then after the 18 s, Figure 5.15b shows the current saturated at 2A. This second figure also shows the mismatch between the demand and actual position. For all of the studied amplitudes, the frequency was increased until finding the point at which the board limits the system.
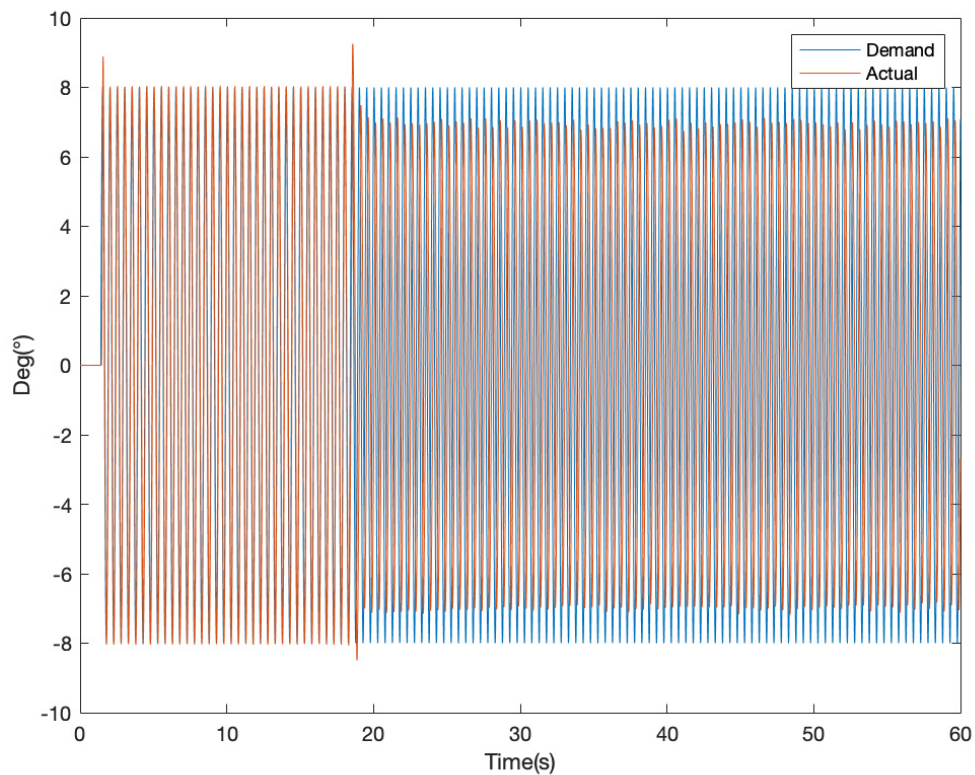

Figure 5.14: Safe mode example

The Matlab curve fitting tool was used to obtain the amplitude and phase of each movement's demand and actual position. The way to analyse the results is to obtain the amplitude ratio between the measured position and the demand (A_{meas}/A_{dem}) and the phase shift (ϕ) between both signals. Besides, two scenarios were considered, first with current limit (using the curve fitting for the whole 60 sampling seconds, even in safe mode is activated) and without current limit (calculating the amplitude and phase only during the seconds before safety mode). This second scenario tries to recreate what could be achieved if the bigger EPOS board was used.

Figure 5.16a shows the results for the amplitudes for the whole 60 s sampling time. The (A_{meas}/A_{dem}) ratio is plotted against the tested frequencies at the bottom y axis, while the corresponding Strouhal number (St) to each frequency is indicated in the upper y axis. The Strouhal number is a dimensionless number describing oscillating flow mechanisms, and is calculated as
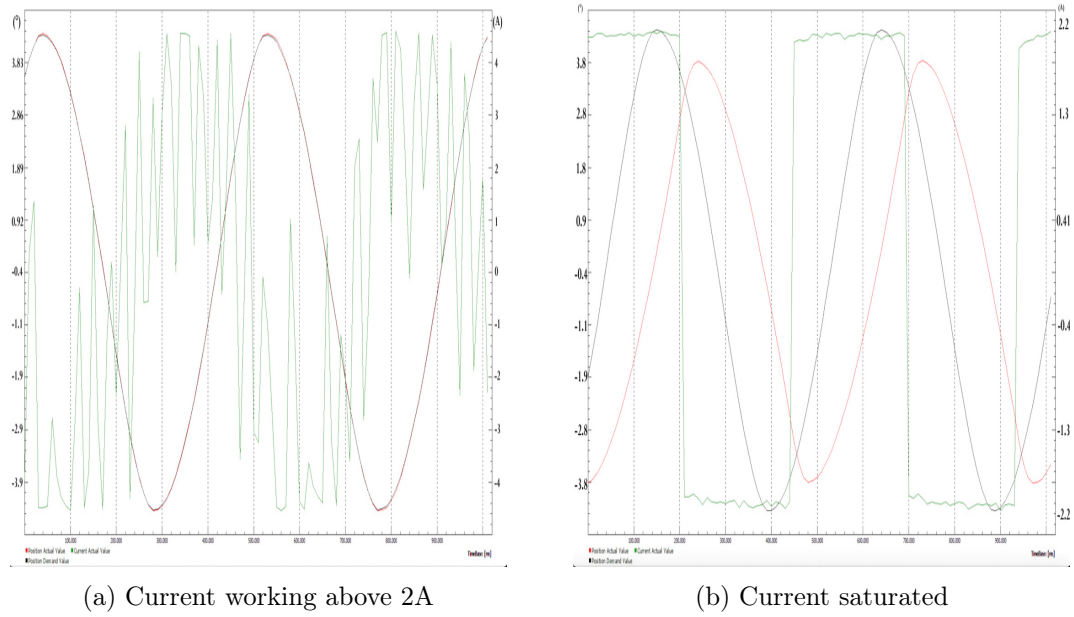
(a) Current working above 2A   (b) Current saturated

Figure 5.15: Current saturation in the EPOS2 board

shown in Equation 5.1 .

$$St = \frac{fL}{U} \tag{5.1}$$

where f is the frequency of vortex shedding, L is the characteristic length (the G06 diameter) and U is the flow velocity (rated wind speed of 10.5 m/s).

It can be seen how the maximal frequency at which the system can move, decreases when increasing amplitude. If a curve point is no longer plotted, the system could not even run for some seconds with that demand. At the last point of each amplitude curve, the board entered safe mode (generally after having been running between 15 and 30 s). The time to entry safety mode varies depending on how long the system has been resting since the board temperature is what triggers this mode. A ratio below 0.9 means that a 10% of the time, the actual position is different to the demand, which can not be accepted as a good performance. However, the system can run without going into the safe mode close to 0.7 ratios.

For 2°, 4 Hz were reached with good performance, and 5 Hz worked, but at 6 Hz the board entered in safety mode quickly and the performance is bad. Generally speaking, it can be seen that 1° of amplitude can be exchanged for 1 Hz until reaching the 8° amplitude, where the system could run for 20 s at 2 Hz. For higher amplitudes, the system worked for 0.5 and 1 Hz without any problems and with good performance, but higher frequencies were not possible for those high amplitudes. Nevertheless, at 30°, which was the maximum tested amplitude, it only worked for some seconds, being 20° the maximum possible amplitude at 1 Hz.

Figure 5.16b shows which of those points worked at least for 15 s. It can be clearly seen that the 5 Hz and 6 Hz frequencies would also not have good performance even if the other board could handle them. At 4 Hz it would be interesting to see how the system would behave for the 4° and 5° amplitude with the bigger board. The conclusion to be drawn is that 3 Hz work fine at even 6°, while at 2° all the interesting points for dynamic yaw are possible (it is strange to use higher amplitudes than 8°), and at 1 Hz all amplitudes should work.

Finally, the phase shift has to be checked to ensure good performance and avoid high delays. Figure 5.16c reflects the same issue as the amplitude for frequencies higher than 4 Hz, in principle, only a good match would be obtained at this frequency for 2° and 3°. 5 Hz and 6 Hz cannot be handled by the system. The movements 30° at 1 Hz and 6° at 3Hz are only possible with the

bigger board as shown in Figure 5.16d. Generally speaking the system shows good performance at 1 and 2 Hz and at 3 Hz for some small amplitudes, for more demanding movements the phase shift is too high.
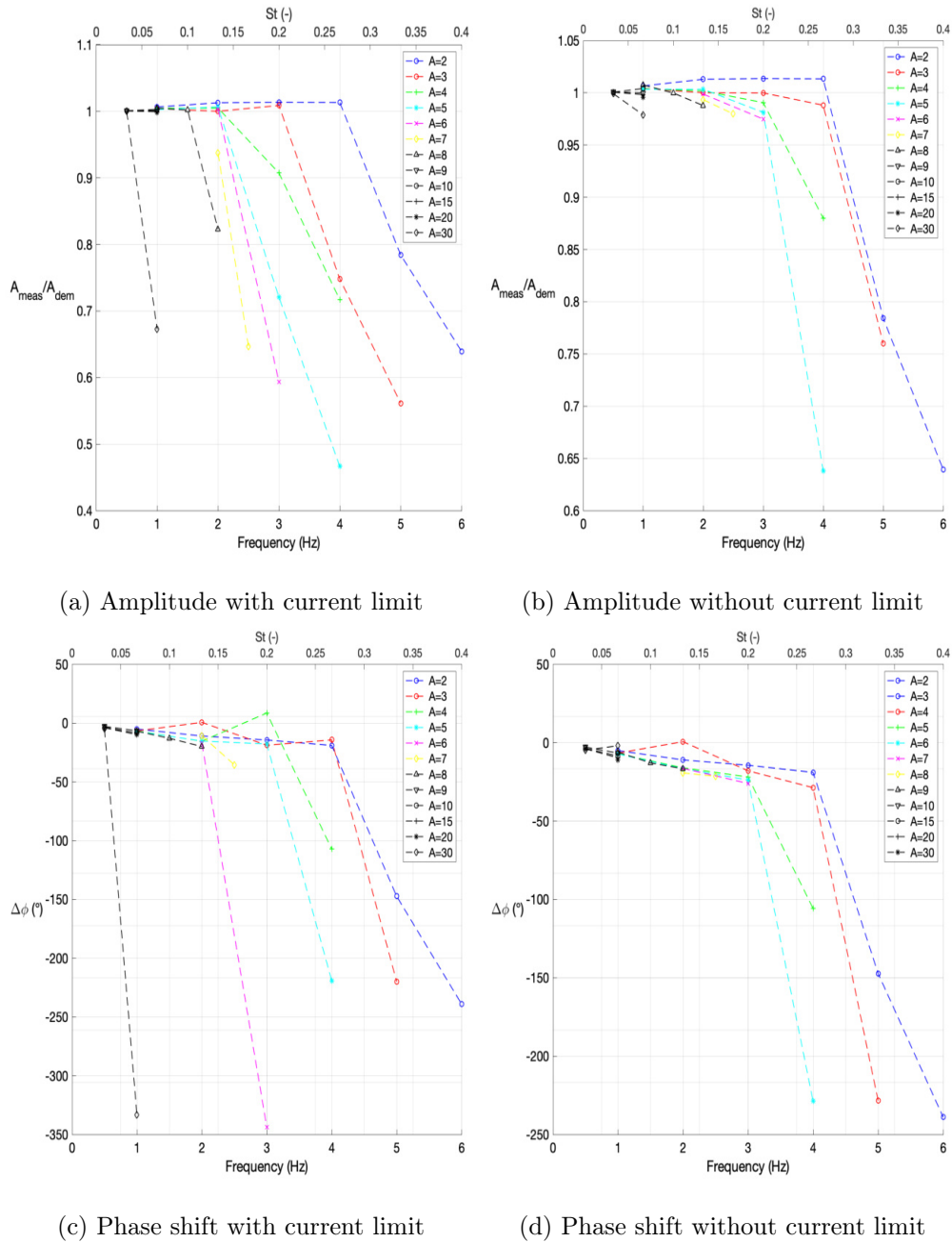

(a) Amplitude with current limit

(b) Amplitude without current limit

(c) Phase shift with current limit

(d) Phase shift without current limit

Figure 5.16: Amplitude and phase shift of the analysed signals

Conclusions

6.1 Yaw system evaluation

A complete operating G06 turbine has been assembled with a new yaw system suitable for the range of movements pretended and preventing major distortions on the wake. Not only was the system the best alternative between four different proposals in terms of price, accuracy and reliability, but also its effect on the wake was tested on the wind tunnel. A NACA0030 with a chord of 50 cm has to be 3D printed to house all the components and obtain the same drag coefficients as in the wind tunnel experiment.

The work is concluded by testing the system with dynamic yaw and checking its limitations. According to the results, the system seems to be fast, robust and accurate for both static and dynamic yaw. Even using a smaller EPOS2 control board, it can perform the design sinusoidal movement of 2° at 2 Hz without problems and can even perform better.

The performance of the system will improve significantly when a bigger EPOS2 board is implemented. This board will have to be programmed, adapting part of the code of the G1 CAN and changing some parameters, as well as the proper assignment of the pins to the Bachmann. According to the last tests, the expectation is that it will be able to run at 3 Hz for amplitudes close to 10° and at 4 Hz up to 3-4° with good performance and low phase shift. However, it will have to be tested.

Regarding the assembly of the turbine, all the process has been documented, and the knowledge has been transmitted to the department and the next student who is in charge of continuing with the development of this project. One hub with active pitch is assembled, which can replace the older hubs, and only the connection to the slip ring is to be done.

To conclude, comment that part of the work consisted of updating all the 3DCAD files of the model and making it easier to understand the different blocks of which it consists. These files were used for the nodal frequency analysis to design the support of the turbine and will be helpful for some of the future work to be done, which will now be explained. The idea is that this work helps to the future assembly of many turbines so they can run together in wind farm configuration.

6.2 Future work

Some minor improvements have to be implemented to the yaw system before running the turbine in the wind tunnel to get the most out of it, apart from implementing the bigger EPOS board. These, in a nutshell, are: printing a new airfoil, thinner and a bit more aerodynamic than the one used in the wind tunnel, but with the same dimensions; integrating a metal plate to plug the connectors similar to the one of the G1 (the aim is to use the same cables) and designing a

homing mechanism for the yaw system since the encoder provides only the relative position.
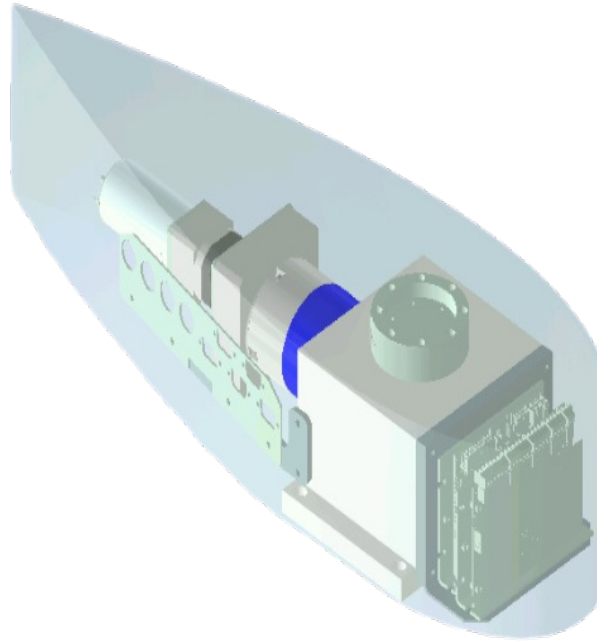

Figure 6.1: Proposal for integrating all the components inside the airfoil

Figure 6.1 shows the proposal made in Inventor to integrate the same connectors plate as in the G1 and to fix the ESCON a bigger future EPOS board in the front. The idea is to stick them together and screw them in an L shape piece while the cables go through a small hole underneath the support. Figure 6.2a and Figure 6.2b show the proposed solution for both pieces. For the connector plate, two designs were considered. The first one would be identical to the one of this figure, while the second one needs an extra piece with a 35° angle part with two holes to connect it to the CP-Motor coupling piece.
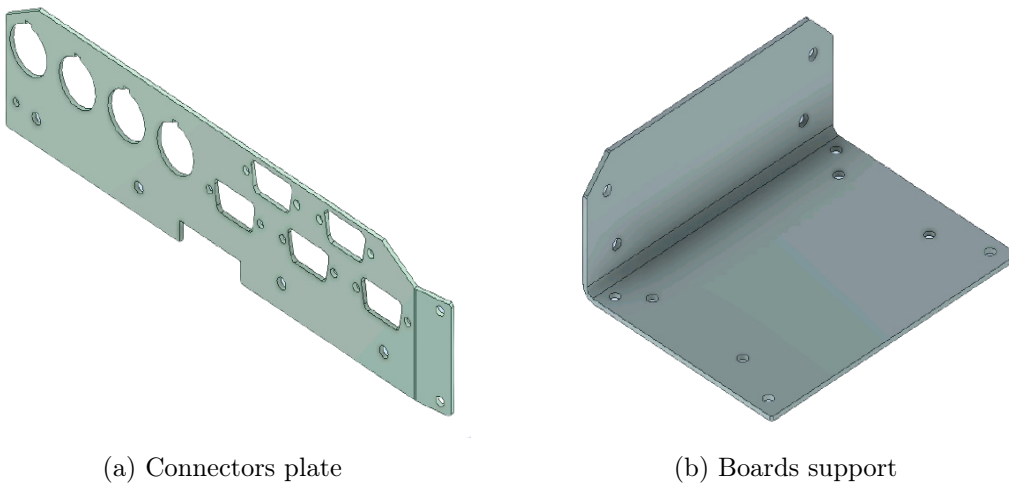
(a) Connectors plate

(b) Boards support

Figure 6.2: Connectors plate and boards support

There are two options for the connectors: it can either be attached to the base designing a

small piece and leave it hanging (Figure 6.3a) or the hole in the coupling piece of the motor can be used (Figure 6.3b). For each option a different piece is designed as shown in (c) and (d).

(a) Ground view option 1

(b) Ground view option 2

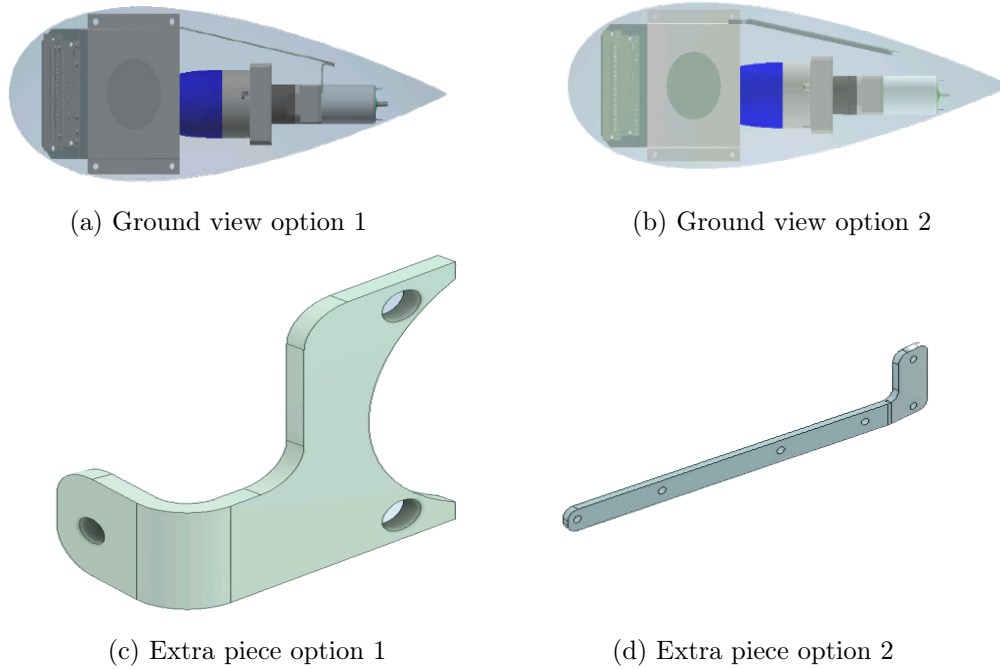(c) Extra piece option 1

(d) Extra piece option 2

Figure 6.3: Connectors plate extra pieces

The final feature to be implemented, is a way to account for the yaw homing position. For this goal normally an optical disk is necessary. The first idea was to copy something similar to the structure used in the G1, by cutting the tower at the bottom and allocate the encoder disk. Nevertheless, this could be complicated, so it was proposed to use Hall sensor like it is done for the pitch position. The sensor should be allocated in the fix part (steel support), while a magnet should be placed at the bottom of the coupling piece with the tower, as shown in Figure 6.4.
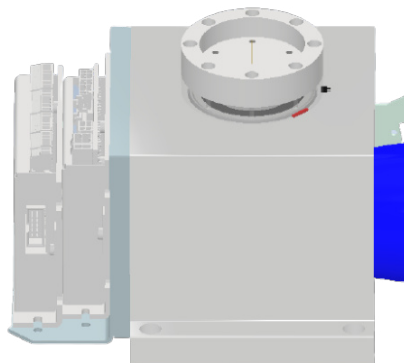

Figure 6.4: Homing position with Hall sensor

Annex

7.1   Rotatory stages

7.1.1   Föhrenbach

Föhrenbach®
Positionier-Systeme

Föhrenbach GmbH, Lindenstraße 34, 79843 Löffingen-Unadingen

TU München
Herrn Juan Llobell
Schleißheimer 56
80333 München

Unser Zeichen:	Horst Oster
Telefon:	+49(0)7707 159-14
Telefax:	+49(0)7707 159-80
Email:	horst.oster@foehrenbach.com
Vertreter-Nr.:	80
Kunden-Nr.:	K12389

Ihr Zeichen:	Juan Llobell
Telefon:	0034/647942-528
Telefax:	
Email:	juanllobell9@gmail.com
Lieferanten Nr.:	

Löffingen-Unadingen, 25.03.2021

Angebot Nr. 1211-0180

Seite 1 von 4

Vertreter:	Klaus-Dieter Kottke	Telefon:	08441/871660	
		Telefax:	08441/871661	
	Adolf - Rebl - Strasse 14	Email:	kottke.mail@t-online.de	
	85276 Pfaffenhofen			

Sehr geehrter Herr Llobell,

vielen Dank für Ihre Anfrage. Unter Zugrundelegung und Beachtung unserer Verkaufsbedingungen (Text umseitig oder als Download unter www.foehrenbach.com erhältlich), bieten wir Ihnen an:

Ihre Anfrage:	HOMEPAGE	Unser Angebot:	1211-0180
Vom:	19.03.2021		

Pos.	Menge	ME	Artikelnr. Bezeichnung	Einzelpreis	Gesamtpreis AP = Alternativposition
1	1,00	Stk	66-400744	2.630,00	2.630,00

RT2A150S36111YY0
Präzisions-Rundtisch

A	Werkstoff	:	Aluminium, schwarz anodisiert
150	Größe	:	150 mm
	Höhe	:	70 mm
S	Qualität	:	Standard
36	Übersetzungsverhältnis	:	i=36:1
1	Endschalterausführung	:	Referenz-Impuls
1	Endschaltertyp	:	PNP - Öffner (NC), 2 -kanalig
1	Antrieb	:	Motoranbau gerade
YY	Motorflansch für	:	Bitte Motortyp bei Bestellung angeben
0	Nacharbeit	:	ohne

TECHNISCHE DATEN:

Durchmesser Drehteller	: 144 mm
Durchmesser Drehtellerdichtung	: 146,5 mm
Bohrung im Drehteller	: 70 H7
Max. Drehzahl mechanisch	: 96 1/min.
Max. Drehzahl mit Motor	: max. 96 1/min.
Positioniergenauigkeit	: 0,040°
Wiederholgenauigkeit	: 0,004°
Umkehrspiel	: 0,025°
Rundlaufgenauigkeit	: 0,012 mm
Planlauf	: 0,018 mm

Föhrenbach®
Positionier-Systeme

Angebot Nr. 1211-0180					Datum: 25.03.2021	
					Seite 2 von 4	

Pos.	Menge	ME	Artikelnr. Bezeichnung		Einzelpreis	Gesamtpreis AP = Alternativposition
			Parallelität	: 0,025 mm		
			Schutzart	: IP 50		
			Gewicht	: 4,8 kg		
			Technische Daten finden Sie im Katalog RT1/RT2 unter: <https://foehrenbach.com/produkte/rundtische-und-rotationsachsen> CAD-Daten zum Download finden Sie unter: <https://foehrenbach.com/download>			
2	1,00	Stk	300004142 SN 5709.2.28.00.0.C.000 2-Phasen-Schrittmotor Drehmoment: 1,4 Nm Nennstrom: 5,0 A 400 Halbschritte / Umdrehung Schutzart Motorgehäuse: IP54 Anschluss über Sub-D 9-polig		189,00	189,00
3	1,00	Stk	300004773 KM 2SN57.CC.B.30.03 Motorkabel, Länge 3 m für 2-Phasen-Schrittmotoren der Baureihe SN 57 mit 9-pol. Sub-D motorseitig passend zur Unipos 330 Aussendurchmesser ca. 8 mm Mindestbiegeradius 7,5xd		133,00	133,00
4	1,00	Stk	300005182 KE 00H.CC.10.03 Endschalterkabel Typ Hall, Länge 3 m passend zur Unipos 330 Aussendurchmesser ca. 6 mm Mindestbiegeradius 45 mm		89,00	89,00
5	1,00	Stk	300004798 Unipos 330 SMI NA 1 Achse 48V - mit Not-Aus-System - 1 Leistungsendstufen 48V / 4,0A Nennstrom - Display: 7"-Touch - 24x Digital-Eingang PNP, 16x Digital-Ausgang - Abmessungen (BxHxT): 345mm x 215mm x 440mm		4.476,00	4.476,00
6	1,00	Stk	IB1000100 Inbetriebnahme, Parametrierung und Testlauf im Hause Föhrenbach		300,00	300,00

Föhrenbach®
Positionier-Systeme

Angebot Nr. 1211-0180	Datum: 25.03.2021
	Seite 3 von 4

Pos.	Menge	ME	Artikelnr. Bezeichnung	Einzelpreis	Gesamtpreis AP = Alternativposition
7	1,00	Stk	D10006614 Dokumentation deutsch auf CD	0,00	

Nettowarenwert	7.817,00
+ USt 19,00 %	1.485,23
Gesamtsumme in EUR	9.302,23

Die genannten Preise verstehen sich zuzüglich der gesetzlichen Mehrwertsteuer bzw. der Einfuhrumsatzsteuer.

Wir behalten uns vor, die Waren direkt aus einem unserer Lieferwerke zu bestätigen und zu liefern (Föhrenbach GmbH in Deutschland, Föhrenbach AG in der Schweiz oder Föhrenbach Precision Slides GmbH in Irland).
Bei Lieferungen aus dem Ausland übernehmen wir die damit verbundenen Mehrkosten wie z.B. die Zollabwicklung.

Haftung für Mängel:

Bis 12 Monate nach Gefahrenübergang. Bei freier Anlieferung des Gerätes sind Material und Arbeitszeit kostenlos.
Bei Beseitigung des Mangels in Ihrem Hause berechnen wir die Fahrtzeit und die Fahrtkosten.
Unsere Lieferungen erfolgen ausschließlich zu unseren umseitigen Verkaufsbedingungen, soweit nichts anderes vereinbart ist.

Die Inbetriebnahme dieser Maschine / dieses Maschinenteils ist so lange untersagt, bis festgestellt wurde, daß die Maschine, in die es eingebaut werden soll, den Bestimmungen der EG-Richtlinien Maschinen, den harmonisierten Normen, Europanormen oder den entsprechenden nationalen Normen entspricht.

Lieferbedingung: Die Lieferung erfolgt ab Werk, unverpackt und selbstversichert

Zahlungsbedingung: Zahlbar innerhalb 30 Tagen rein netto

Lieferzeit:
3-4 Arbeitswochen nach Auftragseingang bzw. Klärung sämtlicher Details

Bitte beachten Sie:
Aufgrund der Corona-Pandemie kann sich die Lieferzeit gegebenenfalls verlängern!

Föhrenbach®
Positionier-Systeme

Unser Zeichen:	Horst Oster	
Telefon:	+49(0)7707 159-14	
Telefax:	+49(0)7707 159-80	
Email:	horst.oster@foehrenbach.com	
Vertreter-Nr.:	80	
Kunden-Nr.:	K12389	

<u>Föhrenbach GmbH, Lindenstraße 34, 79843 Löffingen-Unadingen</u>

TU München
Lehrstuhl für Windenergie
Herrn Juan Llobell
Boltzmannstr. 15
85748 Garching

Ihr Zeichen:	Juan Llobell
Telefon:	0034/647942-528
Telefax:	
Email:	juanllobell9@gmail.com
Lieferanten Nr.:	

Löffingen-Unadingen, 29.04.2021

Angebot Nr. 1211-0253

Seite 1 von 4

Vertreter:	Klaus-Dieter Kottke	Telefon:	08441/871660
		Telefax:	08441/871661
	Adolf - Rebl - Strasse 14	Email:	kottke.mail@t-online.de
	85276 Pfaffenhofen		

Sehr geehrter Herr Llobell,

vielen Dank für Ihre Anfrage. Unter Zugrundelegung und Beachtung unserer Verkaufsbedingungen (Text umseitig oder als Download unter www.foehrenbach.com erhältlich), bieten wir Ihnen an:

Ihre Anfrage:	HR. KOTTKE	Unser Angebot: 1211-0253
Vom:	28.04.2021	

Pos.	Menge	ME	Artikelnr. Bezeichnung	Einzelpreis	Gesamtpreis AP = Alternativposition
1	1,00	Stk	66-400852	2.102,00	2.102,00

RT2A075S25111YY0
Präzisions-Rundtisch

A	Werkstoff	: Aluminium, schwarz anodisiert	
075	Größe	: 75 mm	
	Höhe	: 46 mm	
S	Qualität	: Standard	
25	Übersetzungsverhältnis	: i=25:1	
1	Endschalterausführung	: Referenz-Impuls	
1	Endschalteryp	: PNP - Öffner (NC), 2 -kanalig	
1	Antrieb	: Motoranbau gerade	
YY	Motorflansch für	: Bitte Motortyp bei Bestellung angeben	
0	Nacharbeit	: ohne	

TECHNISCHE DATEN:

Durchmesser Drehteller	: 72 mm
Durchmesser Drehtellerdichtung	: 74,5 mm
Bohrung im Drehteller	: 42 H7
Max. Drehzahl mechanisch	: 120 1/min
Max. Drehzahl mit Motor	: motorabhängig
Positioniergenauigkeit	: 0,050°
Wiederholgenauigkeit	: 0,01°
Umkehrspiel	: 0,035°
Rundlaufgenauigkeit	: 0,010 mm
Planlauf	: 0,012 mm

Angebot Nr. 1211-0253

Pos.	Menge	ME	Artikelnr. Bezeichnung		Einzelpreis		Gesamtpreis AP = Alternativposition

Parallelität   : 0,015 mm
Schutzart   : IP 50
Gewicht   : 1,2 kg

Technische Daten finden Sie im Katalog RT1/RT2 unter:

<https://foehrenbach.com/produkte/rundtische-und-rotationsachsen>

Optionen:

	1,00	Stk	9450208 *Kabeldose ESG 32AH0500* Kabel für Referenzpunktschalter, L=5 m, Stecker gerade (Kabeldose gerade) 4-polig 5 m Kabellänge PUR halogenfrei	53,00	AP	53,00
	1,00	Stk	300004141 *SN 5707.2.28.00.0.C.000* 2-Phasen-Schrittmotor Drehmoment: 0,8 Nm Nennstrom: 5,0 A 400 Halbschritte / Umdrehung Schutzart Motorgehäuse: IP54 Anschluss über Sub-D 9-polig	162,00	AP	162,00
	1,00	Stk	300004229 *KM 2SN57.C0.B.0.03* *Motorkabel, Länge 3 m* *für 2-Phasen-Schrittmotoren der Baureihe SN 57* *Aussendurchmesser ca. 8 mm* *Mindestbiegeradius 7,5xd*	103,00	AP	103,00
5	1,00	Stk	D10006614 Dokumentation deutsch auf CD	0,00		

		Nettowarenwert	2.102,00
		+ USt 19,00 %	399,38
		Gesamtsumme in EUR	2.501,38

Mechanische Spezifikation
Mechanical specifications
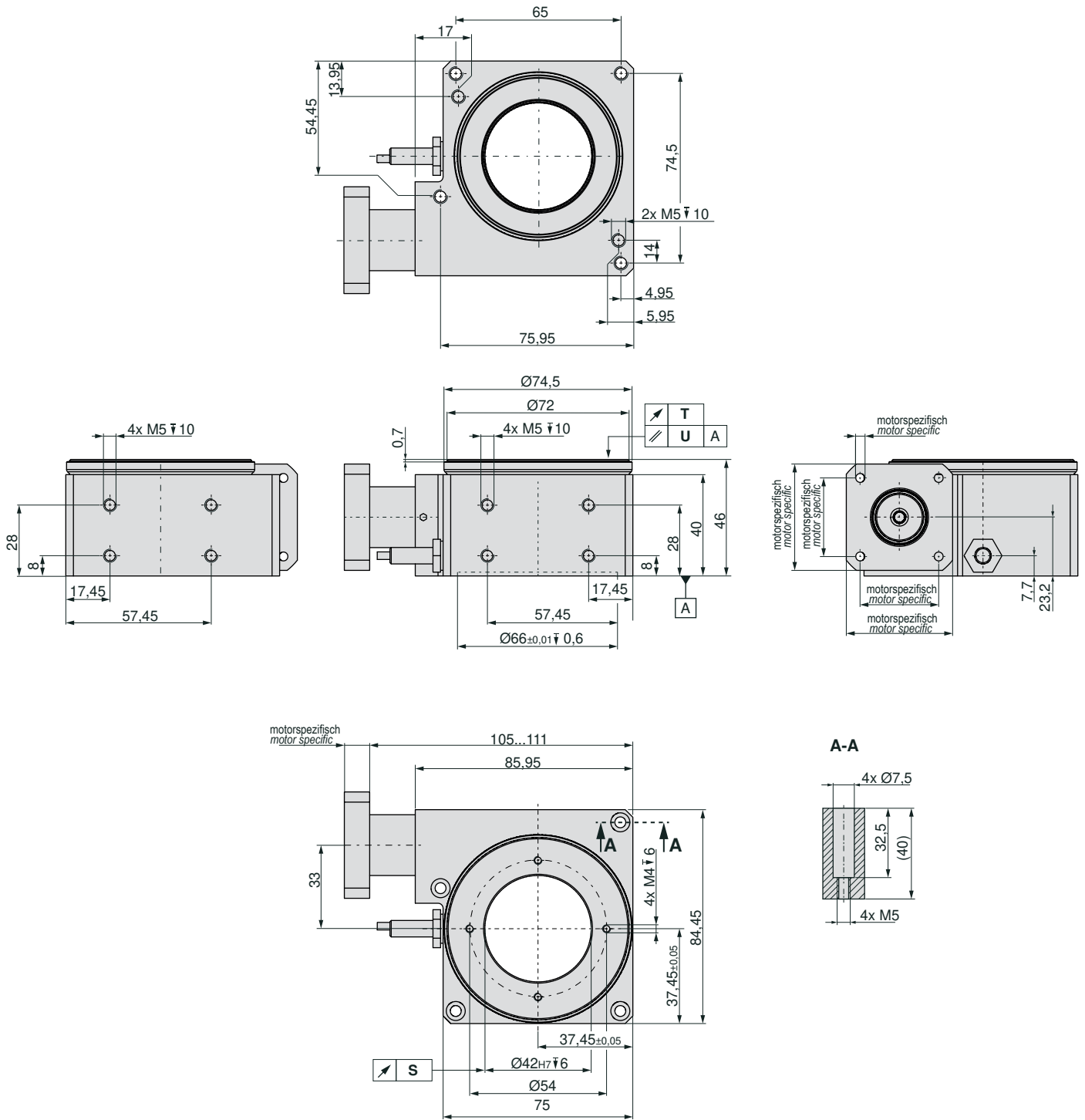
Übersetzung Schneckentrieb *Ratio worm gear drive*		i=25:1
max. Leerlaufmoment *max. no-oad moment*	Ncm	8
max. Drehmoment an der Welle *max. torque at the shaft*	Nm	0,75
n_{max} Drehteller *n_{max} rotary plate*	min^{-1}	120
Positioniergenauigkeit mechanisch *Positioning accuracy mechanical*	°	0,05
Wiederholgenauigkeit mechanisch *Repeating accuracy mechanical*	°	0,010 / 0,005*
Umkehrspiel *Reversing backlash*	°	0,035 / 0,025*
Rundlaufgenauigkeit **S** *Radial run-out accuracy **S***	µm	10 / 3*
Planlaufgenauigkeit **T** bei Ø60 mm *Axial run-out accuracy **T** at Ø60 mm*	µm	12 / 4*
Parallelität **U** *Parallelism **U***	µm	15 / 10*
Taumelfehler *Wobble error*	arcsec	6
Gewicht ohne Motor *Weight without motor*	kg	1,2
Schutzart *Protection class*		IP50

* = Werte bei Präzisionsausführung | *Values on precision versions*
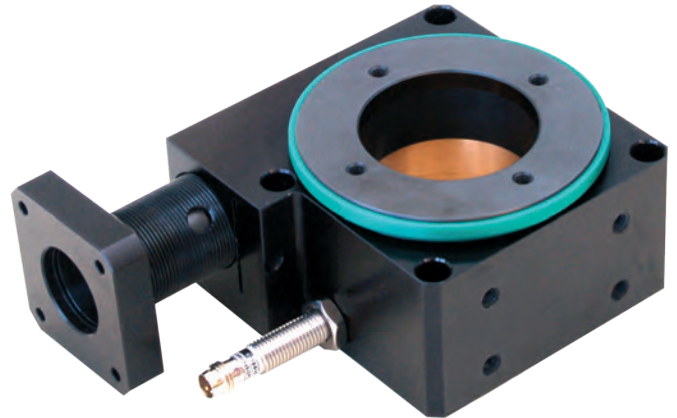
zulässige Belastung auf den Drehteller *allowable load on the rotary plate*			zulässiges Kippmoment *allowable tilting moment*		zulässiges Tangentialmoment *allowable tangential moment*
[N]	[N]	[N]	[Nm]	[Nm]	[Nm]
440	80	125	18	18	6,2

Abmessungen
Dimensions

- Abmessungen in mm
- Toleranzen DIN ISO 2768-1 mittel
- gezeichnetes Bohrbild im Drehteller entspricht der Referenzlage

- *Dimensions in mm*
- *Tolerances DIN ISO 2768-1 middle*
- *Drill hole pattern in the rotary plate is shown in the reference position*

7.1.2 Busch

BUSCH
MICROSYSTEMS

<table>
<tr><td colspan="2">Angebot</td></tr>
<tr><td>Projektnummer</td><td>P21-099</td></tr>
<tr><td>Vorgangsnummer</td><td>3248</td></tr>
<tr><td>Belegnummer</td><td>2021-30115</td></tr>
<tr><td>Datum</td><td>06.04.2021</td></tr>
<tr><td>Kundennummer</td><td>12927</td></tr>
<tr><td>Bearbeiter</td><td>T.Weigele</td></tr>
<tr><td colspan="2">Bitte bei allen Rückfragen angeben !</td></tr>
</table>

BUSCH Microsystems Consult GmbH - An der Altnah 34 - 55450 Langenlonsheim

Firma
TU München
Gebäude 7 – II Stock
Boltzmannstraße 15
85748 Garching

Versandart	Spedition (Stückgut)	Unsere UStIDNr	DE249384496
Lieferbedingung	Ab Werk (EXW) zzgl. Verpack.	Unsere SteuerNr	06/655/1098/6
Bezug		Ausländ. StNr	
Ihr Zeichen	Juan Llobell	Ihre UStIDNr	DE811193231
Ihr Beleg	E-Mail 22.03.2021		

Sehr geehrte Damen und Herren,

vielen Dank für Ihre Anfrage. Gerne unterbreiten wir Ihnen folgendes Angebot:

******************** Liefertermin 12 - 14 Wochen nach Auftragseingang ********************

Pos.	Artikelnr.	Bezeichnung	Termin	MengeME	Einzelpreis	Gesamtpreis	SC
1	DT-180	Drehtisch 180 mm Material: Aluminium Max. Durchmesser: 180 mm Durchmesser Drehteller: 155 mm Antrieb: Torquemotor Max. Geschwindigkeit: 150 rad/s Messsystem: 26-Bit, BiSS Höhenschlag & Rundlauf: 4 μm Max. Tragkraft: 5 kg Gesamtgewicht: 5,5 kg	2021/14	1 Stk	7.871,00	7.871,00	101

* * *
**Steuerungsmodule & Inbetriebnahme
optional erhältlich**
* * *

Gewicht: 5,5000 kg / 5,5000 kg
BUSCH Microsystems bietet die Modifikation der Basissysteme nach Kundenwunsch und
entsprechend Ihrer Anforderungen an.
Folgende Alternativen und zusätzliche Optionen sind möglich:

- Verschiedene Materialien, wie z. B. Aluminium, Granit, Edelstahl oder Keramik
- Skalierbare Verfahrwege
- Optimierung für höhere Traglasten
- Individuelle Montagebohrungen
- Mit und ohne Controller
- Anschlusskabel in gewünschter Länge
- Kombinierbar mit weiteren Achsen
- Auslegung für den Reinraumbetrieb
- Abdeckung (z.B. Faltenbälge)
- Energiekette

Sie möchten eine dieser - oder weitere, nicht genannte - Anpassungen?

	Übertrag	7.871,00

Pos.	Artikelnr.	Bezeichnung	Termin	MengeME	Einzelpreis	Gesamtpreis SC

Sprechen Sie uns an - gemeinsam finden wir eine Lösung!

Bitte beachten Sie, dass unsere Systeme für einen einwandfreien Betrieb regelmäßig gewartet werden müssen.
Gerne bieten wir Ihnen die Wartung Ihres Systems als Option an. Sprechen Sie uns einfach an, wenn Sie dies wünschen

			Zwischensumme	EUR		7.871,00 SC
zzgl. MwSt. mit Steuercode	101	19,00	% von	7.871,00		1.495,49
			Endsumme	EUR		9.366,49

BUSCH Microsystems Consult GmbH - Ihr Systempartner für Präzision in Perfektion.
Wir bieten Ihnen perfekt aufeinander abgestimmte Lösungen des Ultrapräzisionsmaschinenbaus mit intelligenten Hochleistungssteuerungen. Unsere Produkte werden individuell nach den Anforderungen Ihrer Anwendung gefertigt.

Mit unserer Ware erhalten Sie ein deutsches Prüfzeugnis, erstellt in unserem Haus. Bitte beachten Sie, dass die angegebenen Werte/Spezifikationen für eine Raumtemperatur von 20°C (+/- 1°C) gelten.
Das Ursprungsland unserer Produkte ist Deutschland (EEC/EU).

Bei der Lieferung von Positioniersystemen und Granitstrukturen mit Führungsschienen gilt:
Die gesetzliche Gewährleistung wird nur gewahrt, wenn die Wartung der Anlage gemäß Wartungsanleitung durchgeführt wurde. Für eine unsachgemäße Nutzung der unvollständigen Maschine haftet allein der Auftraggeber.
Mit der Auslieferung des Produktes erhalten Sie eine **unvollständige Maschine** gemäß Maschinenrichtlinie 2006/42/EG. Die Anlage wird ohne Schutzeinrichtungen geliefert. Gemäß Maschinenrichtlinie Kapitel 1.4. sind entsprechende Schutzeinrichtungen zu installieren. Die Inbetriebnahme des Produktes ist so lange untersagt, bis festgestellt wurde, dass die Maschine allen grundlegenden Sicherheits- und Gesundheitsschutzanforderungen der Maschinenrichtlinie entspricht.

Granitteile werden von uns aus Kostengesichtspunkten grundsätzlich in der Toleranzklasse mittel (m) nach den Allgemeintoleranzen für Längen- und Winkelmaße (DIN ISO 2768-1) gefertigt. Sollte ein „enger" toleriertes Maß notwendig sein, muss dies einzeln in der Zeichnung angegeben werden.

Im Fall einer angedachten Beistellung von Komponenten bitten wir Sie, dass diese spätestens 2 Wochen vor dem bestätigten Auslieferungstermin bei uns eingegangen sind, um den vereinbarten Liefertermin halten zu können.
Bei Eingang der Beistellungen werden diese auf Vollständigkeit geprüft. Eine vorherige Qualitätsprüfung wird vorausgesetzt. Bitte beachten Sie, dass wir unsere Qualität nur garantieren können, wenn die beigestellten Komponenten den Genauigkeitsanforderungen des gesamten Systems entsprechen.
Des Weiteren möchten wir Sie darauf hinweisen, dass wir nur original verpackte Waren verarbeiten können.

Das Recht an Konstruktionsarbeiten behält sich BUSCH Microsystems Consult GmbH vor. Diese bleiben auch nach Umsetzung eines Projektes Eigentum der BUSCH Microsystems Consult GmbH und dürfen nicht an Dritte weitergegeben werden oder nach Umsetzung des Projektes für Dritte verwendet werden, es sei denn, dies wurde bei Auftragsvergabe explizit vereinbart.

Es gelten die AGB der BUSCH Microsystems Consult GmbH, die Sie unter www.busch-microsystems-consult.de downloaden können; gerne senden wir Ihnen diese auf Wunsch zu.

Mit freundlichen Grüßen

BUSCH Microsystems Consult GmbH

Dieses Schreiben wurde maschinell erstellt und ist daher ohne Unterschrift gültig.

NEWS & MESSEN: www.busch-microsystems-consult.de/news-media/termine/

Sofern nicht anders ausgewiesen, verstehen sich die Preise exklusive der Kosten für Verpackung und Fracht sowie Anschluss und Inbetriebnahme von Steuerungslösungen.
Ist bei Auftragsvergabe vom Auftragsgeber nicht explizit ausgewiesen, dass dieser sich um den Transport kümmert, übernimmt BUSCH Microsystems die Organisation des Transportes (inkl. Verpackung) der Ware zum Auftraggeber und fakturiert diese entsprechend nach Aufwand.

Zahlungsvereinbarungen:

14Tage	ohne Abzug	9.366,49EUR

7.1.3   Aerotech

Angebot

Angebotsdatum:	

Pos	Menge	Teilenummer/Beschreibung	
1	1	AGR75-M1-ML1-3-PL0-TAS	
		Produktdetails: AGR75 Gear-Driven Rotary Stage AGR75-M1-ML1-3-PL0-TAS AGR75 Gear-Driven Rotary Stage Motor: BMS35 Brushless Servomotor and 2000-Line TTL Encoder (-M1) Motor Location: Motor Located on Right Side of Stage Housing, Standard (-ML1) Motor Orientation: Motor Orientation 3, Standard (-3) Travel: Continuous Travel Limits: None Direct Rotary Feedback: None Tabletop: None Mounting Plate: None Seals: None Metrology: No Metrology Performance Plots (-PL0) Integration: Test as System (-TAS)	
2	1	Ensemble-MACHINE-MATLAB-USB-MAINTENANCE-1-00	
		Produktdetails: Ensemble Motion Control Software Ensemble-MACHINE-MATLAB-USB-MAINTENANCE-1-00 Ensemble Motion Control Software License Type: Ensemble Installation on a Single PC (MACHINE) MATLAB: MATLAB Library for Motion, Parameters and Data Collection (MATLAB) Media: Installation Media Provided on a USB Drive (USB) Maintenance Years: Software Maintenance for 1 Year After Purchase (MAINTENANCE-1-00) [Software Version]: Default	
3	1	EnsembleMP10	
		Produktdetails: EnsembleMP Standalone PWM Digital Drive/Controller EnsembleMP10 EnsembleMP Standalone PWM Digital Drive/Controller Current: 10 A Peak, 5 A Cont. Current (10) Low Voltage Control Supply: Standard Control Power Input Voltage IO Expansion Board: None MXU Multiplier: None Aux Encoder: None Real Time Clock: None Five Axis Contouring: None EtherNet IP: None Dynamic Controls Toolbox: None Enhanced Throughput Module: None Enhanced Tracking Control: None Lock Calibration File: None Firmware Version: Default	
4	1	PS-MP/PS-12048/1AX	
		Produktdetails: PS-MP Din-Rail DC Power Supply, Up to 4 Axes PS-MP/PS-12048/1AX PS-MP Din-Rail DC Power Supply, Up to 4 Axes Power Options: 120 W; 48 VDC; Autoranging 100-240 VAC Supply (/PS-12048) Number of Axes: 1 Axis of Wiring (/1AX) Brake Control: None	

Angebot

Angebotsdatum:	

Pos	Menge	Teilenummer/Beschreibung	
5	1	C19360-50	
		Produktdetails: Motor Cable C19360-50	
6	1	C18391-50	
		Produktdetails: Feedback Cable C18391-50	
7	1	ENET-XOVER-30	
		Produktdetails: Communication Cable ENET-XOVER-30 Communication Cable Cable: ENET-XOVER-30 - Ethernet Crossover, 30DM	
8	1	Prod-Service-TAS	

		Produktdetails:
		Production Services Configurator
		
		System Integration
		Testing, integration, and documentation of a group of components as a complete system that will be used together (ex: drive, controller, and stage). This includes parameter file generation, system tuning, and documentation of the system configuration.
		   Qty 1 - TAS
		
		Standard System Metrology
		   Qty 1 - AGR75 : No Metrology Performance Plots (-PL0)	

Incoterms 2010:		Geschätzter Gesamtbetrag: (€):	7,427.00
Währung:	European Euro		
Alle Preise verstehen sich zuzüglich gesetzlicher Mehrwertsteuer.			

AGR SERIES SPECIFICATIONS

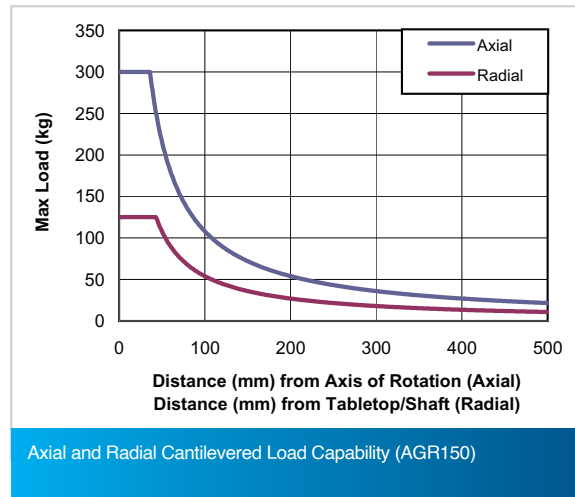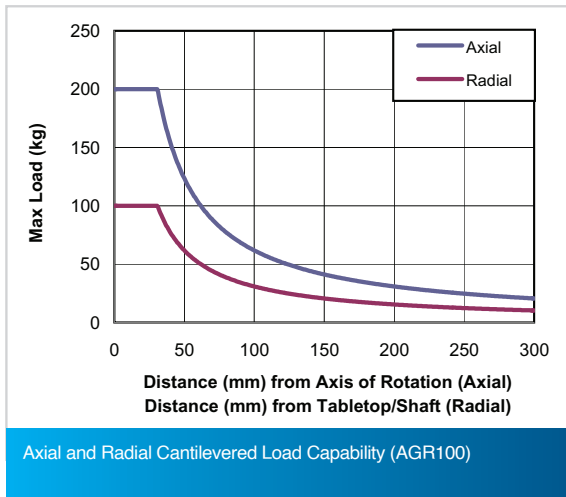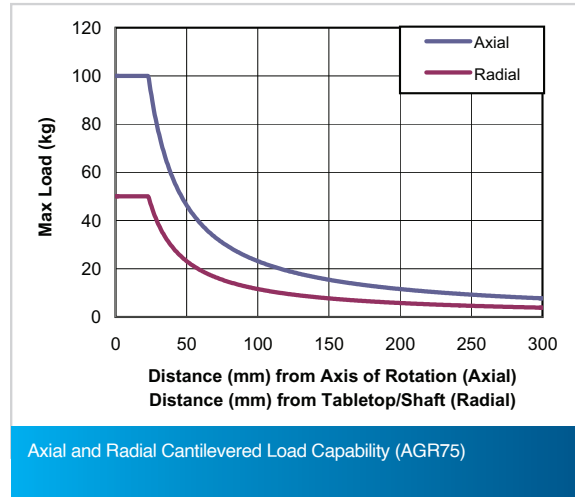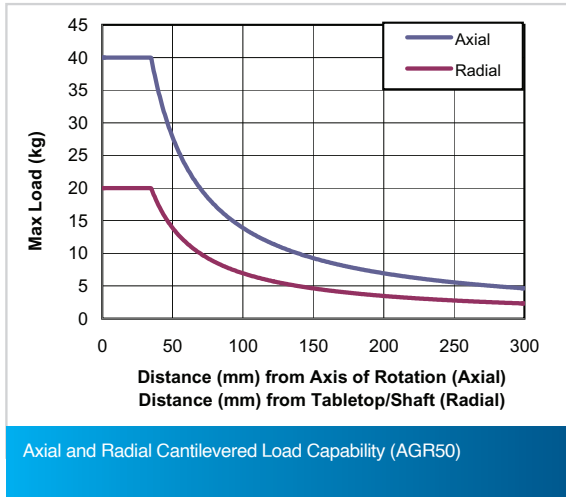| Mechanical Specifications		AGR50	AGR75	AGR100	AGR150	AGR200
Travel		360° (Limited Travel Versions Available)				
Accuracy	Uncalibrated	0.87 mrad (180 arc sec)		0.58 mrad (120 arc sec)		
	Calibrated	0.29 mrad (60 arc sec)	0.24 mrad (50 arc sec)			
	Uncalibrated with Direct Encoder Option	97 µrad (20 arc sec)				
	Calibrated with Direct Encoder Option	58 µrad (12 arc sec)	49 µrad (10 arc sec)			
Repeatability (Uni-Directional)	Standard	49 µrad (10 arc sec)				
	Direct Encoder[1]	24 µrad (5 arc sec)				
Repeatability (Bi-Directional)	Standard[2]	0.22 mrad (45 arc sec)				
	Direct Encoder[1]	39 µrad (8 arc sec)		29 µrad (6 arc sec)		
Tilt Error Motion		49 µrad (10 arc sec)				
Axial Error Motion		5 µm				
Radial Error Motion		10 µm				
Gear Ratio		51:1	67:1	85:1	117:1	126:1
Maximum Speed[3]	with Brushless Servomotor (BM and BMS Models)	180°/s				120°/s
	with Stepper Motor	60°/s		40°/s		
Maximum Acceleration[4]		720°/s²				480°/s²
Aperture	mm	50 mm	75 mm	100 mm	150 mm	200 mm
Load Capacity	Axial	40 kg	100 kg	200 kg	300 kg	425 kg
	Radial	20 kg	50 kg	100 kg	125 kg	200 kg
	Moment	See Moment Load Curves				
Maximum Torque Load to Stage Shaft		2.5 N·m	3.5 N·m	12 N·m	20 N·m	80 N·m
Rotor Inertia (Unloaded)		0.00052 kg·m²	0.0013 kg·m²	0.0035 kg·m²	0.011 kg·m²	0.076 kg·m²
Stage Mass (No Motor)	Standard	1.9 kg	2.4 kg	4.5 kg	6.1 kg	18.6 kg
	Direct Encoder	2.5 kg	3.1 kg	5.6 kg	7.6 kg	21.7 kg
Material		Aluminum				

Notes:
1. Direct encoder repeatability specifications are for systems using the -E1 or -E3 direct encoder options only.
2. Requires the use of an Aerotech controller. Consult factory if using a third-party controller.
3. Maximum speed is load dependent. Contact an Aerotech Application Engineer if imbalanced loads are present.
4. Unloaded acceleration.
5. On-axis loading is listed.
6. Specifications are for single-axis systems measured 25 mm above the tabletop. Performance of multi-axis systems is payload and workpoint dependent.
Consult factory for multi-axis or non-standard applications.

Electrical Specifications		AGR50	AGR75	AGR100	AGR150	AGR200
Drive System		Precision Worm-Gear with Brushless Servomotor or Stepper Motor				
Feedback	Standard	Noncontact Rotary Encoder Contained Within Motor; See Motor Description Under "Ordering Options" Section for Details				
	Direct Encoder	Noncontact Rotary Encoder Directly Mounted to AGR Stage Shaft				
		15744 Lines/Rev	18000 Lines/Rev	23600 Lines/Rev	31488 Lines/Rev	40000 Lines/Rev
Maximum Bus Voltage	with Brushless Servomotor (BM Models)	80 VDC		320 VDC		
	with Brushless Servomotor (BMS Models)	320 VDC				
	with Stepper Motor	40 VDC				80 VDC
Limit Switches		5 V, Normally Closed or Normally Open				
Home Switch		Near Limit (for Limited Travel Stage Version)				

Note:
1. For stepper motors with Aerotech controllers, amplifier bus voltages are 2X values listed

AGR SERIES PERFORMANCE

Axial and Radial Cantilevered Load Capability (AGR50)

Axial and Radial Cantilevered Load Capability (AGR75)

Axial and Radial Cantilevered Load Capability (AGR100)

Axial and Radial Cantilevered Load Capability (AGR150)

Axial and Radial Cantilevered Load Capability (AGR200)
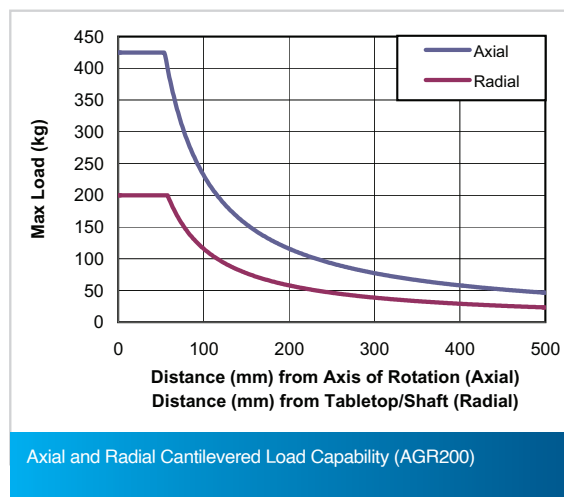
7.2 Handmade Rotatory stage

FACTUREE®
Der Online-Fertiger

Herr Juan Llobell
TUM
Boltzmannstraße 15
85748 Garching
DE - Deutschland

Projekt-Nr.	**103N2004MATU**
Beleg-Nr.	AG2104281436-A_TUM10
Ihre Kunden-Nr.	TUM10
Ansprechpartner	Michael Wallner
Telefon	+49 (0)30 629 3939-15
E-mail	wallner@facturee.de
Datum	28.04.2021

ANGEBOT

Sehr geehrter Herr Llobell,

vielen Dank für Ihre Anfrage vom 20.04.2021. Es freut uns, Ihnen ein Angebot für die Fertigung folgender Einzelpositionen unterbreiten zu können:

Pos.	Bezeichnung	Material	Menge	Stückpreis	Gesamt
1	engranaje-biselado11	EN AW-6061 keine Oberflächenbehandlung Verzahnung nach 3D-Daten Nur 3D-Daten vorhanden - Alle Toleranzen nach ISO 2768-mK	1	298,90 €	298,90 €
2	engranaje-biselado21	EN AW-6061 keine Oberflächenbehandlung für die Fertigung müssen 3D-Daten nachgeliefert werden Verzahnung nach 3D-Daten Nur 3D-Daten vorhanden - Alle Toleranzen nach ISO 2768-mK Wandstärke muss ggfs. angepasst werden für Fertigung muss die STEP-Datei getrennt werden;	1	742,93 €	742,93 €
3	pieza5	EN AW-1050A keine Oberflächenbehandlung Nur 3D-Daten vorhanden - Alle Toleranzen nach ISO 2768-mK	1	202,05 €	202,05 €

Zwischensumme	**1.243,88 €**

1 | 2

FACTUREE®
Der Online-Fertiger

Pos.	Bezeichnung	Material	Menge	Stückpreis	Gesamt
Übertrag					**1.243,88 €**
4	pieza7	EN AW-6061 keine Oberflächenbehandlung Nur 3D-Daten vorhanden - Alle Toleranzen nach ISO 2768-mK	1	459,81 €	459,81 €
5	pieza8	EN AW-6061 keine Oberflächenbehandlung Nur 3D-Daten vorhanden - Alle Toleranzen nach ISO 2768-mK	1	175,71 €	175,71 €

Netto Preis	1.879,40 €
MwSt 19%	357,09 €
Gesamtpreis	**2.236,49 €**

Ihre Konditionen

✔	**Lieferzeit**	18 Arbeitstage
✔	**Versandart**	Kostenloser Express-Versand
✔	**Lieferbedingung**	Lieferung frei Kunde (CIP)
✔	**Zahlungsbedingung**	14 Tage netto
✔	**Gültigkeit**	14 Tage

Die genannten Preise verstehen sich als Nettopreise. Für Rückfragen stehen wir Ihnen gerne unter Tel. +49 (0)30 629 3939-15 zur Verfügung. Das Angebot erfolgt ausschließlich gemäß unserer allgemeinen Verkaufs- und Lieferbedingungen, wie sie auf www.facturee.de/agb aufgeführt sind.

Mit freundlichen Grüßen
Michael Wallner

7.3   Right angle gearbox

Pos.	Material
010	20070533[3]
	CP005S-MF1-10-0B1-2S / Omron - R7M-A03030 ohne Bremse
	alpha Basic Line - Planetengetriebe
	Ausprägung: Standard
	Getriebevariante: Motoranbau
	Getriebeausführung: Standard
	Form des Abtriebs: Welle glatt
	Motoranbindung: Steckhülse

Produktmerkmale[2]	Bestellangaben[3]	Zusatzangaben
Adapterplatte	20075577	
Distanzhülse	20077762	
Zum Anbau an		Omron - R7M-A03030 ohne Bremse
Art der Lackierung		Standard
Lackierung	10038414	Perldunkelgrau
Einbaulage	EHM	Beliebig einbaubar
Schmierstoff	10034768	Tribol GR 100-1 PD

Zusatzinformationen		
Lieferzeit	20 Arbeitstage	
Warennummer	84834029	
Ursprungsland	Deutschland	

Menge	Preis/Einheit	Abgabepreis
1 Stück	130,00 EUR	130,00 EUR
Positionsnetto	**130,00 EUR**	**130,00 EUR**

Pos.	Material
020	20043578[3] TK+ 004S-MF2-100 -5C1-1S10 alpha Advanced Line - Hypoidgetriebe Ausprägung: Standard Getriebevariante: Motoranbau Getriebeausführung: Standard Form des Abtriebs: Flanschhohlwelle Motoranbindung: Steckhülse

Produktmerkmale[2]	Bestellangaben[3]	Zusatzangaben
Art der Lackierung		Standard
Lackierung	10040632	Innovation blue
Einbaulage	EHM	Beliebig einbaubar
Schmierstoff	10034352	Optigear Synthetic 800/220

Zusatzinformationen	
Lieferzeit	40 Arbeitstage
Warennummer	84834023
Ursprungsland	Deutschland

Menge	Preis/Einheit	Abgabepreis
1 Stück	1.638,00 EUR	1.638,00 EUR
Positionsnetto	**1.638,00 EUR**	**1.638,00 EUR**

Gesamtpreis	
Positionen gesamt	**1.768,00 EUR**
Frachtkosten	2,50 EUR
Verpackungskosten	11,00 EUR
Endbetrag netto[4]	**1.781,50 EUR**

[2] Weiterführende technische Informationen zu diesem Produkt finden Sie auf unserer Website unter "Technische Unterlagen"
[3] Bitte bei Bestellung angeben
[4] gegebenenfalls zuzüglich gesetzlicher Umsatzsteuer

Angebotsinformationen	
Zahlungsbedingungen	
Lieferbedingungen	CPT Lieferadresse in Deutschland, Incoterms 2010
Nettogewicht / Bruttogewicht	3,70 kg / 4,26 kg
Gültigkeitsdatum	21.06.2021

02-
STI
V19

Ansicht von rechts / View from right
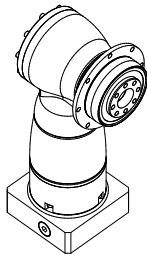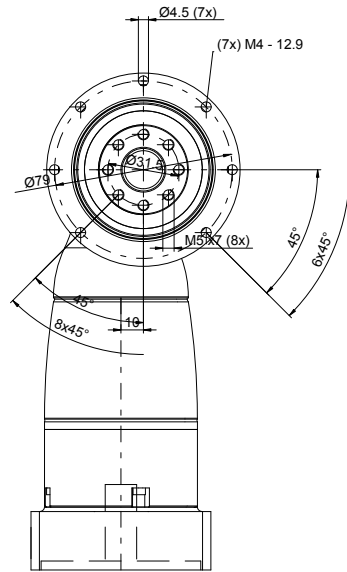
2) Durchgeführtes Element max. Ø16,8 mm
Led through element max. Ø16,8 mm
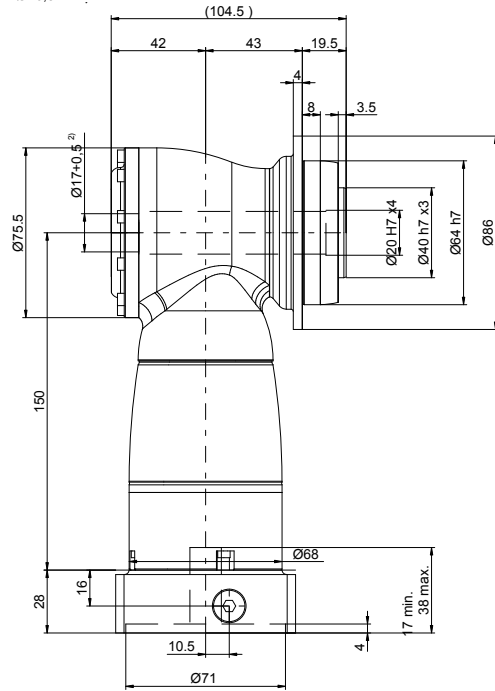
Ansicht von unten / View from bottom

7.3.1 TK+

Ø4.5 (7x)

(7x) M4 - 12.9

Ø79

Ø31

M5x7 (8x)

45°

6x45°

45°

8x45°

10

(104.5)

42

43

19.5

4

8

3.5

Ø117+0.5 2)

Ø75.5

150

Ø20 H7 x4

Ø40 h7 x3

Ø64 h7

Ø86

Ø68

28

16

17 min.

38 max.

10.5

Ø71

4

Ø90

M6 x13

□80

Ø14 F7 1)

45°

1) Motorwellenpassung pruefen / Check motor shaft fit

Technische Aenderungen vorbehalten / Technical modifications reserved

Betriebsanleitung unter www.wittenstein-alpha.de / Operating manual on www.wittenstein-alpha.de

Nicht tolerierte Masse sind Nennmasse / Non-toleranced dimensions are nominal dimensions

gez/draft			
Datum/date	29.04.2021	Massstab Scale auto	WITTENSTEIN alpha
Eigentumsvorbehalt nach DIN 34 beachten !	Observe copyright note according to DIN 34 !		
Benenn. Descr.	TK+004S-MF2-100-5C1-1S10		
Kommentar Note	SIEMENS AG - 1FK2204-5AF10-2xxx (w. brake) (brake. Encoder 22 bit. S210 3AC 400V: 2.3A / S120)		
MN	20043578	DIN A3	Ursp./Ref-Drwg: CAD-Generator V2.0 Blatt/Sheet: 1

nicht vertraulich

Anbauteile / mounting parts		
Adapterplatte adapter plate	MN	20032404
Distanzhuelse bushing	MN	

Produktdatenblatt

WITTENSTEIN | alpha

TK⁺

Spielarmes Servo-Winkelgetriebe

Getriebedaten	
Bezeichnung: TK+004S-MF2-20-5C1-1S	
Getriebetyp	TK⁺
Baugröße	004
Ausführungscode	Standard
Getriebevariante	Motoranbaugetriebe
Stufenzahl	2
Übersetzung i	20
Form des Abtriebs	Flanschhohlwelle + Hohlwelle mit Deckel
Bohrungsdurchmesser Klemmnabe	14 mm
Verdrehspiel	Standard
Getriebe Materialnummer	20042995

Technische Daten		
Max. Drehmoment am Abtrieb (abhängig von applikationsspezifischen Randbedingungen)	$T_{2\alpha}$	36 Nm
Max. Beschleunigungsmoment (max. 1000 Zyklen pro Stunde)	T_{2B}	30 Nm
Nenndrehmoment am Abtrieb (bei n_{1N})	T_{2N}	22 Nm
NOT-AUS-Moment (1000 mal während der Getriebelebensdauer zulässig)	T_{2Not}	50 Nm
Zulässige mittlere Antriebsdrehzahl (bei T_{2N} und 20°C Umgebungstemperatur) [a), b)]	n_{1N}	4400 min⁻¹
Max. Antriebsdrehzahl	n_{1Max}	6000 min⁻¹
Durchschnittl. Leerlaufdrehmoment (bei n_1=3000 min⁻¹ und 20°C Getriebetemperatur) [c)]	T_{012}	0,2 Nm
Max. Verdrehspiel	j_t	≤ 5 arcmin
Verdrehsteifigkeit	C_{t21}	2,8 Nm/arcmin
Max. Axialkraft [d)]	F_{2AMax}	2400 N
Max. Radialkraft [d)]	F_{2RMax}	2700 N
Max. Kippmoment	M_{2KMax}	251 Nm
Wirkungsgrad bei Volllast	η	94 %
Lebensdauer (Berechnung siehe Katalog Kapitel „Informationen")	L_h	> 20000 h
Gewicht inkl. Standard-Adapterplatte	m	3,2 kg
Laufgeräusch (bei n_1=3000 min⁻¹ ohne Last)	L_{PA}	≤ 64 dB(A)
Max. zulässige Gehäusetemperatur		90 °C
Umgebungstemperatur		0 °C bis 40 °C
Schmierung		Lebensdauergeschmiert
Lackierung		Innovation Blue
Schutzart		IP 65
Massenträgheitsmoment (bezogen auf den Antrieb)	J_1	0,19 kgcm²

a) Bei reduziertem Nenndrehmoment sind höhere Drehzahlen möglich
b) Bei höheren Umgebungstemperaturen bitte Drehzahlen reduzieren
c) Leerlaufmomente nehmen im Betrieb ab
d) Bezogen auf Wellen- bzw. Flanschmitte am Abtrieb

Alle technischen Daten für vordere Abtriebsseite gültig.
Technische Daten der rückwärtigen Abtriebsvarianten siehe Produktkatalog.

Für eine optimale Auslegung bei S1-Einsatzbedingungen (Dauerbetrieb) bitte Rücksprache.

7.3.2 CP
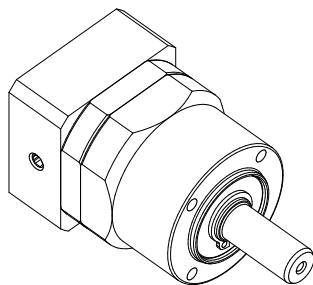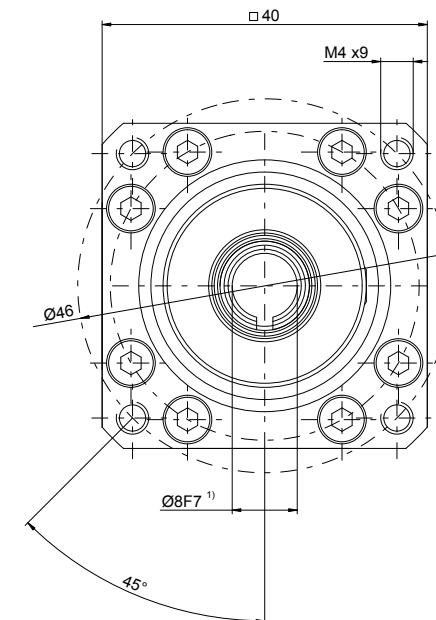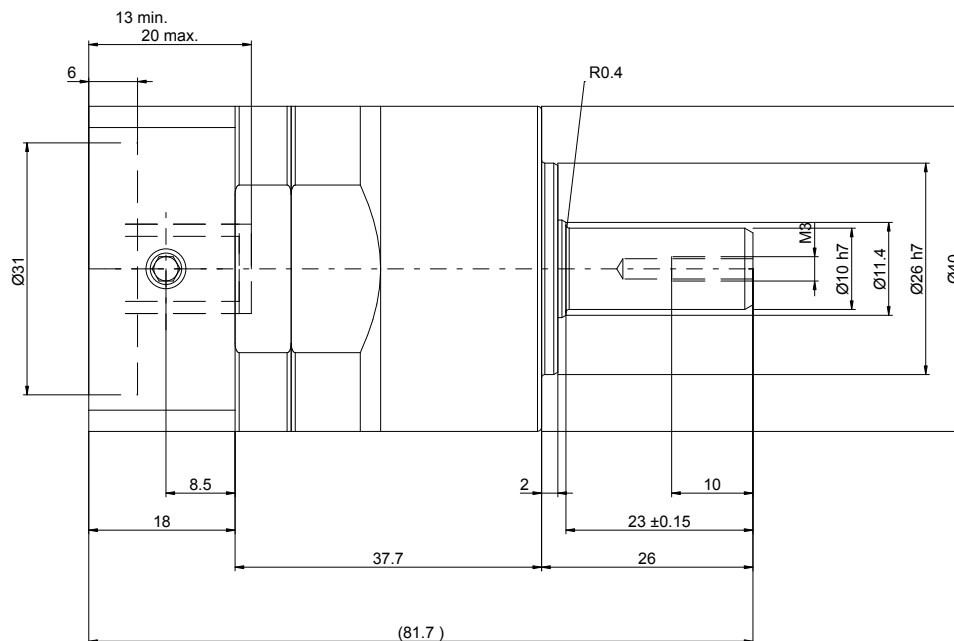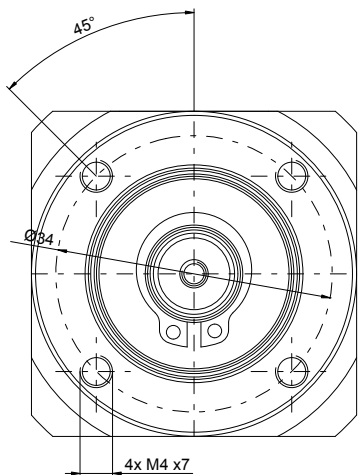
45°

Ø34

4x M4 x7

13 min.
20 max.

6

Ø31

R0.4

M3

Ø10 h7

Ø11.4

Ø26 h7

Ø40

8.5

2

10

18

23 ±0.15

37.7

26

(81.7)

□ 40

M4 x9

Ø46

Ø8F7 [1)]

45°

1) Motorwellenpassung pruefen / Check motor shaft fit

Technische Aenderungen vorbehalten / Technical modifications reserved

Betriebsanleitung unter www.wittenstein-alpha.de / Operating manual on www.wittenstein-alpha.de

Nicht tolerierte Masse sind Nennmasse / Non-toleranced dimensions are nominal dimensions

gez/draft			
Datum/date	30.04.2021	Massstab Scale	
Eigentumsvorbehalt nach	Observe copyright note		
DIN 34 beachten !	according to DIN 34 !	auto	

Benenn. Descr. **CP005S-MF1-10-0B1-2S**

Kommentar Note **SIEMENS AG - 1FK7011-5AK71 (brake)**

| MN | 20070533 | DIN A3 | Ursp./Ref-Drwg: | CAD-Generator V2.0 | Blatt/Sheet: | 1 |

WITTENSTEIN | alpha

nicht vertraulich

Anbauteile / mounting parts		
Adapterplatte adapter plate	MN	20075583
Distanzhuelse bushing	MN	20076984

Produktdatenblatt

CP

Spielarmes Planetengetriebe

Getriebedaten

Bezeichnung: CP005S-MF1-5-0B1-2S	
Getriebetyp	CP
Baugröße	005
Ausführungscode	Standard
Getriebevariante	Motoranbaugetriebe
Stufenzahl	1
Übersetzung i	5
Form des Abtriebs	Glatte Welle
Bohrungsdurchmesser Klemmnabe	11 mm
Verdrehspiel	Standard
Getriebe Materialnummer	20077983

Technische Daten

Max. Drehmoment am Abtrieb (abhängig von applikationsspezifischen Randbedingungen) [a) b) d)]	$T_{2\alpha}$	21 Nm
Max. Beschleunigungsmoment [d)] (max. 1000 Zyklen pro Stunde)	T_{2B}	14 Nm
Nenndrehmoment am Abtrieb (bei n_{1N})	T_{2N}	6,5 Nm
NOT-AUS-Moment (1000 mal während der Getriebelebensdauer zulässig) [a) b) d)]	T_{2Not}	26 Nm
Zulässige mittlere Antriebsdrehzahl (bei T_{2N} und 20°C Umgebungstemperatur) [c)]	n_{1N}	3800 min⁻¹
Max. Antriebsdrehzahl	n_{1Max}	9000 min⁻¹
Durchschnittl. Leerlaufdrehmoment (bei n_1=3000 min⁻¹ und 20°C Getriebetemperatur)	T_{012}	0,06 Nm
Max. Verdrehspiel	j_t	≤ 12 arcmin
Verdrehsteifigkeit	C_{t21}	0,6 Nm/arcmin
Max. Axialkraft [b)]	F_{2AMax}	240 N
Max. Radialkraft [b)]	F_{2RMax}	170 N
Max. Kippmoment	M_{2KMax}	4 Nm
Wirkungsgrad bei Volllast	η	97 %
Lebensdauer (Berechnung siehe Katalog Kapitel „Informationen")	L_h	> 20000 h
Gewicht inkl. Standard-Adapterplatte	m	0,5 kg
Laufgeräusch (bei n_1=3000 min⁻¹ ohne Last)	L_{PA}	≤ 62 dB(A)
Max. zulässige Gehäusetemperatur		90 °C
Umgebungstemperatur		-15 °C bis 40 °C
Schmierung		Lebensdauergeschmiert
Lackierung		Perldunkelgrau
Schutzart		IP 64
Massenträgheitsmoment (bezogen auf den Antrieb)	J_1	0,04 kgcm²

a) Gilt für reine Drehmomentbelastung
b) Bezogen auf Wellen- bzw. Flanschmitte am Abtrieb
c) Bei höheren Umgebungstemperaturen bitte Drehzahlen reduzieren
d) Gilt für: Welle glatt
e) Muss separat bestellt werden

7.3.3 RE40

RE 40 ⌀40 mm, graphite brushes, 150 watt
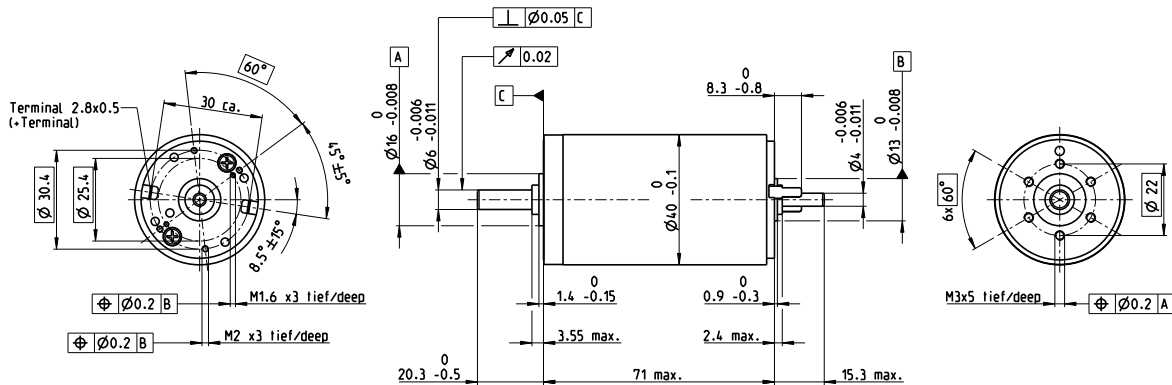
M 1:2

	Stock program
	Standard program
	Special program (on request)

Part Numbers

Motor Data

			148866	148867	148877	218008	218009	218010	218011	218012	218013	218014
	Values at nominal voltage											
1	Nominal voltage	V	12	24	48	48	48	48	48	48	48	48
2	No load speed	rpm	6920	7580	7590	6420	5560	3330	2690	2130	1720	1420
3	No load current	mA	241	137	68.6	53.7	43.7	21.9	16.6	12.5	9.66	7.76
4	Nominal speed	rpm	6380	6940	7000	5810	4930	2710	2060	1510	1080	781
5	Nominal torque (max. continuous torque)	mNm	94.9	177	187	186	180	189	190	192	192	190
6	Nominal current (max. continuous current)	A	6	6	3.17	2.66	2.23	1.4	1.13	0.909	0.73	0.6
7	Stall torque	mNm	1720	2420	2560	2040	1620	1020	814	655	523	424
8	Stall current	A	105	80.2	42.4	28.6	19.7	7.43	4.79	3.06	1.97	1.32
9	Max. efficiency	%	88	91	92	91	91	89	89	88	86	85
	Characteristics											
10	Terminal resistance	Ω	0.115	0.299	1.13	1.68	2.44	6.46	10	15.7	24.4	36.3
11	Terminal inductance	mH	0.024	0.082	0.33	0.46	0.613	1.7	2.62	4.14	6.41	9.32
12	Torque constant	mNm/A	16.4	30.2	60.3	71.3	82.2	137	170	214	266	321
13	Speed constant	rpm/V	581	317	158	134	116	69.7	56.2	44.7	35.9	29.8
14	Speed/torque gradient	rpm/mNm	4.05	3.14	2.97	3.16	3.45	3.29	3.31	3.27	3.29	3.37
15	Mechanical time constant	ms	5.89	4.67	4.28	4.2	4.19	4.16	4.15	4.15	4.15	4.16
16	Rotor inertia	gcm²	139	142	137	127	116	121	120	121	120	118

Specifications

Thermal data
17 Thermal resistance housing-ambient   4.7 K/W
18 Thermal resistance winding-housing   1.9 K/W
19 Thermal time constant winding   41.5 s
20 Thermal time constant motor   809 s
21 Ambient temperature   -30...+100°C
22 Max. winding temperature   +155°C

Mechanical data (ball bearings)
23 Max. speed   12 000 rpm
24 Axial play   0.05 - 0.15 mm
25 Radial play   0.025 mm
26 Max. axial load (dynamic)   5.6 N
27 Max. force for press fits (static)   110 N
   (static, shaft supported)   1200 N
28 Max. radial load, 5 mm from flange   28 N

Other specifications
29 Number of pole pairs   1
30 Number of commutator segments   13
31 Weight of motor   480 g

Values listed in the table are nominal.
Explanation of the figures on page 82.

Option
Preloaded ball bearings

* Industrial version with radial shaft seal ring
(resulting in increased no load current).
IP54 protection only if mounted on brush side, in
compliance with maxon modular system.

Operating Range

Comments

	Continuous operation
	In observation of above listed thermal resistance (lines 17 and 18) the maximum permissible winding temperature will be reached during continuous operation at 25°C ambient. = Thermal limit.
	Short term operation
	The motor may be briefly overloaded (recurring).
	Assigned power rating

n [rpm]

150 W

148877

maxon Modular System — Details on catalog page 38

Planetary Gearhead
⌀42 mm
3 - 15 Nm
Page 405

Planetary Gearhead
⌀52 mm
4 - 30 Nm
Page 410

Recommended Electronics:
Notes   Page **38**
ESCON Mod. 50/5   501
ESCON Mod. 50/8 (HE)   502
ESCON 50/5   503
ESCON 70/10   503
EPOS4 Mod./Comp. 50/5   510
EPOS4 Module 50/8   511
EPOS4 Comp. 50/8 CAN   513
EPOS4 50/5   515
EPOS4 70/15   515
EPOS4 Disk 60/8   516
EPOS4 Disk 60/12   517
EPOS2 P 24/5   520

Encoder MR
256 - 1024 CPT,
3 channels
Page 479

Encoder HED_5540
500 CPT,
3 channels
Page 486/489

Brake AB 28
24 VDC
0.4 Nm
Page 535

Industrial Version IP54*
Encoder HEDL 9140
Page 493
Brake AB 28
Page 536
End cap
Page 541

Encoder HEDS 5540   500 CPT, 3 channels

sensor

Cycle C = 360°e
Pulse P = 180°e

Channel A
Channel B
Channel I (Index)

Phase shift Φ 90°e

s_3 s_4 s_1 s_2 $s_{1..4}$ = 90°e   Δs < 45°e
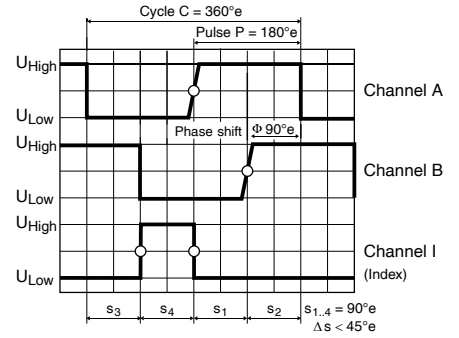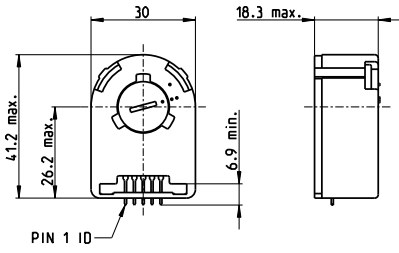
Direction of rotation cw (definition cw p. 78)

■ Stock program
□ Standard program
▨ Special program (on request)

Part Numbers				
110511	110513	110515	110517	**X drives**

Type					
Counts per turn	500	500	500	500	500
Number of channels	3	3	3	3	3
Max. operating frequency (kHz)	100	100	100	100	100
Max. speed (rpm)	12 000	12 000	12 000	12 000	12 000
Shaft diameter (mm)	3	4	6	8	2-4

overall length   overall length
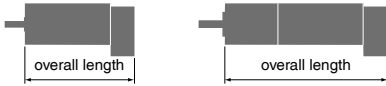
maxon Modular System						
+ Motor	**Page**	**+ Gearhead**	**Page**	**+ Brake**	**Page**	**Overall length [mm] / ● see Gearhead**
RE 25	144/146					75.3
RE 25	144/146	GP 26, 0.75 - 4.5 Nm	390			●
RE 25	144/146	GP 32, 0.75 - 6.0 Nm	392-396			●
RE 25	144/146	KD 32, 1.0 - 4.5 Nm	403			●
RE 25	144/146	GP 32 S	426-433			●
RE 25, 20 W	146			AB 28	535	105.8
RE 25, 20 W	146	GP 26, 0.75 - 4.5 Nm	390	AB 28	535	●
RE 25, 20 W	146	GP 32, 0.75 - 6.0 Nm	392-396	AB 28	535	●
RE 25, 20 W	146	KD 32, 1.0 - 4.5 Nm	403	AB 28	535	●
RE 25, 20 W	146	GP 32 S	426-433	AB 28	535	●
RE 30, 15 W	147					88.8
RE 30, 15 W	147	GP 32, 0.75 - 4.5 Nm	394			●
RE 30, 60 W	148					88.8
RE 30, 60 W	148	GP 32, 0.75 - 6.0 Nm	392-399			●
RE 30, 60 W	148	KD 32, 1.0 - 4.5 Nm	403			●
RE 30, 60 W	148	GP 32 S	426-433			●
RE 35, 90 W	149					91.7
RE 35, 90 W	149	GP 32, 0.75 - 8.0 Nm	392-400			●
RE 35, 90 W	149	GP 42, 3.0 - 15 Nm	405			●
RE 35, 90 W	149	GP 32 S	426-433			●
RE 35, 90 W	149			AB 28	535	124.3
RE 35, 90 W	149	GP 32, 0.75 - 8.0 Nm	392-400	AB 28	535	●
RE 35, 90 W	149	GP 42, 3.0 - 15 Nm	405	AB 28	535	●
RE 35, 90 W	149	GP 32 S	426-433	AB 28	535	●
RE 40, 25 W	150					91.7
RE 40, 150 W	151					●
RE 40, 150 W	151	GP 42, 3.0 - 15 Nm	405			●
RE 40, 150 W	151	GP 52, 4.0 - 30 Nm	410			●
RE 40, 150 W	151			AB 28	535	124.3
RE 40, 150 W	151	GP 42, 3.0 - 15 Nm	405	AB 28	535	●
RE 40, 150 W	151	GP 52, 4.0 - 30 Nm	410	AB 28	535	●
DCX 22 S	99-100					online
DCX 22 L	101-102					online
DCX 26 L	103-104					online
DCX 32 L	106					online
DCX 35 L	106					online

Technical Data		Pin Allocation			Connection example

Technical Data

Supply voltage V_{CC}	5 V ± 10%
Typical current draw	55 mA
Output signal	TTL compatible
Phase shift Φ	90°e ± 45°e
Signal rise time (typically, at C_L = 25 pF, R_L = 2.7 kΩ, 25 °C)	180 ns
Signal fall time (typically, at C_L = 25 pF, R_L = 2.7 kΩ, 25 °C)	40 ns
Index pulse width (nominal)	90°e
Operating temperature range	-40...+100 °C
Moment of inertia of code wheel	≤ 0.6 gcm²
Max. angular acceleration	250 000 rad s⁻²
Output current per channel	min. -1 mA, max. 5 mA

The index signal I is synchronized with channel A or B.
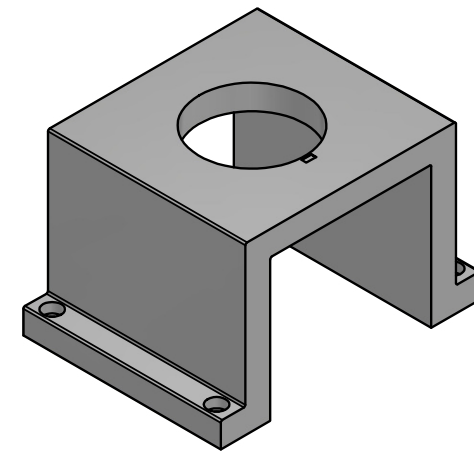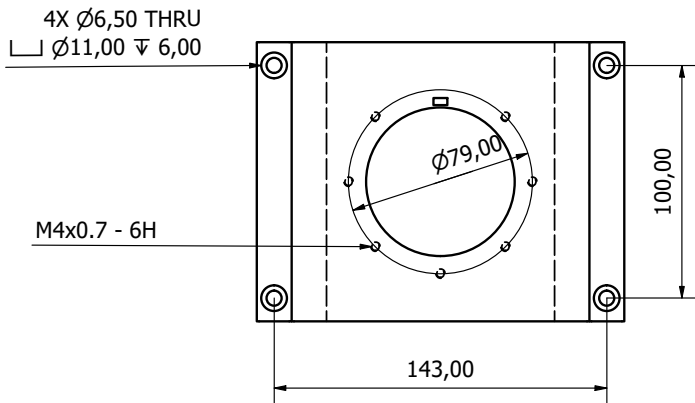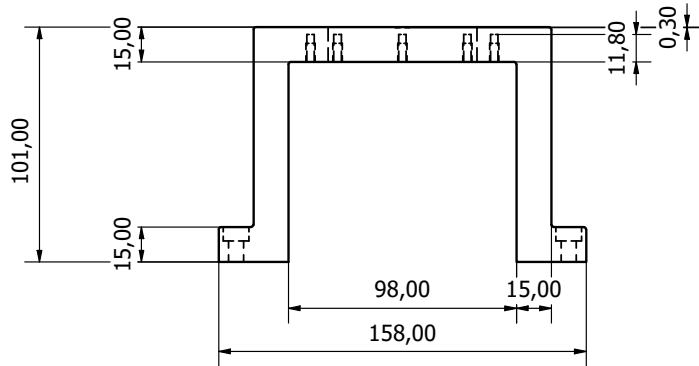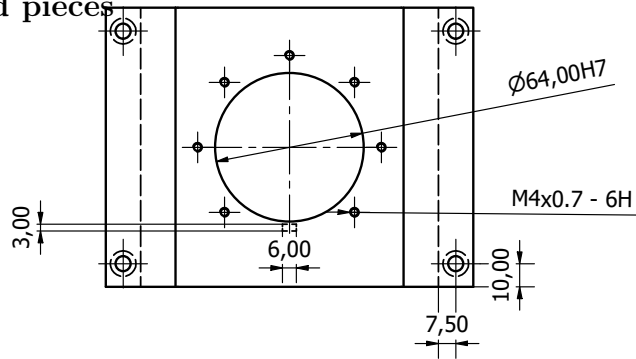
Pin Allocation

Encoder	Description	Pin no. from 3409.506
Pin 5	Channel B	1
Pin 4	V_{CC}	2
Pin 3	Channel A	3
Pin 2	Channel I	4
Pin 1	GND	5

Connection example

Channel A
Channel B
Channel I
Pin 3
Pin 5
Pin 2
TTL
$R_{pull-up}$ 3.3 kΩ
V_{CC} 5 VDC

Ambient temperature range ϑ_U = 25 °C

7.3.4 Designed pieces

Ø64,00H7

M4x0.7 - 6H

3,00

6,00

10,00

7,50

15,00

11,80

0,30

101,00

15,00

98,00

15,00

158,00

Stahl
Eckesrundung 1cm

4X Ø6,50 THRU
⌴ Ø11,00 ▽ 6,00

Ø79,00

M4x0.7 - 6H

100,00

143,00

Diseño de	Revisado por	Aprobado por	Fecha		Fecha	
JUALLOBU					02/08/2021	1:2

5.1 Support yaw		Edición	Hoja
			1 / 1
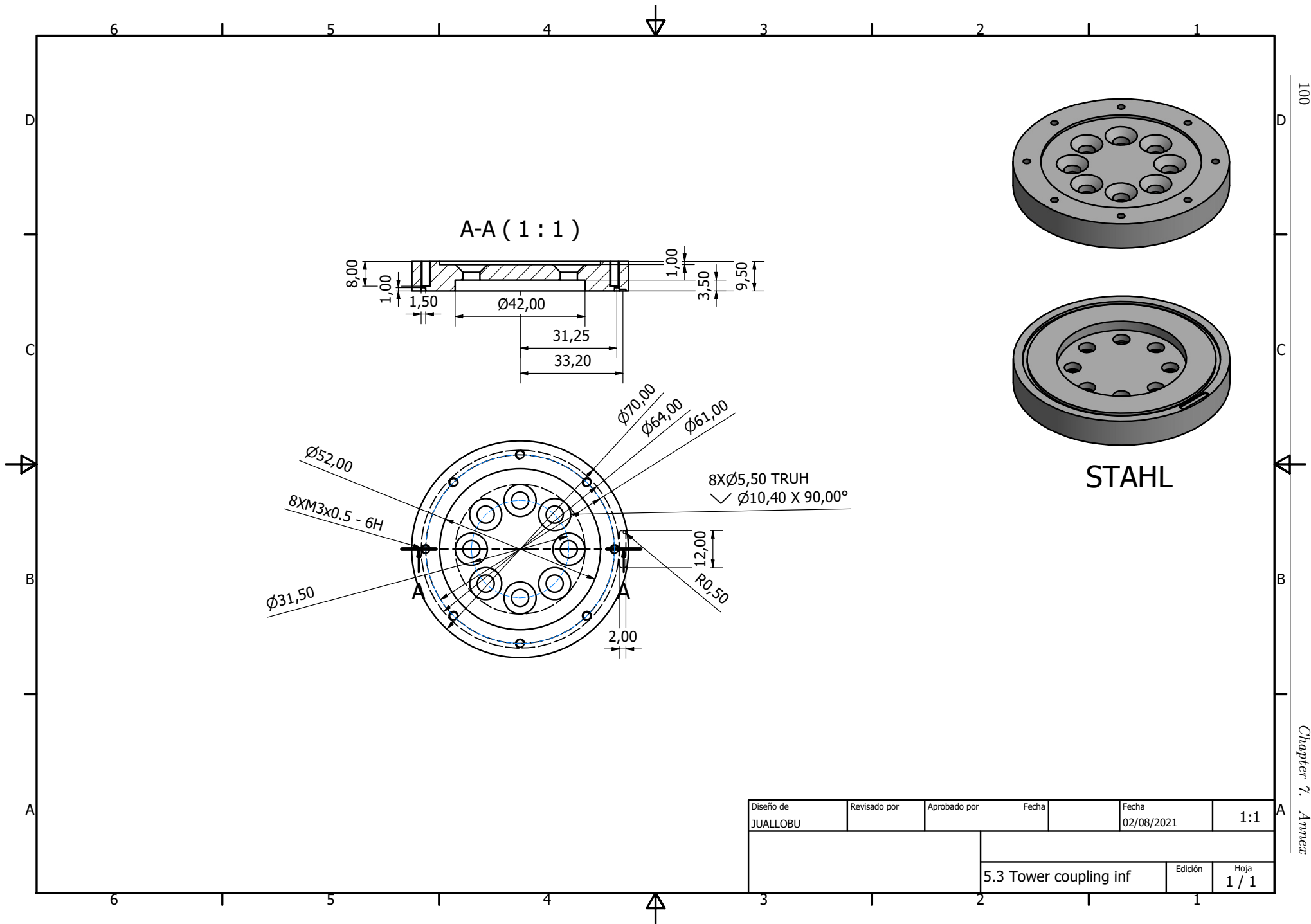
A-A (1 : 1)

8,00
1,00
1,00
1,50
Ø42,00
31,25
33,20
1,00
3,50
9,50

Ø70,00
Ø64,00
Ø61,00

Ø52,00

8XM3x0.5 - 6H

8XØ5,50 TRUH
∨ Ø10,40 X 90,00°

12,00
R0,50

Ø31,50

2,00

A

STAHL

Diseño de	Revisado por	Aprobado por	Fecha		Fecha	
JUALLOBU					02/08/2021	1:1

5.3 Tower coupling inf	Edición	Hoja
		1 / 1

STAHL

A-A (1 : 1)

0,50 4,00

7,00

Ø70,00

10,00

4,00

15,00

A

A

6XM4x0.7 - 6H

Ø3,10 THRU
⊔ Ø7,00

Ø42,00

Ø52,00

Ø61,00

Diseño de	Revisado por	Aprobado por	Fecha		Fecha	1:1
JUALLOBU					02/08/2021	
				5.3 Tower_coupling inf	Edición	Hoja 1 / 1

2,50 X 45,00°

4xØ4,50 DURCH

Ø46,00

Ø9,20

0,50 X 45,00°

1,50

4,50

3,55

Ø16,00 +0,008 / -0,000

ALU

□40,00

6XØ3,50THRU
⌴ Ø5,50 ▽ 2,00

Ø22,00

Ø30,00

Ø31,00 H7

⊕ 0,2 A

Diseño de	Revisado por	Aprobado por	Fecha		Fecha	
JUALLOBU					02/08/2021	2:1

	Edición	Hoja
5.7 Coupling_CP-RE40		1 / 1

[1] E.M.Nanos, J.Robke, F.M.Heckmeier, M.Cerny, and C.L.Bottasso, "Wake characterization of a multipurpose scaled wind turbine model," *American Institute of Aeronautics and Astronautics*, vol. 1, no. 1, pp. 1–11, 2018.

[2] E.M.Nanos, C.L.Bottasso, F.Campagnolo, and A.M.Rotea, "Design, performance and wake characterization of a scaled wind turbine with closed-loop controls," *European Academy of Wind Energy*, vol. 1, no. 1, pp. 1–32, 2021.

[3] E.M.Nanos, N. Kheirallah, F.Campagnolo, and C.L.Bottasso, "Design of a multipurpose scaled wind turbine model," -, vol. 1, no. 1, pp. 1–10, 2018.

[4] IRENA, "Irena wind energy data," *https://www.irena.org/wind*, 2021.

[5] J.Lee and F.Zhao, "Global wind report 2021," *GWEC, https://gwec.net/global-wind-report-2021/*, pp. 1–80, 2021.

[6] NREL, "The leading edge: April 2020 wind energy newsletter," *https://www.nrel.gov/wind/newsletter-202004.html*, 2021.

[7] IRENA, "Sustainability times," *https://www.sustainability-times.com/low-carbon-energy/the-future-of-wind-power-is-looking-bright-energy-agency-says/*, 2021.

[8] C.L.Bottasso and F.Campagnolo, "Wind tunnel testing of wind turbines and farms," *Handbook of Wind Energy Aerodynamics*, vol. 1, no. 1, pp. 1–20, 2020.

[9] L.P.Chamorro and F.Porté-Agel, "A wind-tunnel investigation of wind-turbine wakes: Boundary-layer turbulence effects, boundary- layer meteorology," *https://doi.org/10.1007/s10546-009-9380-8*, vol. 1, no. 1, pp. 129–149, 2009.

[10] H.Hu, Z.Yang, and P.Sarkar, "Dynamic wind loads and wake characteristics of a wind turbine model in an atmospheric boundary layer wind," *https://doi.org/10.1007/s00348-011-1253-5*, vol. 1, no. 1, pp. 1227–1294, 2012.

[11] G.V.Iungo, F.Violfa, and F.Porté-Agel, "Linear stability analysis of wind turbine wakes performed on wind tunnel measurements," *Journal of Fluid Mechanics:https://doi.org/10.1017/jfm.2013.569*, vol. 1, no. 1, pp. 499–526, 2013.

[12] F.Violfa, G.V.Iungo, and F.Porté-Agel, "Prediction of the hub vortex instability in a wind turbine wake: Stability analysis with eddy-viscosity models calibrated on wind tunnel data," *Journal of Fluid Mechanics:https://doi.org/10.1017/jfm.2014.263*, vol. 1, no. 1, pp. 1–10, 2014.

[13] C.L.Bottasso and F.Campagnolo, "Wind tunnel testing of scaled wind turbine models :beyond aerodynamics," *Journal of Wind Engineering and Industrial Aerodynamics:https://doi.org/10.1016/j.jweia.2014.01.009*, vol. 1, no. 1, pp. 11–28, 2014.

[14] K.Howard, L.Hu, and L.P.Chamorro, "Characterizing the response of a wind turbine model under complex inflow conditions," *Wind Energy:https://doi.org/10.1002/we.1724*, vol. 1, no. 18, pp. 729–743, 2015.

[15] H.Hu, Z.Yang, and P.Sarkar, "An experimental investigation on the aeromechanic performance and wake characteristics of a wind turbine model subjected to pitch motions," *29th AIAA Applied Aerodynamics Conference*, vol. 1, no. 1, pp. 1–20, 2016.

[16] J.Schreiber, E.M.Nanos, F.Campagnolo, and C.L.Bottasso, "Verification and calibration of a reduced order wind farm model by wind tunnel experiments," *Journal of Physics: Conference Series:https://doi.org/10.1088/1742-6596/854/1/012041*, vol. 1, no. 1, pp. 1–15, 2014.

[17] J.Schottler, F.Mühle, J.Bartl, and C.L.Bottasso, "Comparative study on the wake deflection behind yawed wind turbine models," *Journal of Physics: Conference Series:https://iopscience.iop.org/article/10.1088/1742-6596/854/1/012032/pdf*, vol. 1, no. 1, pp. 1–11, 2017.

[18] F.Campagnolo, R.Weber, J.Schreiber, and C.L.Bottasso, "Wind tunnel testing of wake steering with dynamic wind direction changes," *Wind Energy Science:https://doi.org/10.5194/wes-5-1273-2020*, vol. 1, no. 5, pp. 1–12, 2020.

[19] M.Bastankhah and F.Porté-Agel, "A new miniature wind turbine for wind tunnel experiments. part ii: wake structure and flow dynamics," *Energies:https://doi.org/10.3390/en10070923*, vol. 923, no. 10, pp. 1–16, 2017.

[20] C. Garrido, "Development of a scaled wind turbine model for wind tunnel experiments," *Lehrstuhl für Windenergie*, vol. 1, no. 1, pp. 1–76, 2014.

[21] J.Schottler, A.Holling, J.Peinke, and M.Holling, "Design and implementation of a controllable model wind turbine for experimental studies," *Journal of Physics: Conference Series:https://doi.org/10.1088/1742-6596/753/7/072030*, vol. 753, no. 1, pp. 506–541, 2016.

[22] R.Lanfazame, S.Mauro, and M.Messina, "Numerical and experimental analysis of micro hawts designed for wind tunnel applications," *Int J Energy Environ Eng:https://doi.org/10.1007/s40095-016-0202-8*, vol. 7, no. 1, pp. 199–210, 2016.

[23] J.Winslow, H.Otsuka, B.Govidarajan, and I.Chopra, "Basic understanding of airfoil characteristics at low reynolds numbers," *Journal of Aircraft:https://doi.org/10.2514/1.C034415*, vol. 55, no. 1, pp. 104–105, 2018.

[24] J.F.Manwell, J.G.McGowan, and A.L.Rogers, *Wind energy explained : theory, design, and application.* John Wiley and Sons, Ltd, 2009.

[25] N. T.Burton, D.Shape and E.Bossanyi, *Wind Energy Handbook.* John Wiley and Sons, Ltd, 2001.

[26] J.Yang, L.Fang, and D.Song, "Review of control strategy of large horizontal-axis wind turbines yaw system," *WILEY, https://doi.org/10.1002/we.2564*, vol. 1, no. 1, pp. 1–19, 2019.

[27] T.Bracchi, "Yaw moments of a three-axis wind turbine with yaw error," *Dept. Energy and Process Engineering, Norwegian University of Science and Technology, NTNU Trondheim, Norway*, vol. 1, no. 1, pp. 1–8, 2012.

[28] P. Hu and C.Chang, "Research on optimize application of buckingham pi theorem to wind tunnel test and its aerodynamic simulation verification," *Journal of Physics: Conference Series:https://doi.org/1742-6596/1507/8/082047*, vol. 1, no. 1, pp. 1–10, 2020.

[29] R.P.Coleman, A.M.Feingold, and C.W.Stempin, "Evaluation of the induced velocity field of an idealised helicopter rotor," *N.A.C.A. A.R.R,. No. L5E10.*, vol. 1, no. 1, pp. 1–27, 1945.

[30] J.G.Scheper and H.Snel, "Joint investigation of dynamic inflow effects and implementation of an engineering method'," *Netherlands Energy Research Foundation (ECN)*, vol. 1, no. 1, pp. 1–326, 1995.

[31] C.W.Tan, "Development and wind tunnel testing of yaw and individual pitch control systems for scaled wind turbine models," *Lehrstuhl für Windenergie*, vol. 1, no. 1, pp. 1–143, 2015.

[32] A. Paula, J.Meneghini, and R.D.Girardi, "The wavy leading edge performance for a very thick airfoil," *ARC: https://doi.org/10.2514/6.2017-0492*, vol. 1, no. 1, pp. 1–27, 2017.

[33] Princeton-edu, "Drag of blunt bodies and streamlined bodies," *https : //www.princeton.edu/asmits/Bicycle$_w$eb/blunt.html*, vol. 1, no. 1, p. 1, 2018.

[34] F.M.Heckmeier, D.Iglesias, and C.Breitsamter, "Development of unsteady multi-hole pressure probes based on fiber-optic pressure sensors," *Engineering Research Express*, vol. 1, no. 1, pp. 1–18, 2019.